ADVANCED MATERIALS
www.advmat.de

Progress and Opportunities for Machine Learning in Materials and Processes of Additive Manufacturing

Wei Long Ng, Guo Liang Goh, Guo Dong Goh, Jyi Sheuan Jason Ten, and Wai Yee Yeong**

In recent years, there has been widespread adoption of machine learning (ML) technologies to unravel intricate relationships among diverse parameters in various additive manufacturing (AM) techniques. These ML models excel at recognizing complex patterns from extensive, well-curated datasets, thereby unveiling latent knowledge crucial for informed decision-making during the AM process. The collaborative synergy between ML and AM holds the potential to revolutionize the design and production of AM-printed parts. This review delves into the challenges and opportunities emerging at the intersection of these two dynamic fields. It provides a comprehensive analysis of the publication landscape for ML-related research in the field of AM, explores common ML applications in AM research (such as quality control, process optimization, design optimization, microstructure analysis, and material formulation), and concludes by presenting an outlook that underscores the utilization of advanced ML models, the development of emerging sensors, and ML applications in emerging AM-related fields. Notably, ML has garnered increased attention in AM due to its superior performance across various AM-related applications. It is envisioned that the integration of ML into AM processes will significantly enhance 3D printing capabilities across diverse AM-related research areas.

1. Introduction

In recent years, the growing interest in machine learning (ML) has been driven by a convergence of technological advancements, data availability, community collaborations, and its practical applications in various domains. ML, a subset of artificial intelligence, empowers systems to learn from data, recognize patterns, and make intelligent decisions.[1] There are four types of ML algorithms (**Table 1**): supervised learning,[2] unsupervised learning,[3] semi-supervised learning[4] and reinforcement learning.[5] Supervised learning learns from a labeled dataset (input-output pairs) and creates a mapping between the input data and the corresponding output, allowing the algorithm to make predictions when presented with new data. Although supervised learning requires a lot of human effort and domain knowledge to label the data and define the goal, it can produce accurate predictions with repeated training iterations with large relevant dataset, and has found applications in various industries such as sports[6] and robotics.[7] In contrast, unsupervised learning is trained on a dataset without labeled output. It aims to find patterns or relationships within the large and complex data without human intervention. Semi-supervised learning is an ML algorithm that combines the elements of both supervised and unsupervised learning; it is trained on a dataset that contains both labeled and unlabeled data to improve the model performance. It makes efficient use of available data and reduces the reliance on costly labeled data to achieve good performance. Lastly, reinforcement learning focuses on regimented learning processes, whereby the algorithm undergoes a trial-and-error process based on the provided set of actions, parameters, and end values to achieve the best possible result.

Additive manufacturing (AM), often known as 3D printing, has revolutionized the field of manufacturing by enabling the fabrication of customized, complex 3D structures in a layer-by-layer manner. It can be categorized into seven main groups based on ISO/ASTM 52900:2021: 1) binder jetting, 2) directed energy deposition, 3) material extrusion, 4) material jetting, 5) powder bed fusion, 6) sheet lamination, and 7) vat photopolymerization. When applied to AM, ML opens new avenues for enhancing the entire manufacturing process, from material formulation, design optimization, and process optimization to quality control. The synergy between ML and AM has the potential to revolutionize the way AM-printed parts are designed or produced. By harnessing the vast amount of generated data, ML algorithms can unlock deeper insights into AM processes such as optimizing designs, predicting material properties, or even improving production quality (**Figure 1**).

W. L. Ng, W. Y. Yeong
Singapore Centre for 3D Printing
Nanyang Technological University
50 Nanyang Avenue, Singapore 639798, Singapore
E-mail: ng.wl@ntu.edu.sg; wyyeong@ntu.edu.sg
G. L. Goh, W. Y. Yeong
School of Mechanical and Aerospace Engineering
Nanyang Technological University
50 Nanyang Ave, Singapore 639798, Singapore
G. D. Goh, J. S. J. Ten
Singapore Institute of Manufacturing Technology (SIMTech)
Agency for Science
Technology and Research (A*STAR)
5 CleanTech Loop #01-01, Singapore 636732, Singapore
The ORCID identification number(s) for the author(s) of this article can be found under https://doi.org/10.1002/adma.202310006

DOI: 10.1002/adma.202310006

Table 1. Different classifications of ML techniques.

Category	Techniques
Supervised Learning	Linear Regression
	Logistic Regression
	Support Vector Machine
	Decision Trees (e.g., Classification and Regression Tree)
	Random Forest
	Gradient Boosted Trees (e.g., XGBoost, LightGBM, CatBoost)
	Neural Networks (e.g., DNN, RNN, U-Net, RandLA-Net, LSTM)
	K-Nearest Neighbours (K-NN)
	Gaussian Process Modelling
	Ensemble learning (e.g., Adaboost, Bayes optimal classifier, bagging, stacking)
Unsupervised Learning	K-means Clustering
	Hierarchical Clustering
	Principal Component Analysis (PCA)
	Independent Component Analysis (ICA)
	Autoencoders (e.g., variational autoencoder)
	Gaussian Mixture Models
Semi-supervised Learning	Self-training
	Multi-view Training
	Generative Adversarial Networks (GANs)
	Domain Adversarial Neural Network
Reinforcement Learning	Q-learning
	Deep Q Networks (DQN)
	Monte Carlo Methods
	Policy Gradient Methods
	Actor-Critic

2. Publication Landscape for ML in AM

An analysis of the publication landscape was conducted to determine the influence of ML on different 3D printing techniques using the following set of keywords on Web of Science ("machine learning" + "3D printing/additive manufacturing" + "printing technique"). As there are many variants of 3D printing technique under each ASTM classification, numerous keywords for each printing technique were used: 1) binder jetting—binder jetting, multi-jet fusion; 2) directed energy deposition—directed energy deposition, wire arc additive manufacturing; 3) material extrusion—extrusion, fused deposition modeling, fused filament fabrication, direct ink writing; 4) material jetting—jetting, inkjet, microvalve; 5) powder bed fusion—powder bed fusion, selective laser sintering, selective laser melting, electron beam melting, laser powder bed fusion; 6) sheet lamination—sheet lamination; and 7) vat photopolymerization—vat photopolymerization, stereolithography, digital light processing (DLP), and continuous liquid interface production. As shown in **Figure 2a**, a total of 528 ML-related AM publications were published over the last 10 years and the adoption of ML for each 3D printing technique varies—powder bed fusion (225 publications) > material extrusion (135 publications) > material jetting (80 publications) > directed energy deposition (59 publications) > vat photopolymerization (20 publications) > binder jetting (8 publications) > sheet lamination (1 publication). The ML-related AM research has grown substantially over the last ten years; it has increased significantly from one publication in the year 2013 to 213 publications in the year 2022 (Figure 2b).

As ML is prevalently used in AM processes, further analysis was conducted on Web of Science to determine some common ML applications in AM research using the following set of keywords ("machine learning" + "3D printing/additive manufacturing" + "application"). The top five most common ML applications in AM research over the last 10 years include 1) Quality control (301 publications), 2) Process optimization (222 publications), 3) Design optimization (183 publications), 4) Microstructure analysis (45 publications), and 5) Material formulation (14 publications) (Figure 2c). These ML applications are applied in various key AM-related research areas such as aerospace and defense, bioprinting, construction printing, drug printing, electronics printing, and marine and offshore and unmanned aerial vehicles (Figure 2d). A more in-depth discussion of these five common ML applications and their specific roles in different key AM-related research areas will be presented in subsequent sections.

3. Common ML Applications in AM Research

Over the years, ML has attracted increasing attention in AM due to its superior performance in different applications such as quality control, process optimization, design optimization, microstructure analysis, and material formulation. In-depth discussion on the common ML applications will be categorized based on their AM technique to provide a comprehensive overview of how machine learning can be applied to each specific AM technique, thereby highlighting the unique challenges and solutions that each method presents.

3.1. Quality Control

Quality control plays a crucial role in enhancing the efficiency and reliability of additive manufacturing processes. Many studies have explored the application of ML algorithms and sensor data analysis to achieve real-time process monitoring and quality assurance. Signals from in situ sensors are used to train ML models to monitor the stability of the process and detect defects within successful builds. Different ML techniques (supervised, unsupervised, semi-supervised, and reinforcement learning) have been used for quality control in AM; the choice of ML approach for quality control is dependent on the nature of the data and the objectives of the quality control system. Supervised learning is most used ML technique for quality control in AM and most of the studies demonstrated high prediction accuracies > 90%. Although it is well-suited for quality control with labeled historical data from both good and defective products/processes, it may not be useful for the detection of novel defects or anomalies not seen in the training data. **Figure 3** provides a summary of the techniques involved and applications of ML in quality control and more discussion on the different types of ML used in quality control will be provided in the subsequent sections.

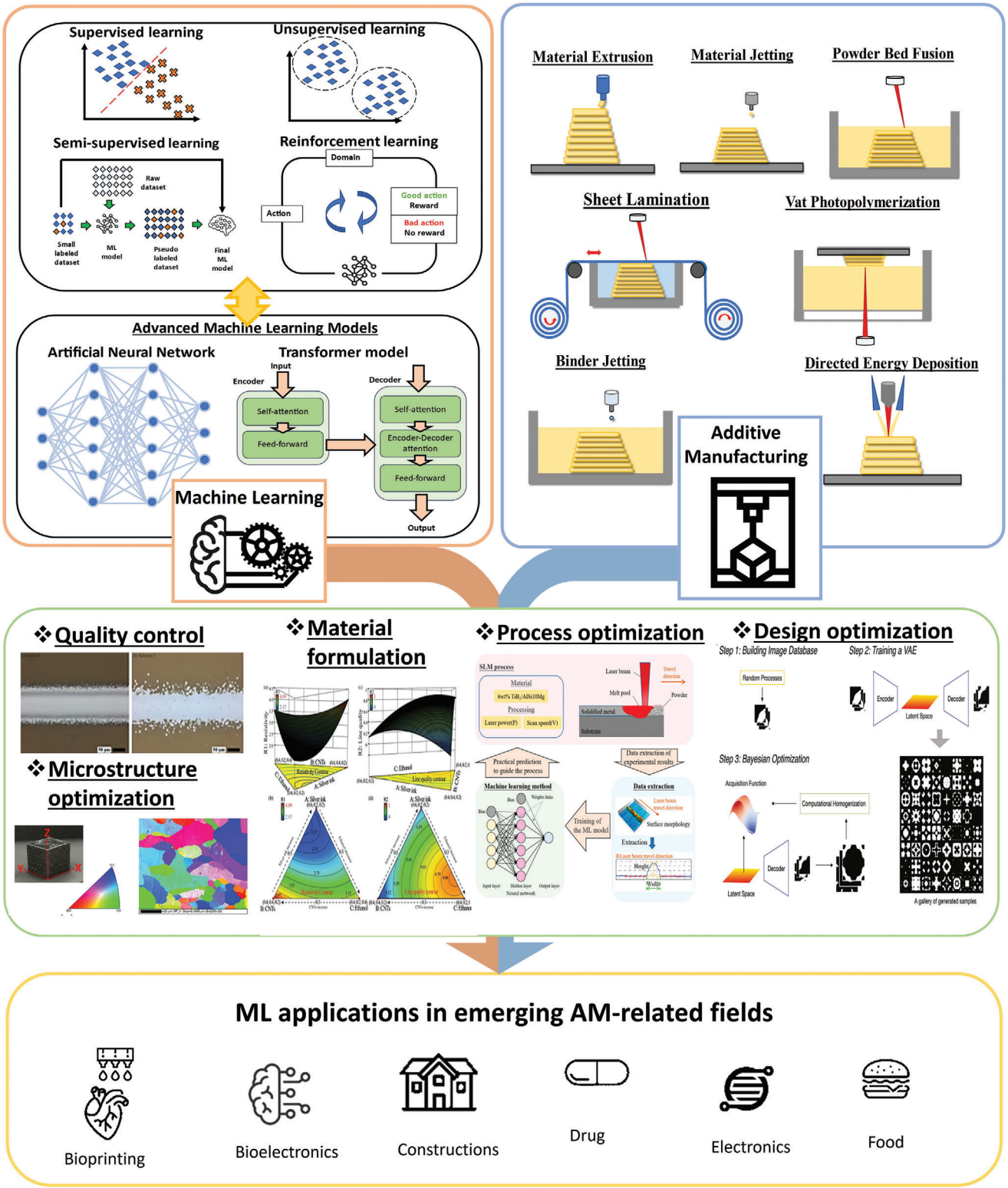

Figure 1. An overview of the integration of ML into AM processes for diverse optimizations and applications. The left section classifies ML into four types—supervised, unsupervised, semi-supervised, and reinforcement learning—while introducing the emerging transformer model for ML applications. On the right, various AM techniques are detailed. The central part of the figure illustrates the potential benefits that ML can offer to AM and the bottom part showcases practical applications across a wide range of industries, from aerospace and defense to electronics, and food, underscoring the extensive impact of integrating ML with advanced manufacturing methods. Reproduced with permission.[53,76,115,176] Copyright 22 Mar 2024, Elsevier.

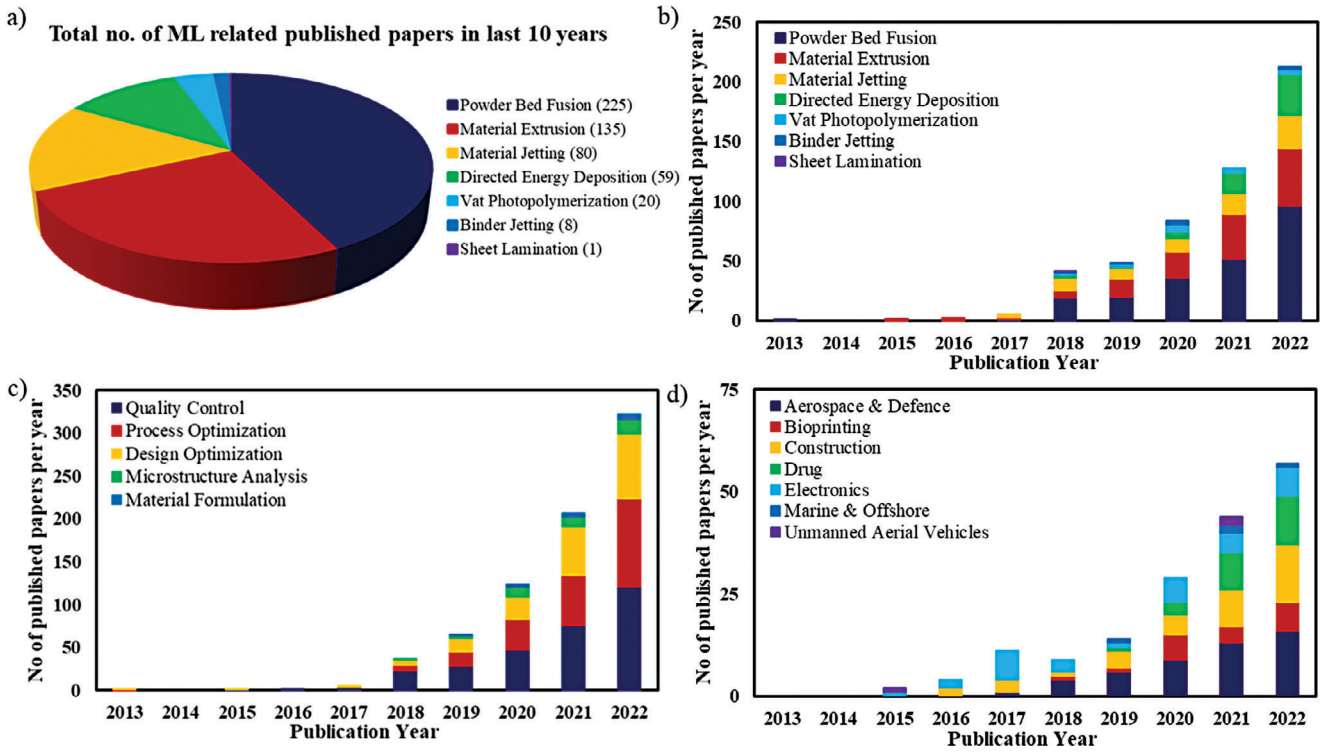

Figure 2. a) Number of ML-related additive manufacturing publications over the past 10 years. b) Detailed annual breakdown of the number of publications for each printing technique from years 2013 to 2022. c) Detailed annual breakdown of the number of publications for different ML applications in AM from years 2013 to 2022. d) Detailed annual breakdown of the number of publications on ML applications in various key AM research areas from years 2013 to 2022.

3.1.1. Powder Bed Fusion

It is common to observe high porosity, balling, incomplete fusion, and spattering during the AM process. These defects arise from factors such as process instability and poor material interactions. Such defects are detrimental to the quality of printed parts, leading to compromised mechanical strength, surface roughness, inaccurate geometries, and potential delamination. It is important to address these defects to ensure the reliability and performance of AM-fabricated components across industries.[8]

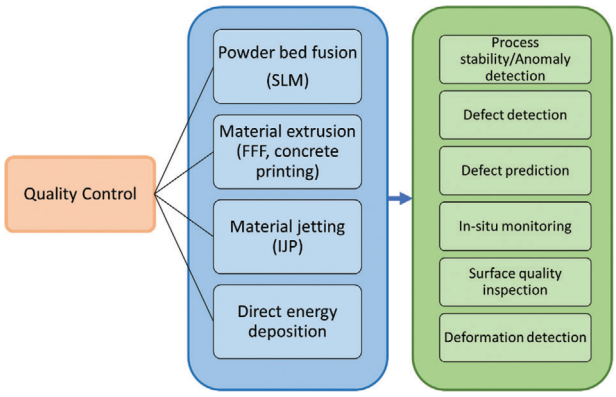

Figure 3. Graphical overview summarizing the diverse applications of ML in quality control across various AM processes.

To monitor the process stability, a study used data from the supplied EOS M290 powder bed images to predict anomalies during the powder spreading process (**Figure 4**).[9] The powder-based materials included Ti6Al4V, AlSi10g, IN718, SS316L, SS17-4, and bronze. The images were first filtered using 37 different 2D image processing filters, and the filter responses were stored in vectors for each pixel. The response vectors were then grouped into 100 groups using a standard k-means unsupervised clustering algorithm. The mean response vector for each group was then stored as visual words in a dictionary. Then, the pixel at each training image patch was matched to the closest visual word, and the histogram for the occurrence frequency of each word in the patch was calculated and termed "fingerprints". The rationale was that training images with similar powder-spreading anomalies would result in similar "fingerprints". During the method execution, the powder bed image was divided into different patches and the "fingerprint" from each patch was then calculated. The quality of a patch was determined by matching its "fingerprint" to a database of 2402 "fingerprints". These "fingerprints" were manually labeled under six conditions: anomaly-free: 1040 "fingerprints", recoater hopping: 264 "fingerprints", recoater streaking: 228 "fingerprints", debris: 187 "fingerprints", super-elevation: 314 "fingerprints", part failure: 264 "fingerprints", incomplete spreading: 105 "fingerprints". The top three matches from this database were then used to assess the patch's quality. The algorithm managed to classify the powder spreading based on the six conditions with precision ranging from 65.0% to 98.9%

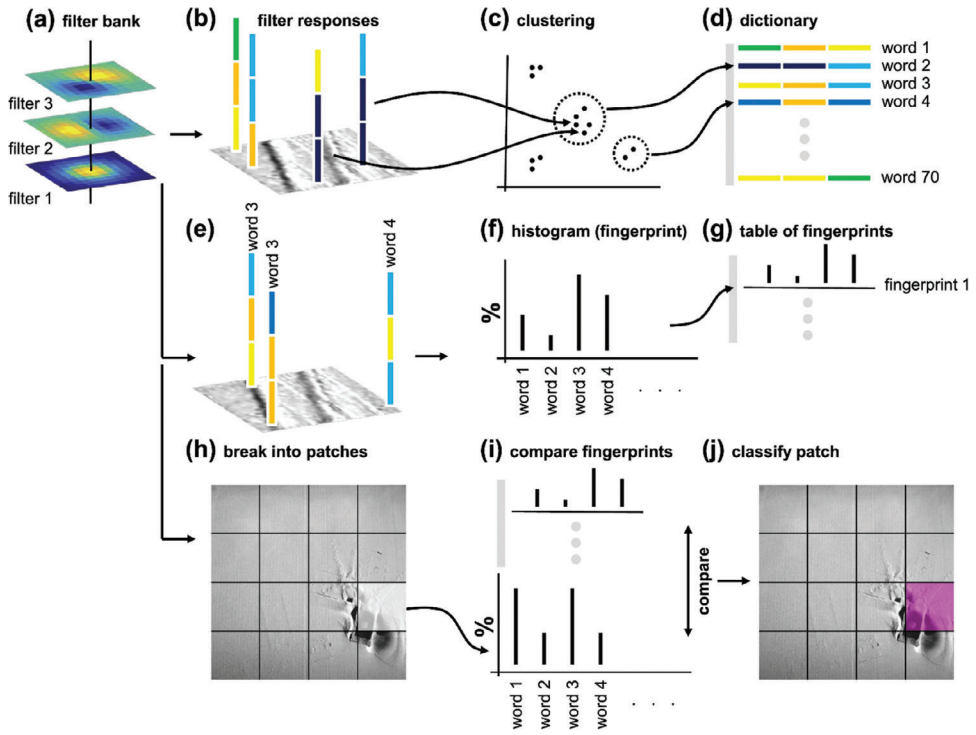

Figure 4. Flow chart of ML process to detect anomaly in laser powder bed fusion. Reproduced with permission.[9] Copyright 2018, Elsevier.

For defect detection in laser powder bed fusion (LPBF) builds, various sensor technologies were used in conjunction with ML techniques. These technologies included visible light cameras, infrared cameras, high-speed cameras, photodiodes, and acoustic sensors. There were also efforts that combined multiple sensor technologies for ML training. Using a high-resolution 36.3-megapixel digital single-lens reflex (DSLR) camera, images of each layer were taken before and after LPBF laser scanning to predict the locations of voids.[10] Multiple images were taken under different lighting conditions for each build layer and were combined using an *ensemble* classification. It was possible to combine data from multiple sensors through the *ensemble* technique instead of only using data from a single sensor under different conditions. The ground truths were obtained from X-ray computed tomography (CT) convolved with a Gaussian filter and labeled using support vector machine (SVM) binary classifiers before being manually checked by a certified non-destruction inspection inspector. The *ensemble* method improved the accuracy of prediction from 65% to 85% for single sensor image input to 85% for multiple images.

A four-phase (sliding, convolutional neural networks (CNN), smoothing, and compensation) modeling approach was developed for online surface measurement in additive manufacturing.[11] This approach utilized a window-based data reformulation technique and CNN to predict 3D surface data directly from 2D images without the need for time-consuming triangulation computations. The method proved to be highly accurate, with an average relative prediction error mostly lower than 10%. Its computational efficiency and ability to acquire data layer-wise in real-time made it suitable for online quality monitoring and control in additive manufacturing processes.

In-process monitoring using infrared cameras followed by ML for data analysis was performed using the original equipment manufacturer and customized hardware.[12] The EOSTATE Exposure OT captured a long exposure image at ≈900 nm of the laser scanning over one whole layer. Both groups changed the process parameters to create the training dataset. The unsupervised K-means clustering was used to enlarge the manually labeled training dataset followed by k-nearest neighbors (K-NN) supervised learning to identify anomalies (*drifts*) in the images.[12a] These anomalies were then shown to have a correlation with high porosity occurrence in X-ray CT scans of the actual samples. Random forest-bagged tree ensemble labeled with X-ray CT data are used (**Figure 5**) and the use of multiple consecutive layers improved the prediction accuracy. The interpretability of the random forest (RF) model showed that the lack of fusion defects prediction was dependent on the adjacent layers while keyhole defects prediction was heavily dependent on the 10th subsequent layer. The model could determine the average density of a small area measuring 1 mm × 1 mm.

An infrared thermographic camera was integrated to an SLM 280 LPBF system to capture short videos of delamination, splatters, and defect-less processes that were then converted to image frames to train a CNN.[13] The training dataset was augmented by rotating the image, flipping the images, and random image noise and blur. Delamination and splatter defects were detected at an average accuracy of 96.8%.

High-speed cameras with frame rates above 1000 Hz in the visible and infrared range were also used as inputs for ML models. A short wavelength infrared high-speed camera was used to capture the thermal history of the part and train a customized CNN for the identification of defect locations within the part.[14]

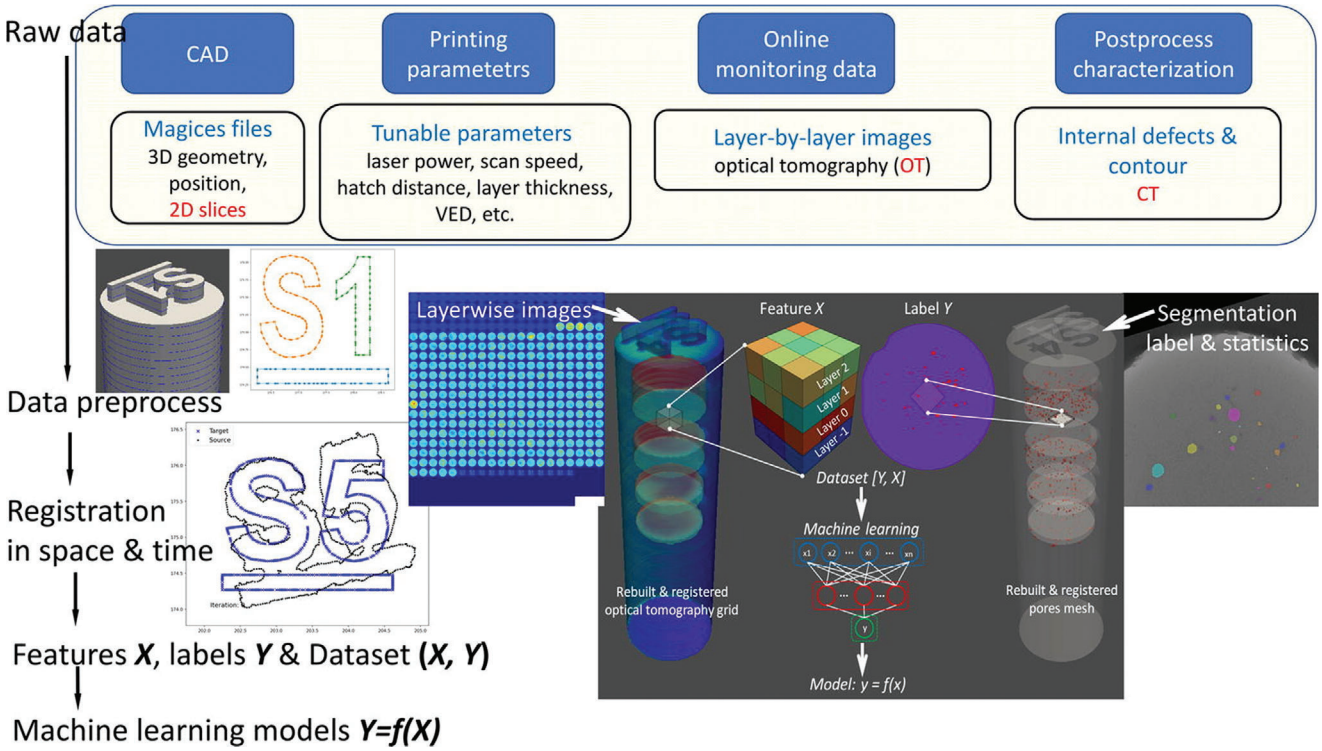

Figure 5. Workflow of training the ML model using labeled X-ray CT data. Initially, a compilation of through-process data encompassing Computer-Aided Design (CAD), processing parameters, real-time online monitoring data captured via Optical Tomography (OT) images, and subsequent post-processing characterization data derived from X-ray Computed Tomography (CT) was performed. Subsequently, an ML model was developed to glean valuable insights into the mechanisms underlying defect generation. The adeptly trained ML model is proficient in accurately forecasting porosity occurrences within individual layers, leveraging the composite data from multiple layers of OT information. Reproduced with permission.[12b] 2022, Elsevier.

Melt-pool and time-dependent attributes were extracted from the thermal images for groups of pixels and a threshold was set for a binary outcome of pore and non-pore groups. The data was labeled in comparison to X-ray CT data with details from their previous work[15] and a 1D CNN model was trained using Bayesian Optimization. It was found that a group of pixels representing a volume of 700 × 700 × 50 μm produced the best prediction accuracy for keyhole porosities above 0.1% in volume and decreasing the volume size reduced the prediction accuracy. A high-speed visible light camera at 6,400 Hz was used to capture melt pool images.[16] The feature extraction, classification, and subsequent unsupervised ML model training were similar to another work for build failure detection and modifications were made to achieve a scale-invariant representation of the melt pool morphology.[9] The "fingerprints" that were identified for five outcomes include desirable, under-melting, keyhole porosity, severe keyhole porosity, and balling. Two infrared (IR) high-speed cameras at 700 and 950 nm wavelengths respectively were used to take images of melt pools at 100 kHz (**Figure 6**).[17] Multiple feature types from the raw sensor data and calculated thermal field were extracted to train various ML models ranging from K-NN, SVM, to CNN. The algorithms were used to 1) detect out-of-focus laser and 2) porosity level and were able to achieve a true positive rate of 90%. The computationally light ML models produced subpar results when trained on single feature types but generated on-par results with the deep learning models when trained on inputs from the multiple feature types (melt pool morphology, spatter characteristics, and melt pool temperature features).

One of the challenges for training ML models with high-speed camera data was the difficulty in volumetrically matching the ground truth data typically obtained by X-ray CT. Synchrotron X-ray imaging was used to obtain real-time defect formation data for comparison with the in situ visible and NIR imaging above 50 kHz instead of measuring the defects after the process.[18] The frequency response of the intensity of the high-speed camera images was grouped into wavelets shorter than 1 ms for training a deep neural network model to identify pore and non-pore events. Simulation models were then used to provide further insights into the pore formation mechanism. The developed simulation model was then used to generate data to train a deep learning model for a high-speed camera integrated into a commercial LPBF system SLM 280. Accuracies up to 87% were obtained for identifying the pores.

Due to the limited penetration depth of visible and IR waves in metals, the signals obtained from electromagnetic emissions of these wavelengths typically only capture signals from the surface of the metal during the process. Besides using synchrotron X-ray to penetrate the metal, others have captured acoustic emissions to potentially detect process signals originating from below the metal surface. A microphone was secured 25–30 cm on top of the build plate to sample acoustic emissions at 100 kHz.[19] Features from the signal were extracted based on three primary groups: time-series statistics, frequency domain characteristics,

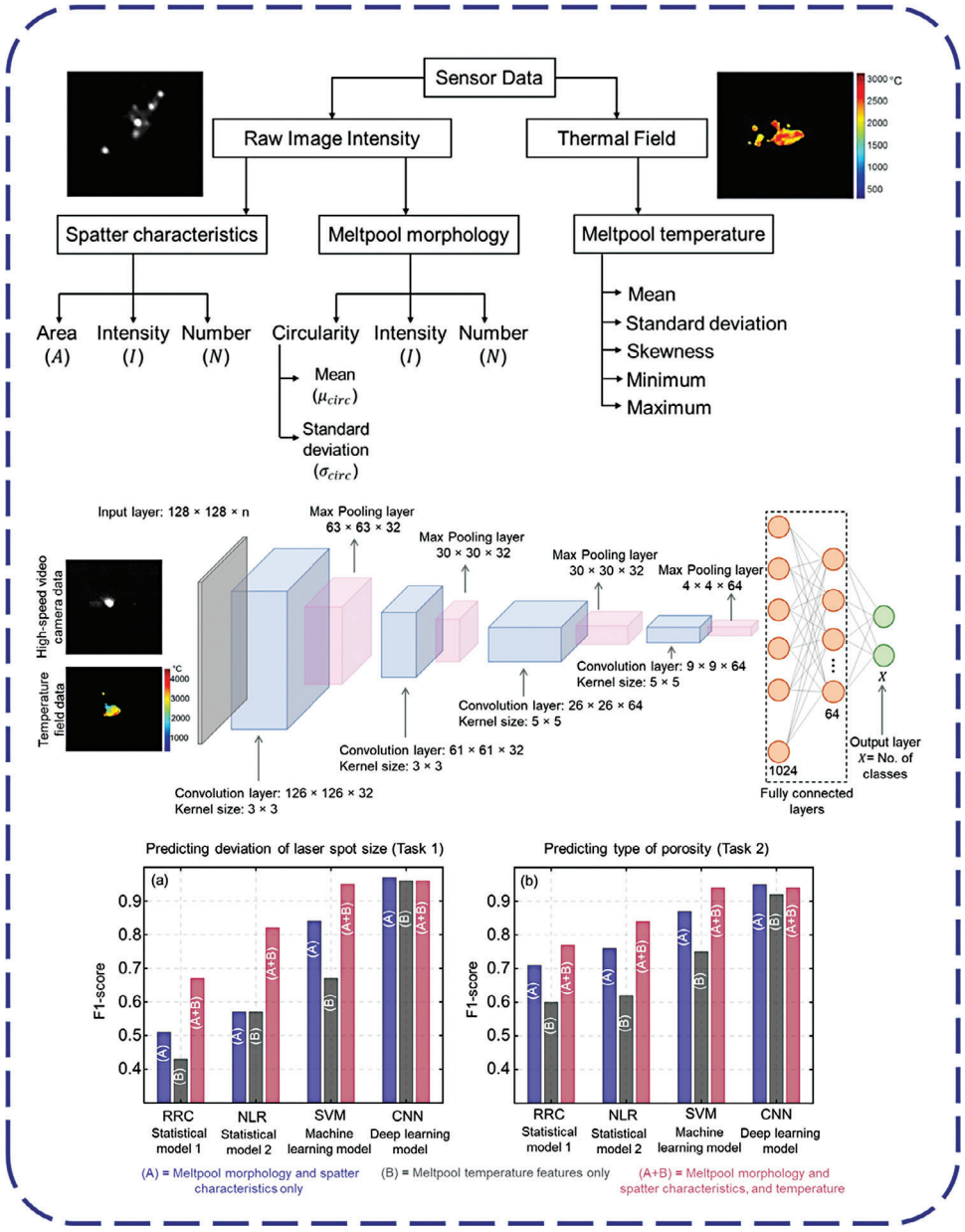

Figure 6. Diagram illustrating the diverse physics-derived attributes extracted from various sensing methods, which are then used to train the CNN architecture. A visual depiction of the efficacy of various models in classifying a) the size of the laser spot and b) the kind of porosity, measured using the F1-score. RRC stands for ridge regression classifier, NLR denotes nonlinear logistic regression classifier, SVM represents support vector machine classifier, and CNN signifies convolutional neural network classifier. Adapted with permission.[17] 2022, Elsevier.

and oscillatory modes via an ensemble empirical mode decomposition technique. An SVM was then trained based on X-ray radiograph ground truths for signal windows of 1–15 ms. A window of 7.5 ms showed the best accuracy of 97% in predicting keyhole pore and keyhole-free scan lengths that corresponded to the window. A sensor measuring a wideband of 100–900 kHz at the center bottom of a circular build plate was used to detect acoustic emissions from coupons separated radially from the sensor.[20] The noise from the acoustic signal was first removed and three methods were explored: k-means, principal component analysis, and a general deep learning. K-means clustering achieved a 90% prediction rate when paired with a deep learning classifier, cracks were detected using principal component analysis and lastly the general deep learning model (trained on raw H13 signals) demonstrated good adaptability for prediction when tested on SS316L data. A 1D CNN model accurately detected the spattering event in the LPBF process up to 85% (**Figure** 7a).[21] Conversely, acoustic emission from the powder bed fusion process was used to predict possible defect formation within the printed parts (Figure 7b).[22] The developed model was able to predict different types of defects (lack of fusion pores, conduction mode, and keyhole pores) within

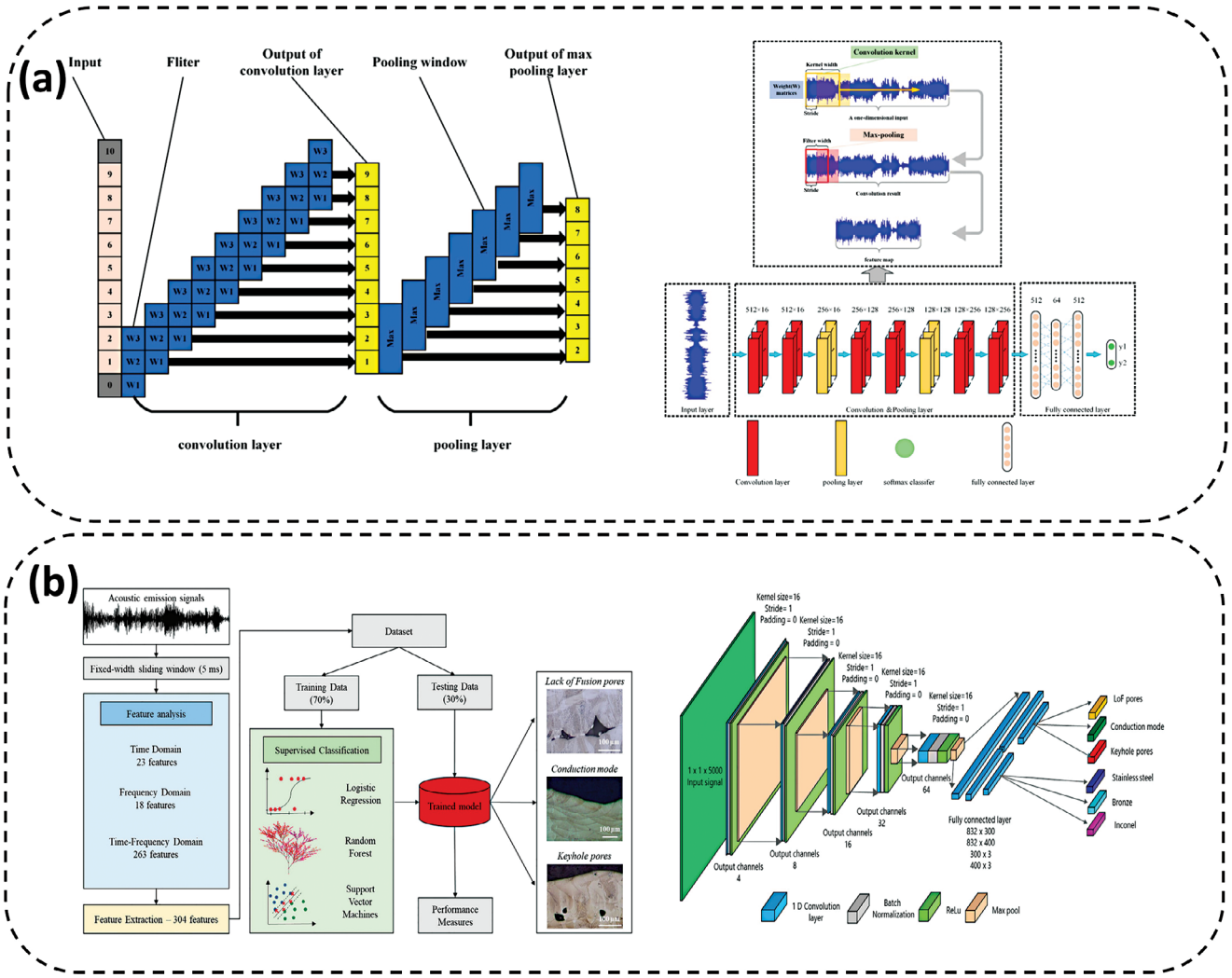

Figure 7. a) Schematic showing the ID-CNN model that is used for detecting spattering event using acoustic signal. Reproduced with permission.[21] 2021, MDPI. b) Schematic showing the flowchart of model that is used for detecting various types of defects using acoustic signal. Reproduced with permission.[22] 2022, Taylor & Francis.

different materials (316L stainless steel, bronze (CuSn8), and Inconel 718) with an accuracy of ≈93%. It was challenging to collect the acoustic emissions as the signal passed through the previously melted layers and the build plate to reach the sensor. Another study collected the acoustic signals via an optoacoustic fiber Bragg grating with sampling rates up to 10 MHz.[23] Reinforcement learning was used to recognize acoustic emissions from three classes of material: poor quality, medium quality, and high quality, and achieved detection accuracies above 74%. A monitoring strategy for LPBF process was developed using a hybrid deep learning (DL) model that combined CNN and long–short-term memory (LSTM) (**Figure 8**).[24] The proposed model achieved high prediction accuracy ranging from 95.9% to 100% in classifying lack of fusion, conduction mode, and keyhole across various time scales, based on data from a heterogeneous time-synced sensing system. The study emphasized the importance of back reflection and structure-borne acoustic emission sensors in the decision-making process. Although the model demonstrated high accuracy, further validation is necessary for complex geometries and scanning paths, other types of defects, and optimization of hardware and data collection pipeline, and the inclusion of physics-based inference from the trained models.

The previous studies were either based on derived or raw data taken from one sensor type. There were also efforts to use ML for multiple sensor types to achieve improved defect detection rates. Sensor data from the optical layer images, process multispectral emission, and the vector scan path of the laser were combined (**Figure 9**).[25] The combined sensor data input was trained against X-ray CT ground truths in a CNN model to classify volumes of 940 μm × 940 μm × 660 μm into flaw and nominal build regions. The training accuracy was 97.3% when trained solely on multi-spectral emissions but decreased to 88.7% for the test dataset. Similarly, the training accuracy was 97.0% when trained on all data modalities but decreased to 91.9% for the test dataset.

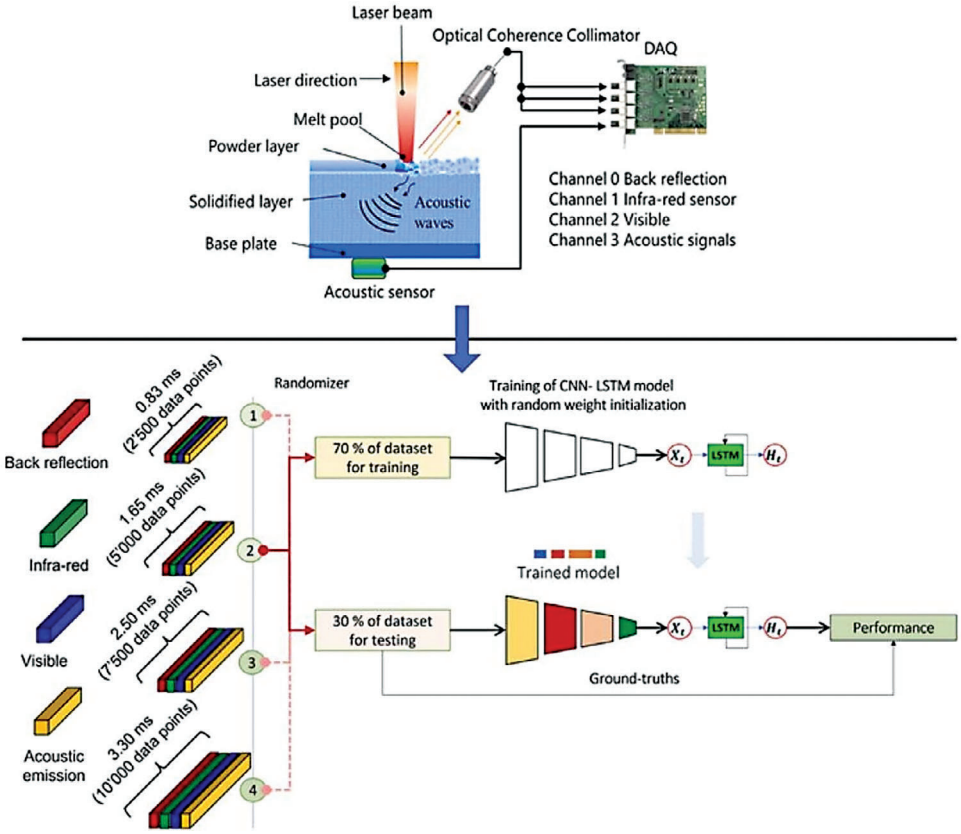

Figure 8. Overview of the variable time scale monitoring of LPBF using a hybrid DL model. The proposed DL model can operate over variable time scales for LPBF monitoring. A hybrid DL architecture combining CNN and LSTM was introduced. Heterogeneous signals, including optical and acoustic emissions from the process zone, were used to train the DL model. The DL model demonstrated accurate classification of lack of fusion, conduction, and keyhole regimes within time scales ranging from 0.5 to 4 ms. Adapted with permission.[24] 2022, Elsevier.

3.1.2. Material Extrusion

Material extrusion, a prevalent additive manufacturing technique, is prone to specific defects that impact the quality of printed parts. Common defects include layer misalignment caused by inaccurate deposition, voids stemming from incomplete material fusion, inconsistent extrusion leading to irregular wall thickness, and delamination due to weak adhesion between layers. These defects are dependent on factors like improper temperature control, inadequate material flow, and incorrect print settings. These undesirable defects compromise the structural integrity, mechanical strength, and dimensional accuracy of printed parts, making defect mitigation essential for producing reliable and functional components.

To improve print quality and consistency of fused filament fabrication (FFF) processes, an innovative approach to quality assurance in additive manufacturing processes was implemented by leveraging environmental data and ML.[26] Various environmental parameters (temperature, humidity, air pressure, and gas particles) were recorded and analyzed during fused deposition modeling (FDM) processes and different ML algorithms (multilayer perceptron (MLP), 1D CNN, RNN, LSTM, Inception Time, XceptionTime, and eXplainable CNN for multivariate time series classification (XCM)) were employed for classification. The XceptionTime architecture was found to be the most effective, achieving a minimum accuracy of 95% with both small and large datasets. This ML algorithm provided faster and cheaper quality assurance compared to traditional optical 3D scan methods.

Nozzle clogging is also a common issue when dealing with fiber-reinforced polymers. Nozzle clogging is usually undetected by the printer and would cause an eventual print failure. A multi-head encoder-decoder temporal convolutional network (MH-ED-TCN) algorithm utilized time-series data from collaborative sensors to detect nozzle clogging.[27] This algorithm outperformed other ML approaches including SVM, LSTM, LSTM autoencoder, and a simple CNN to achieve a remarkable 97.2% accuracy in identifying nozzle clogging. Further improvements to the algorithm were also recommended and the addition of appropriate sensors addressed the printing malfunctions caused by the viscoelastic behavior of polymer materials. Although prediction of nozzle clogging can be performed using ML approaches, it is challenging to predict the quality of extruded materials from the nozzle. To solve that, image-based anomaly detection techniques were developed to realize real-time monitoring and correction. Image classification model[28] and object detection models[29] were used to predict under-extrusion and over-extrusion phenomena during the FDM process and accuracies of 98.0% and 89.8% were achieved respectively. The system outperformed human response times in detecting and correcting defects. The framework proposed can be extended to other 3D printing

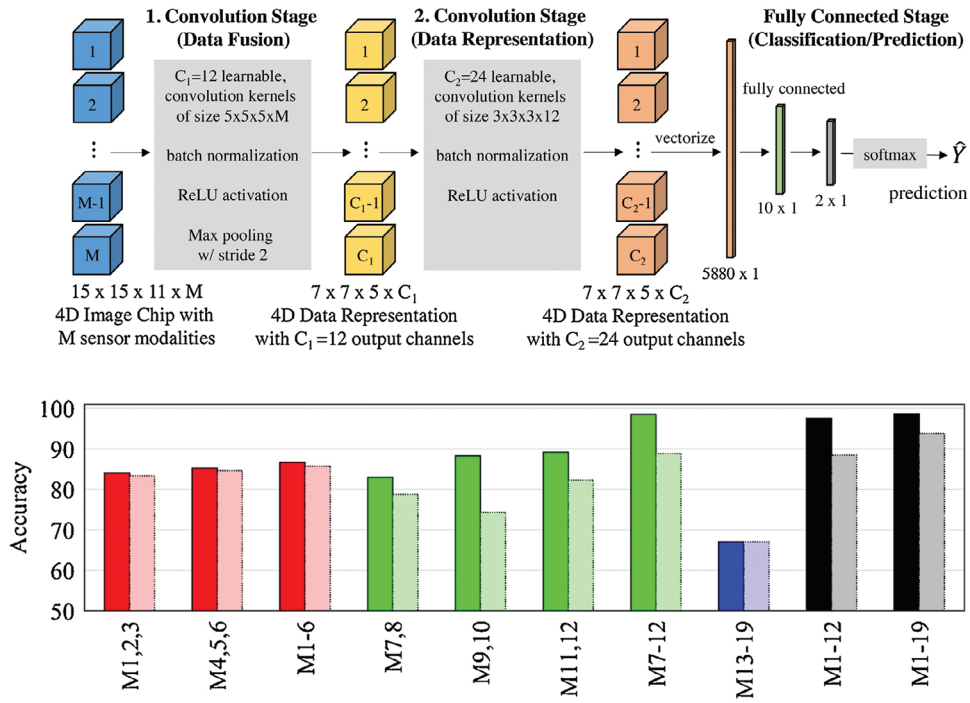

Figure 9. A Convolutional Neural Network (CNN) design for defect identification uses 3D image slices from M different sensor types. This network is structured with two convolutional phases followed by a dense layer comprising one hidden layer. The model's output predictions are produced through a softmax classification layer. Bar chart showing sensor fusion performing better than the individual layer-wise optical layer images, process multi-spectral emission, and the vector scan path of the laser. Reproduced with permission.[25] 2022, Elsevier.

technologies for fabricating high-performance materials in challenging environments without human intervention.

A study was performed to diagnose faults and identify causes, particularly regarding the drift of process parameters. A deep adversarial learning system that utilized captured upper-layer images during the manufacturing process was proposed.[30] It employed a conditional generative adversarial network (CGAN) to address data imbalance and a domain adversarial neural network (DANN) to handle domain-shifting problems caused by drifting process parameters. The experimental validation demonstrated the effectiveness and accuracy (91.01%) of the proposed method. Although many approaches have been developed to provide automated monitoring, current automated methods cannot be universally applied to various components, materials, and printing systems. A study focused on generalizing the 3D printing defects and correcting errors in material extrusion additive manufacturing (**Figure 10**).[31] A multi-head neural network trained on a large and diverse dataset (≈1.2 million images) was developed to identify deviations from optimal printing parameters. The system allowed for real-time error detection and rapid correction across different printing scenarios. The trained network achieved an overall accuracy of 84.3% in classifying the flow rate, lateral speed, Z offset and hot end temperature and demonstrated the effectiveness of gradient-based visual explanations for understanding network decisions. The methodology offered a cost-effective and scalable solution that can be easily integrated into existing printers and workflows, leading to improved quality and reliability of end-use products (**Figure 11**).

Defect detection is critical for large-scale printing due to the high cost involved, especially so in building and construction. A study has demonstrated automated layer defect detection in construction 3D printing using deep CNN.[32] The system comprised a deep CNN model that took images as input and distinguished concrete layers from surrounding objects via semantic pixel-wise segmentation. Data augmentation techniques generated 1 million images for training, tuning, and testing the CNN model. Furthermore, a defect detection module was developed to detect deformations in the printed concrete layers using the images output by the CNN model. The evaluation results showed a high level of accuracy and F1 score (>90%) in differentiating concrete and non-concrete pixels, while the defect detection module achieved a total accuracy of 97.5% and a miss rate of less than 6% for printed layers with and without defects. A similar study with fewer images resulted in poorer performance of 80% mean average precision.[33] These studies demonstrated the potential of computer vision and deep learning techniques for automated inspection and quality monitoring in construction 3D printing.

In construction printing, the bigger size (cm-scale) of the extrudate allowed the utilization of 3D scanners for detecting deformations in printed structures.[34] This was unlike smaller-scale polymer printing (in mm scale) where the precision of 3D cameras imposed limitations on this capability. A study evaluated the performance of a monocular camera, LiDAR, and LiDAR-camera in terms of point cloud density and 3D map reconstruction for defect detection. The results showed that the RGB-L camera outperformed the other sensors in all scenarios, with an error below 4% when using K-means clustering at a distance of 0.5m.

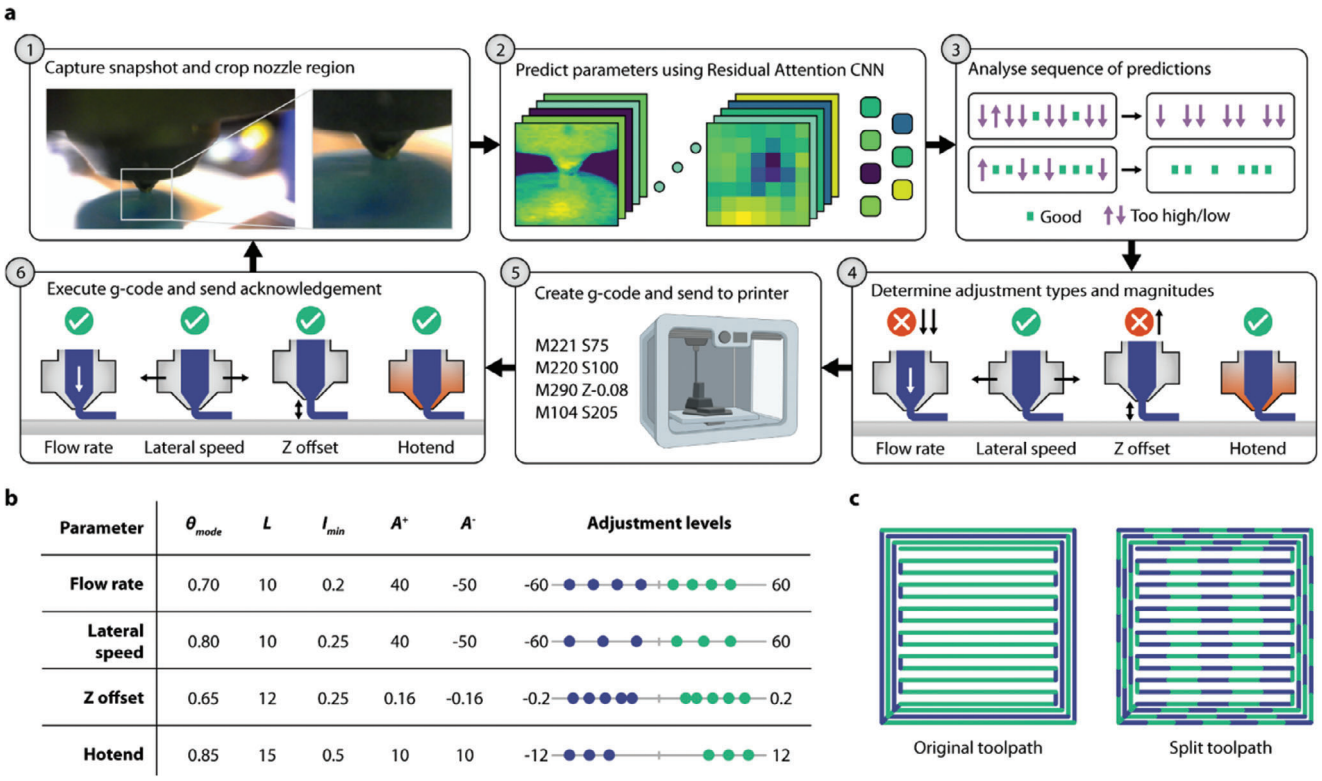

Parameter	θ_{mode}	L	I_{min}	A^+	A^-	Adjustment levels
Flow rate	0.70	10	0.2	40	-50	-60 … 60
Lateral speed	0.80	10	0.25	40	-50	-60 … 60
Z offset	0.65	12	0.25	0.16	-0.16	-0.2 … 0.2
Hotend	0.85	15	0.5	10	10	-12 … 12

Figure 10. a) The feedback pipeline consists of six key steps that facilitate the online updating of parameters based on image data obtained during the extrusion process. b) The provided table presents the values for θ_{mode} (mode threshold), L (sequence length), I_{min} (interpolation minimum), A^+ (maximum increase), and A^- (maximum decrease) for each printing parameter, along with the corresponding possible levels of update amounts. c) A simple example is presented to illustrate the geometric structure of a single layer and the subdivision of the toolpath into smaller segments of equal length. This subdivision, using 1 mm segments, enables swift correction and reduces the response time in the feedback process. Reproduced with permission.[31] 2022, Nature Portfolio.

However, the execution time of the algorithm was currently too high for real-time applications. It was suggested that future work can focus on validating the system by analyzing concrete printed areas, incorporating color information to better identify points belonging to each printed layer, and developing the more advanced algorithm in C/C^{++} to reduce computational cost and enable real-time applications.

A novel methodology for real-time quality assurance in 3D-printed electronics using U-Net was presented.[35] An FFF printer equipped with an extruder was used for conductive paste dispensing, pick-and-place unit, and dual cameras. The cameras captured images during the printing process and a trained neural network was used to distinguish the conductive wires from the plastic substrate. The method was used to identify common printing flaws such as connection breaks, shorts, and inaccuracies in wire width, comparing the actual output with the intended G-code instructions with an overall accuracy of 96.6%. The results facilitated high-resolution documentation and provided data to improve the printing process. This innovation enabled the detection of errors and can be potentially used for automated flaw rectification, paving the way for more reliable and autonomous 3D-printed electronics production.

In situ monitoring is commonly implemented during the bioprinting process to improve the dimensional accuracies of 3D-bioprinted tissue constructs. The error (missing or excess material) within each printed layer is compounded with increasing layers and it would lead to poor dimensional accuracies for large 3D-bioprinted tissue constructs, which typically require a long printing time and involve high material cost. The CNN-based classifiers are typically utilized for defection detection in most manufacturing processes; they can be implemented to monitor and improve the printing outcome in 3D bioprinting processes using computer vision. The captured images can be labeled as "under-extrusion", "good-quality" and "over-extrusion" images for training. A DL model can be used to optimize the printing parameters iteratively and adaptively using a real-time in situ monitoring and correction system. An ad hoc optimized CNN and a mathematical model were used to perform in-process and parameter optimization of the extrusion-based bioprinting process.[36] The dataset was constructed by capturing videos of multi-layered scaffolds fabricated using the extrusion bioprinting process; the inputs include type of extrusion system (pneumatic or mechanical), type of material, layer thickness, and infill density while the output is based on extrusion multiplier (which represents the ratio of printing resolution to nozzle diameter). The printing quality can be optimized by tuning the printing parameters through a series of consecutive prints in a feedback loop manner using the CNN model. The results showed an accuracy of 94.3% for overall printing; acceptable printing has a precision of 87.2% and recall of 96.5%, over-extrusion has a precision of 98.3% and recall of

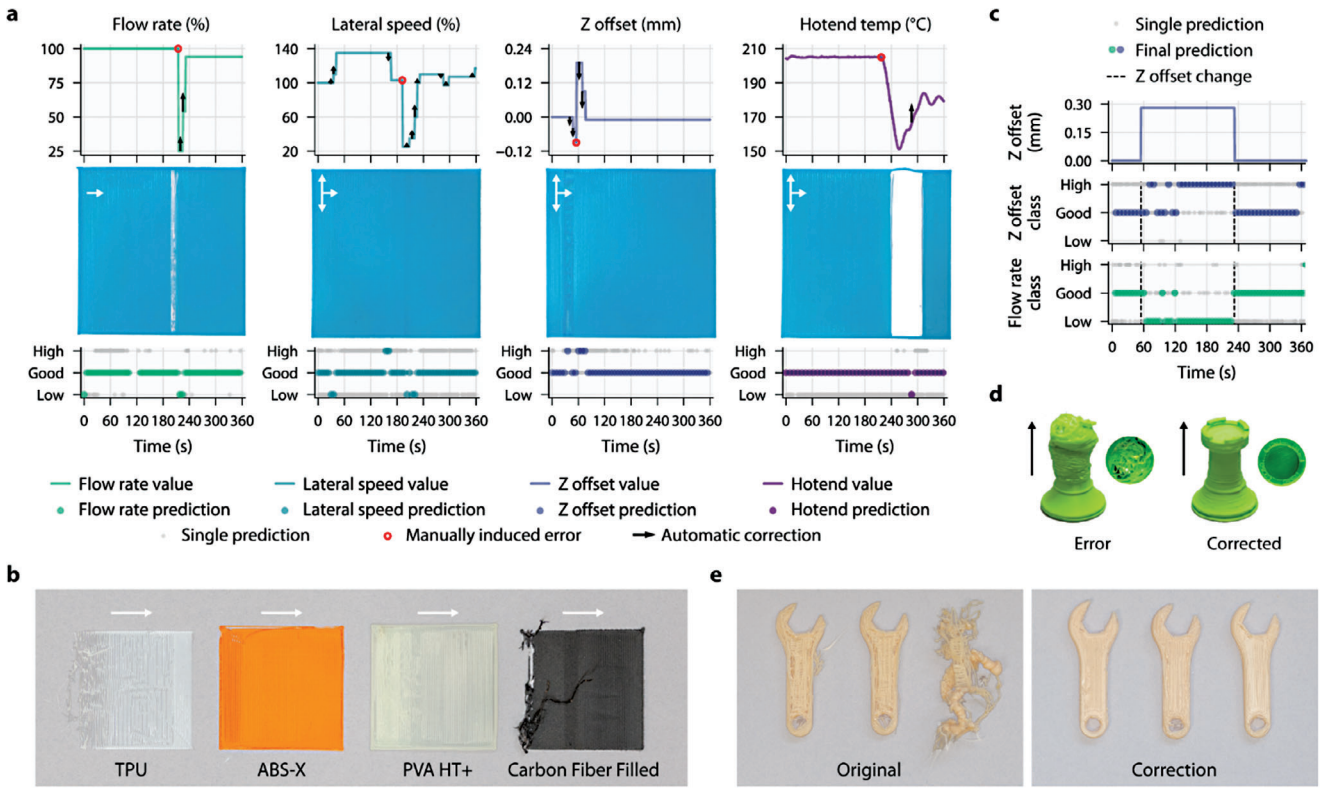

Figure 11. a) The multi-head neural network allows for quick correction of errors caused by manual intervention in a single parameter. It has been trained on a particular printer and PLA feedstock. The correction procedure is used on a hidden 0.4 mm nozzle that was not part of the training set of data. b) The control pipeline shows that multiple incorrect parameters for thermoplastic polymers that were not seen during the training phase can be simultaneously optimized online. This demonstrates the system's adaptability to a variety of feedstocks with various material characteristics, colors, and initial conditions. c) The system uses self-learned relationships between parameters to make corrective predictions, much like human operators do. By decreasing the Z offset value and/or increasing the material flow rate, for example, a high Z offset can be corrected. d) The system successfully fixes numerous wrong printing parameters that were added during a print job. The only difference between the two identical rooks printed under the same circumstances was how the correction process was used. e) Prints started with the wrong parameter combinations are successfully handled by the system. The same conditions were used to print a set of six spanners, demonstrating the system's capacity to correct mistakes and produce the desired results. Reproduced with permission.[31] 2022, Nature Portfolio.

94.5% and lastly under-extrusion has a precision of 97.6% and recall of 92.2%.

These research efforts collectively demonstrate the growing potential of ML and computer vision in automating quality inspection and monitoring in a material extrusion process. By addressing the limitations of manual inspection methods, these advanced solutions offer enhanced accuracy, efficiency, and the potential for real-time applications. Further developments in dataset size, sensor technology, and algorithm optimization hold promise for broader adoption and improved quality control in the field of AM.

3.1.3. Material Jetting

A technique for in-process monitoring of droplet properties during liquid metal jetting AM was developed using an in-process millimeter wave (MW) sensor and ML.[37] The MW sensor provided a real-time monitoring solution that circumvented the computing requirements of high-speed image sensors by producing efficient time series data to anticipate droplet size, velocity, and shape. An MLP-based non-linear autoregressive model was trained to predict droplet size and velocity with a statistical fidelity exceeding 90%, outperforming traditional statistical models. Furthermore, a supervised ML model was trained to classify droplet shapes using spectral frequencies from the MW sensor data, achieving an F1-score of over 95%. This approach presented a practical and computationally efficient solution for quality control in liquid metal jetting AM. It was even suggested that future research should aim to develop and use ML models for the prediction of defect formation and build failures and contribute to improved part quality and higher manufacturing efficiency.

A novel in situ monitoring method employing vision-based techniques was introduced to observe droplet formation in inkjet printing.[38] A drop watcher camera was implemented to capture video sequences of droplet properties which include size, velocity, aspect ratio, and the existence of satellite droplets under various voltage and frequency combinations. The influence of these parameters on distinct droplet modes (namely normal, satellite, and no-droplet) was analyzed through computer vision, and a backpropagation neural network (BPNN) was constructed to categorize the droplet modes based on these properties with a high

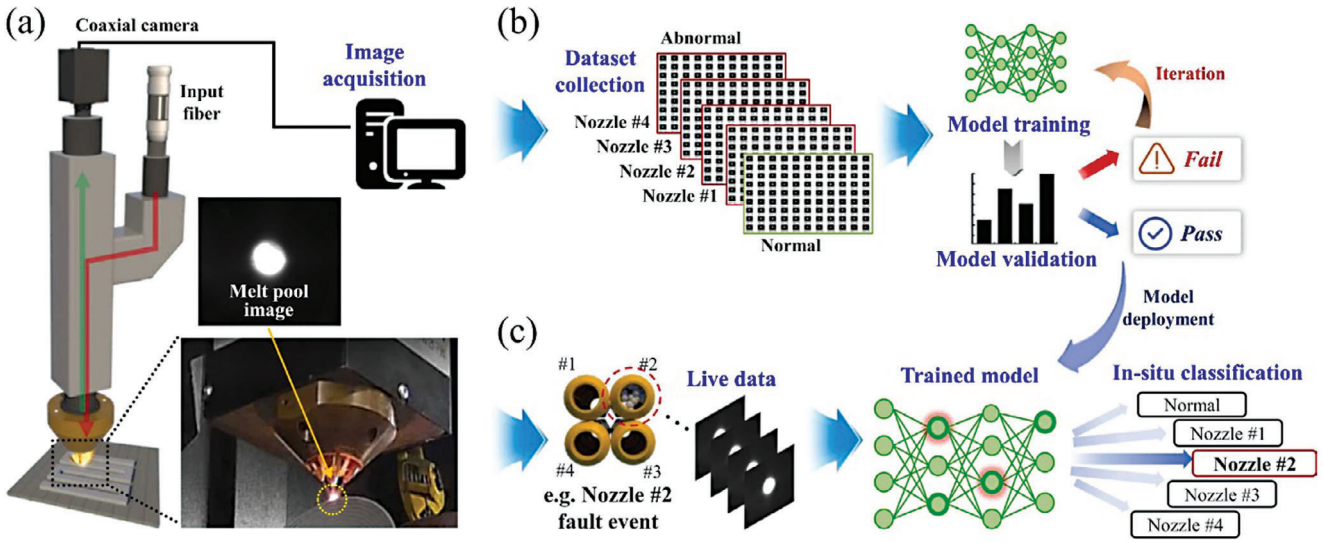

Figure 12. Illustration of the process for detecting irregular powder feeding. a) Deposition head featuring four side nozzles and a central camera for monitoring the melt pool region, b) Training and validation of the model using image datasets representing both regular and irregular conditions, and c) Real-time application of the pre-trained model for immediate inference. Reproduced with permission.[43] 2022, Elsevier.

degree of classification accuracy at 90%. This method offered a sturdy framework for real-time quality inspection during inkjet printing, which can potentially facilitate process enhancement and predictive analysis. The work laid the foundation for the future development of a digital twin model for inkjet printing and other related electronic printing technologies.

Another study proposed the adoption of predictive models and nonlinear autoregressive neural networks with external input (NARX) for quality assurance and process control in AM for electronics. The challenges of using 3D printing in electronics manufacturing were highlighted and modeling techniques such as finite element analysis (FEA) and data-driven ML can be applied for predicting product performance, quality, and reliability.[39] A novel model-based approach for inkjet printing process is demonstrated using state-space models derived from measured process data.[40] This approach helped to anticipate process trends and associated product quality characteristics over large prediction horizons, even in the case of moderately non-linear dynamics of the 3D printing process. Both studies emphasized the importance of proactive, model-based assessment over conventional post-manufacture techniques to mitigate common reliability and quality risks associated with AM. These advancements have significant potential in enhancing the acceptance of 3D printing technology in the electronics industry, while ensuring improved and more robust process performance.

3.1.4. Directed Energy Deposition (DED)

The occurrence of defects is common in the DED process; these defects include balling, lack of fusion, porosity, warping, and waviness. The defects are caused by improper laser parameters, material interactions, and heat accumulation. These issues compromise the structural integrity, surface finish, and dimensional accuracy of the manufactured parts, highlighting the importance of meticulous parameter control and real-time monitoring in DED processes for achieving high-quality components.

An infrared camera coaxial to the laser beam was used to train a deep CNN to identify process stability at four categories: normal laser power, low laser power, low scanning speed, and high scanning speed with accuracies above 80%.[41] Another study analyzed process parameters to predict the melt pool temperatures via extreme gradient boosting ensemble learning and LSTM neural networks.[42] The melt pool temperatures were trained on infrared camera measurements and the coefficient of determination between the prediction and actual measured temperatures was higher than 51% in all cases tested. Another study used coaxial camera images to determine abnormal powder supply in DED due to issues such as restricted powder flow (**Figure 12**).[43] A few ML models were trained and the accuracies were above 55.1%, 69.8%, 70.6%, and 95.9% for K-NN, decision tress (DT), RF, and CNN, respectively. Furthermore, an in situ monitoring system was developed for DED process.[44] The monitoring system consisted of a hyperspectral camera for melt pool width and temperature control, a coaxial camera for melt pool data, and a laser scanning system for material height measurement. Independent tuning of the process parameters was challenging due to the highly interconnected process parameters that significantly influenced the deposited geometry and material properties. Hence, ML-based optimization is helpful in finding the optimal controller output for the in situ process monitoring system.

Beyond process stability, neural network-based ML such as RandLA-Net with in situ sensors were used to detect defects within the DED built parts. Geometrical defects were classified based on a laser line scanner trained on a DL model to classify surfaces into normal, convex, and concave at accuracies of 91.3%.[45] A similar study used data from a laser profiler to first cluster the points via an unsupervised ML model followed by supervised learning to classify the clusters into no defect, bulging,

dents, and wavy surfaces.[46] For the supervised learning, a few ML models were explored, and K-NN achieved the highest accuracy of 93.2%. Another work combined optical emission spectrometer and CCD camera images through Kronecker product of graphs as inputs into an SVM model.[47] The model was trained against X-ray CT data to classify the layers into three categories: low, medium, and high severity. The combination of input from the two sensors via a Kronecker product improved the statistical fidelity score from 35% to 75%. A microphone with a sampling rate of 44.1 kHz was used to gather acoustic emissions from the DED.[48] A deep learning model that consisted of a fully connected regression deep neural network (F-DNN) and a redundant convolutional encoder-decoder network (R-CED) was trained to remove the signal noise from the machine motion, inert gas motion, and powder supply based on the ground truth signal that was equalized, filtered and processed using audio-based algorithms.[48a] The acoustic signal was first denoised by audio-based signal processing algorithms, followed by extraction of time and frequency features to construct a sequence of Mel-Frequency Cepstral Coefficients (MFCC).[48b] These coefficients were used as inputs to train a CNN model and compared against simpler ML models such as RF, SVM, gradient boosting, and K-NN with a subset of the audio signal features used as inputs. The MFCC CNN model produced the highest accuracies above 89% at predicting defect free, cracks, and keyhole pores in the built part (**Table 2**).

3.2. Process Optimization

Process optimization plays a crucial role in maximizing the efficiency and reliability of AM processes. With the complexity and intricacy involved in AM, fine-tuning the printing parameters, and optimizing the process parameters are essential for achieving consistent and desirable results. One of the major challenges in process optimization for 3D metal printing is the intricate interplay of numerous variables, including laser power, scanning speed, layer thickness, and powder characteristics. The optimal combination of these parameters is dependent on the specific metal alloy, part geometry, and desired mechanical properties. This is where ML is important in process optimization for metal printing. ML algorithms can analyze large amounts of data from previous printing runs, identifying patterns and relationships between process parameters and part quality. By learning from these patterns, ML models can predict the optimal process parameters for a given set of conditions, thereby reducing the need for trial and error, and minimizing material waste. In general, ML can be implemented in metal printing to predict printability of a material under specific set of process parameters, to optimize the toolpath to decrease the residual stress, and to predict the thermal gradient for process optimization purposes.

Supervised learning is commonly used for process optimization in AM; it is suitable for process optimization when historical data with well-defined input-output pairs are available, but it may not adapt well to dynamic processes. **Figure 13** provides an overview of ML applications in optimizing processes across diverse AM processes, along with various objectives related to process optimization. The choice of ML approach is often dependent on the specific process optimization problem, the availability of data (labeled or unlabelled), and the level of complexity involved and more discussion will be provided in the subsequent sections.

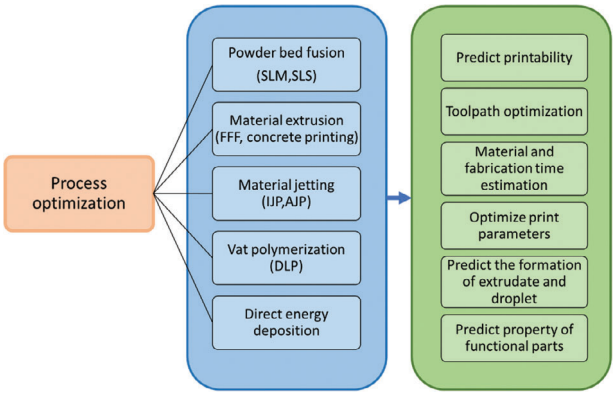

Figure 13. Graphical overview of ML applications in optimizing processes across diverse AM processes, along with various objectives related to process optimization.

3.2.1. Powder Bed Fusion

The quality of LPBF-fabricated parts is heavily influenced by process parameters, but existing methods for determining the parameter window are time-consuming and subjective. A supervised ML method was implemented to optimize the LPBF process in additive manufacturing (**Figure 14**).[53] An ML approach was proposed to detect and track defects and predict material printability in LPBF. It classified printed tracks into five groups based on surface characteristics and developed a data-driven model using BPNN. The model utilized the classification results as target output and four quantitative indicators calculated from surface morphology as input variables. The proposed method significantly improved the efficiency of parameter window search, enabling defect-free printing and excellent part performance. The integration of a 3D microscope for in situ measurement further enhanced its applicability in unmanned factories. Overall, the work highlighted the importance of ML in optimizing the LPBF process, offering an intelligent solution for parameter determination and paving the way for more efficient and automated manufacturing processes.

The primary object of another study was to determine the optimal laser tool path by minimizing the average thermal gradient. The study showcased the capability of accurately predicting optimal laser paths using a DL model, which was trained on 33000 physics-based simulation results that contain "good" labels (low-temperature gradient) and "bad" labels (high-temperature gradient) in a 1:1 ratio, despite limitations in training data and binary information.[54] Notably, the DL simulation, implemented with a CNN, significantly outperformed brute force simulations in terms of speed. This work underscored DL's potential in tool path optimization within AM, highlighting its ability to comprehend tool path patterns and reconstruct comprehensive path performances. Furthermore, the research illustrated the feasibility of applying a physics-based DL approach to other AM techniques, providing lower simulation costs while maintaining accuracy. Thus, a trade-off between computational expenses and accuracy

Table 2. ML for quality control in AM.

Research target	Fabrication process	ML technique	Sample size	Inputs	Outputs	Performance	Refs.
Process stability: anomalies in powder spreading	PBF	Unsupervised: K-means unsupervised clustering followed by labelling based on expert knowledge of the powder spreading defects	2402 image patches	Powder bed images	Powder spreading quality: anomaly-free, recoater hopping, recoater streaking, debris, super-elevation, part failure, or incomplete spreading	Able to classify the powder spreading with precision ranging from 65 to 98.9%.	[9]
Defect prediction: location of voids	PBF	Supervised: Ensemble classification	840 samples of DSLR voxels	Build layer images taken with DSLR camera at eight different lighting conditions	Binary quality of a group of voxels as a flaw or nominal build	Prediction accuracy: 85%	[10]
Layer-wise Surface morphology measurement	PBF	Supervised: CNN	70 000 samples	300 × 300-pixel images	Surface morphology	Average relative prediction error lower than 10%	[11]
Defect prediction through labelling of anomalous in situ data	PBF	Unsupervised: K-means clustering to enlarge the manually labelled training dataset k-nearest neighbours supervised learning to identify anomalies	200	Long exposure IR camera images (OEM EOSTATE Exposure OT)	Labelling of in situ IR camera images as either normal or anomalous	Accuracy close to 100%	[12a]
Defect prediction through average porosity in a local volume	PBF	Supervised: Random forest bagged tree ensemble.	100 000 to 1 000 000	Long exposure IR camera images (OEM EOSTATE Exposure OT)	Average porosity of a local volume	Accuracy greater than 90%	[12b]
Defect prediction of delamination and splatters	PBF	Supervised: Convolutional neural networks	4314 RGB color images converted into 18 short video sequences	Infrared thermographic camera images	Delamination, splatter, or defect-less	Average accuracy of 96.8%.	[13]
Defect prediction of porosities within a volume	PBF	Supervised: 1D CNN model was trained using Bayesian Optimization	Up to 836426 samples	Short wavelength infrared high-speed camera images	Binary outcome of pore and non-pore in local volume	Best prediction accuracy for keyhole porosities above 0.1%	[14]
Defect prediction of balling, under-melting, keyholes, porosity, spatter	PBF	Supervised: Feature extraction using Scale Invariant Feature Transforms followed by Bag-of-Words unsupervised ML then labelling by experts	24 385	High speed visible light camera images	Prediction of melt pool outcome into 5 types of desirables conditions, balling, under-melting, keyholes, porosity, spatter	Accuracy close to 85.1%	[16]

(*Continued*)

Table 2. (Continued)

Research target	Fabrication process	ML technique	Sample size	Inputs	Outputs	Performance	Refs.
Process stability in predicting laser focus	PBF	Supervised: Various ML models ranging from k-nearest neighbours, support vector machines, to convolutional neural network	18 000 data points of 9 classes (162 000 input vectors)	Two IR high speed cameras at 700 and 950 nm wavelengths	Prediction of laser focus 4-class porosity: severe lack of fusion, lack of fusion, optimal, keyhole	False positive rate: 0.1-0.001%; true positive rate:~90%	[17]
Defect prediction in identifying pore locations	PBF	Supervised: Deep neural network	Varies with each configuration up to ≈500 videos	Visible and NIR high speed camera images	Prediction of keyhole defect formation	Prediction accuracies up to 87% were achieved	[18]
Defect prediction of keyhole pore location	PBF	Supervised: Support vector machine	1176 time series segments	Acoustic emissions captured via a microphone fixed 25 – 30 cm on top of the build plate	Prediction of keyhole or keyhole-free formation within a time window	Best accuracy of 97%	[19]
Quality prediction of produced coupon	PBF	Unsupervised and Supervised: K-means clustering Deep learning convolutional neural network	22 263 data points	Acoustic emissions captured by a wideband sensor at the center bottom of a circular build plate	Part quality (minimum defects or cracks only or porosities)	90% prediction rate	[20]
Anomaly detection	PBF	Supervised: 1D-CNN, 2D-CNN, RNN, LSTM, Gated Recurrent Unit (GRU)	1809 samples	Sampling rate: 51.2 kHz 512 acoustic signal data points	Spattering event	Highest classification confidence of models is 85.08%	[21]
Defect detection	PBF	Supervised: : Logistic Regression (LR), Random Forest (RF), and SVM and CNN	3000	ML: 23-time domain features, 18 frequency domain features, and 263 time-frequency domain features. CNN: raw acoustic signal with windows of 5 ms, which is a time-series signal consisting of 5000 data points.	Three processing regimes (lack of fusion pores, conduction mode and keyhole pores)	Classification accuracy of ~93%	[22]
Quality prediction of produced coupon	PBF	Reinforcement learning	180 spectrograms	Optoacoustic fiber Bragg grating	Part quality (poor, medium, high)	Prediction accuracies above 74%	[23]
Defect detection	PBF	Supervised: CNN-LSTM	>15 000	Four sensors were split into four different running windows (w1, w2, w3, and w4), whose time duration is 0.83, 1.65, 2.5, and 3.30 ms, respectively.	Lack of Fusion (LoF), conduction mode, and keyhole across various time scales	95.9% to 100%	[24]
Defect detection	PBF	Supervised: CNN	4004	Layer-wise imagery, multi-spectral emissions, and laser scan vector data	"flaw" and "no flaw"	93.9% and 98.9%	[25]

(*Continued*)

Table 2. (Continued)

Research target	Fabrication process	ML technique	Sample size	Inputs	Outputs	Performance	Refs.
Defect detection	Material extrusion (FFF)	Supervised: MLP, 1D CNN, RNN LSTM, Inception time, XceptionTime, XCM	20 000 value pairs	Temperature, humidity, air pressure, gas particle resistance	Normal, defect	Accuracy: 95%	[26]
Anomaly detection	Material extrusion (FFF)	Supervised: multi-head encoder–decoder temporal convolutional network (MH-ED-TCN)	328 470	Humidity, temperature, acoustic sensor	Normal, anomaly	Accuracy obtained was 97%	[27]
Defect detection	Material extrusion (FFF)	Supervised: CNN-pre-trained ResNet 50	120 000	224 × 224-pixel images	Over-extrusion, good quality, Under-extrusion	98% accuracy	[28]
Defect detection	Material extrusion (FFF)	Supervised: CNN- yolov4	>8000	512 × 512-pixel images	Over-extrusion, good quality, Under-extrusion	89.8%	[29]
Fault diagnosis	Material extrusion (FFF)	Semi-supervised: conditional generative adversarial network (CGAN), and domain adversarial neural network (DANN)	13 025 images (3.5% for normal images, 16% each for other classes)	128 × 128-pixel images	standard (STD), low nozzle flow rate (Low NFR), high nozzle flow rate (High NFR), low filling speed (Low FS), high filling speed (High FS), low liquefier temperature (Low LT), and high liquefier temperature (High LT).	Accuracy for DANN_CGAN is the highest (91.01%)	[30]
Real-time defect detection and rapid correction	Material extrusion (FFF)	Multi-head deep residual attention network with a single backbone and four output heads, one for each parameter	946 283	320 × 320 RGB image	Good, low, high (for flow rate, lateral speed, Z offset, and hot end temperature)	Overall accuracy: 84.3%	[31]
Detect deformations in the printed concrete layers	Material extrusion	Supervised: CNN model Line and edge detections Thresholding line angles	1 M images	RGB image from camera	Cropped concrete layers	F1 scores for detect and non-detect are 82% and 98.05%	[32]
Detect crack on concrete surface	Material extrusion	Supervised: Mobile Net-SSD	20 000+ images	300 × 300-pixel images	cracks	80% mean average precision	[33]
Detect deformations on printed concrete structures	Material extrusion	Unsupervised: Principal component analysis and clustering methods (K-means and spectral cluster)	-	3D point clouds	Circle radius estimation Deformation detection	inaccuracy of 0.3%	[34]

(*Continued*)

Table 2. (Continued)

Research target	Fabrication process	ML technique	Sample size	Inputs	Outputs	Performance	Refs.
In situ monitoring	Material extrusion	Supervised: Image segmentation using U-net neural network	20 000 images	512 × 512-pixel image input	512 × 512-pixel image output	The pixels in the segmentized output have an accuracy of 96.6%,	[35]
Optimization of printing outcome	Material extrusion	Supervised: ad hoc optimized convolutional neural network (CNN) and mathematical model	128	Printing set-up, material type, layer height, infill density	Extrusion multiplier	The results showed an accuracy of 94.3% for overall printing.	[36]
In-process monitoring	Material jetting (Inkjet printing)	Supervised: Multilayer perceptron-based non-linear autoregression (MLP-NARX) model Support vector machine	A total of 345 droplets were used	20 data points before and after each local minimum a	Droplet size, velocity, and morphology	Achieve >95% accuracy for droplet morphology classification	[37]
In situ droplet monitoring	Material jetting (Inkjet printing)	Supervised: Back propagation neural network	N.A.	Droplet size, velocity, aspect ratio, presence of satellites	Normal dispensing, non-dispensing, and satellite modes	Accuracy: 90%	[38]
In-line process control	Material jetting (Inkjet printing)	State-space modeling	N.A.	Nozzle temperature	Film thickness	Accuracy metric of 92.3%	[39]
In-line monitoring	Material jetting (Inkjet printing)	Supervised: nonlinear autoregressive neural network with external input (NARX)	150 past datapoints	Thickness of printed line	Thickness of printed line	-	[40]
Process stability of laser power and scan speed	DED	Supervised: Deep convolutional neural network	211 images	Coaxial infrared camera	Four process conditions: normal, low laser power, low scanning speed, high scanning speed	Prediction accuracies above 80%	[41]
Process stability by prediction of melt pool temperature	DED	Supervised: Extreme gradient boosting ensemble Long short-term memory neural networks	70 112 data points	Laser power, scan speed, layer index, time index, average height, average width	Melt pool temperature	R^2 values above 0.51	[42]
Process stability relating to the condition of the powder nozzles	DED	Supervised: K-nearest neighbours Decision tree Random forest Convolutional neural network	80 000 images	Coaxial camera	Condition of nozzles (i) normal case, (ii) #1 nozzle clogged, (iii) #2 nozzle clogged, (iv) #3 nozzle clogged, and (v) #4 nozzle clogged	Accuracy of 95.9% for CNN model	[43]
Realtime monitoring	DED	Supervised: Artificial Neural Network	-	Laser power (P), powder mass flow (m) and scanning speed (s)	Close-loop feedback	-	[44]

(*Continued*)

Table 2. (Continued)

Research target	Fabrication process	ML technique	Sample size	Inputs	Outputs	Performance	Refs.
Surface geometrical quality classification	DED	Supervised: RandLA-Net	247 samples with ≈10 000 points per sample	Laser line scanner	Surface conditions: normal, convex, concave	Prediction accuracies above 91.3%	[45]
Surface geometrical quality classification	DED	Clustering via unsupervised ML model followed by several supervised learning models: Support Vector Machine, K-Nearest Neighbours, Gaussian Process, Decision Tree, Naive Bayes, Artificial Neural Network, Random Forest, and AdaBoost	73 samples	Laser profiler	Surface conditions: no defect, bulging, dented, and wavy.	Highest accuracy of 93.2%.	[46]
Quality of each layer	DED	Supervised: Support Vector Machine	400 layers	Optical emission spectrometer and CCD camera images	Quality of the layer: low severity, medium severity, high severity	Fidelity score from 35% to 75%	[47]
Defect prediction (defect free, cracks, or keyhole pores) in local area of part	DED	Supervised: Random forest, support vector machine, gradient boosting, and k-nearest, convolutional neural network	1300 signal samples	Acoustic emissions gathered using a microphone	Acoustic signal with removed noise Prediction of defect free, cracks, or keyhole pores within the part	Highest accuracies above 89%.	[48]
Predict surface roughness	PBF	Supervised: The roughness prediction models are developed using linear regression, polynomial regression, support vector regression (SVR), Gaussian process regression (GPR), and artificial neural networks (ANNs)	59	The image texture features such as the contrast from the GLCM method, and the second moment from the NGLDM method	Surface roughness parameters	R^2 value of more than 0.9	[49]
Defect inspection (ST and Inconel)	PBF	Supervised: Neural Learning Based Blind Source Separation (NLBSS) and Spatial-Temporal Sparse Dictionary Learning (STSDL) Algorithm	–	Thermogram sequence	Defect detection	F-score of 0.96 for large detects, 0.57 for small defects	[50]
Detect detection	PBF	Supervised: Image classification via U-net	Nil	1280 × 1024	Prediction classes: Holes, Spattering, Vertical defects, Horizontal defects, and Incandescence.	Accuracy >90% for most tested features.	[51]
Pore size prediction	PBF	Supervised: Dynamic time warping and k-Nearest Neighbor classifiers are used on the time-series data	–	Time-series temperature information	Pore size	Classification accuracies of 92% to 94% are achievable	[52]

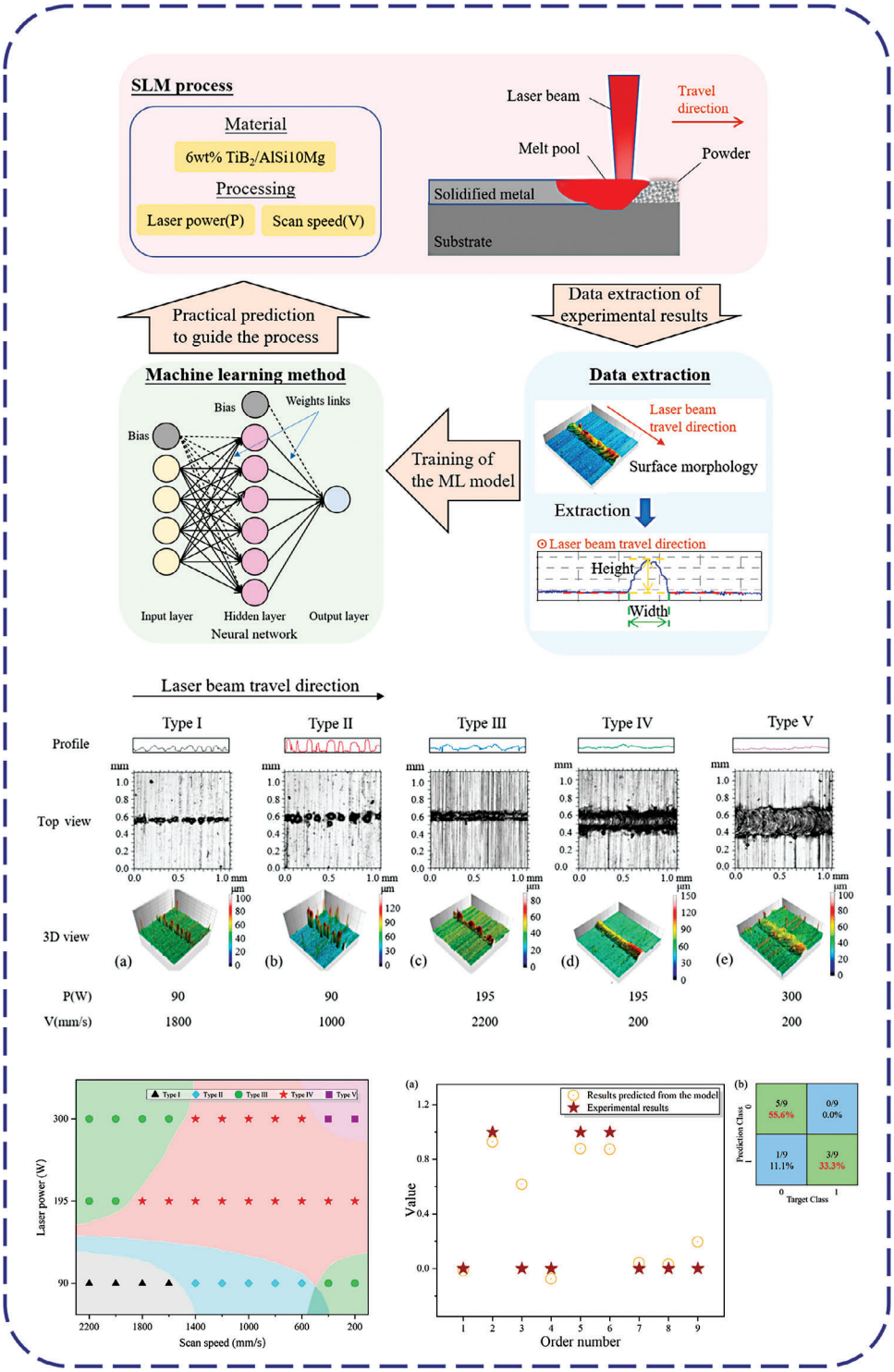

Figure 14. Illustration showing the different types of line morphology created by powder bed fusion using different process parameters and the use of ML to classify and predict the printability of the parts. Reproduced with permission.[53] 2020, MDPI.

was identified, emphasizing the importance of striking an optimal balance for future investigations in this domain. It is crucial to note that, despite the DL's model's substantial speed advantage over traditional brute force simulation methods, this does not imply that the predictions are flawless and devoid of the need for further refinement. The model's success lies in its rapid narrowing identification of a singular perfect solution. The model's predictions serve as a highly informed starting point, and subsequent optimizations can be applied using additional criteria or constraints not fully captured by the training data. This iterative refinement process is essential for tailoring the model's output to the specific nuances. It is important to note that while the DL model significantly outperforms traditional brute force simulation methods in processing speed, this does not imply that the predictions are flawless and devoid of the need for further refinement. The model's success lies in its rapid narrowing down of potential tool paths to a subset likely to include the optimal path, rather than guaranteeing the identification of a singular, perfect solution. The model's predictions serve as a highly informed starting point, and subsequent optimizations can be applied using additional criteria or constraints not fully captured by the training data. This iterative refinement process is essential for tailoring the model's output to the specific nuances of any given LPBF task. Additionally, the well-known challenge of ML models not precisely adhering to hard constraints is addressed. In the context of LPBF tool path optimization, this limitation necessitates the integration of supplementary optimization algorithms or constraint-satisfaction techniques post-prediction. These steps ensure that the final tool paths not only approximate the model's predictions but also align with the physical and operational constraints of the LPBF process.

3.2.2. Material Extrusion

Multiple process parameters such as the nozzle and bed temperatures, raster angle, layer thickness, nozzle size, and print speed are known to affect the quality of the printed parts during material extrusion. The high dimensionality of the dataset warrants the use of ML techniques to identify the most optimum process parameters.

A data-driven ML platform using MLP and CNN models was developed to predict optimized parameters for the FFF process.[55] Spatial features were first extracted using CNN and were then transferred to the MLP model together with other process parameters such as extrusion width, layer height, print speed, infill, area, and volume. The approach enabled quick and accurate predictions of decisive parameters such as time, weight, and length, even with fuzzy input information. It did not require consideration of the shape, size, and material of the printed object and can perform the process automatically. The proposed ML approach has several advantages, including better stability and clearer rules compared to previous research, fast estimation of printer parameters in approximately one second, and applicability to various types of 3D printing materials and domains like construction, medical, and architecture. In a different study, a data-driven predictive model for the FDM process was created using a variety of ML algorithms.[56] The model predicted dimensional deviations between the printed model and the original one by fusing temperature and vibration data from various sensors with process parameters. In terms of parts dimensional accuracy prediction, the residual attention neural network model performed better than other ML models such as 1D CNN and LSTM networks. However, more advancements are required to consider environmental factors from the outside, develop an online feedback system for real-time prediction, and create a comprehensive digital twin system for AM.

Bayesian optimization was used in a recent work to accelerate the printability optimization for extrusion-based bioprinting.[57] The input variables for bioink compositions consist of 3-gelatin methacryloyl (GelMA) concentrations and 3 GelMA/hyaluronic acid methacrylate, whereas the input variables for printer parameters include bioink reservoir temperature, extrusion pressure, print-head speed, and platform temperature. A scoring system was then implemented to assess the filament morphology during extrusion and pore architecture on layer stacking. The study has shown that the Bayesian optimization algorithm can be used to analyze the optimal printer parameters and accelerate the extrusion bioprinting experimentation process in comparison to the traditional trial and error approach.[57] Another work utilized Uniform Design (UD) technique to select 12 experiment data points based on three parameters four-level data space $U_{12}(P_3^4)$[58] and SVM algorithm to generate a process map that identified optimal printing parameters to fabricate high-quality printed parts using Pluronic F127 bioink with a high probability of > 75%.[59] It provided a simple tool to improve the printability of extrusion-based bioprinting process based on width index with minimum dataset using inputs such as printing temperature, material composition, and path height.

An interesting study used optimized ML models to predict material printability for FDM-printed pharmaceutical products.[60] A total of 318 materials and 1594 formulations obtained from online literature and in-house formulations were used as dataset for this study; three different ML techniques (ANN, SVM, and RF) were used and a 75:25 split was used for training and testing. RF emerged as the best ML model for predicting all targeted variables (filament mechanical characteristics, extrusion temperature, printing temperature, and printability) with the highest accuracy. Another work compared the optimization of 3D printing properties for assistive devices using traditional ANN and deep neural networks (DNN).[61] The DNN outperformed the traditional ANN approach, offering improved calculation speed, higher print quality, and decreased errors. It highlighted the effectiveness of DL-based optimization in 3D printing processes.

Another study proposed the use of both open-loop and closed-loop ML models to monitor the effects of processing parameters on the quality of 3D-printed parts.[62] The open-loop approach utilized multiple ML classification algorithms such as deep neural network (DNN), support vector machine (SVM), decision tree (DT), random forest (RF), and logistic regression (LR) to determine the relationship between processing parameters and printed lines' quality (large space, little space, good connection, little material flow, large material flow). A closed-loop system is constructed based on this relationship using a fuzzy inference system that generates optimized processing parameters. The ML-based closed-loop system improved the quality of printed parts and enabled a self-adjusting 3D printing process by effectively monitoring and optimizing processing parameters. More

research could be conducted to include additional processing parameters and conducting real-time closed-loop 3D printing experiments.

In larger-scale construction printing, printing parameters such as pumping, extrusion, and printing speeds, nozzle diameter, and standoff height have a direct impact on the printing process and the final mechanical properties of the concrete structures. It is a daunting task to identify the optimal printing process due to the large number of variables involved. One approach to address this challenge is through nozzle shape optimization. A predictive modeling approach using ANN was proposed to directly control the geometry of concrete printing extrudate by optimizing nozzle shapes.[63] Thirteen different nozzle shapes were predetermined and used in the experiments, with their corresponding extrudate geometries analyzed using MATLAB. The ANN model was then developed to correlate nozzle and extrudate shapes, and a nozzle-extrudate database was formed for analyzing the optimal nozzle shape for specific target extrudate shapes. The results showed a noticeable improvement in surface finish quality without additional post-finishing effort, offering flexibility for various printing structures with different outer-surface shapes. The proposed approach has the potential to improve surface finish quality in concrete printing, as it directly controls extrudate geometry without the need to reduce nozzle size.

Researchers are making significant advancements in process optimization for 3D printing by exploring nozzle shape optimization, predictive modelling for mechanical properties, and AI-based control systems. These approaches offer potential for enhanced surface finish quality, improved mechanical properties, and better control over the printing process, paving the way for further innovation and application of 3D printing in various industries.

3.2.3. Material Jetting

There are many variants of jetting-based printing techniques which include inkjet printing, aerosol jet printing, electrohydrodynamic jet printing, acoustic printing, laser-induced forward transfer printing, etc., that facilitate drop-on-demand high-resolution printing. Each of these printing techniques are designed differently and they have their unique sets of process parameters that can be controlled to adjust the print quality. Typically, these print parameters are adjusted such that a printed pattern with well-defined edges is obtained. However, most printing processes have multiple process parameters that make it difficult to identify the most optimum print settings for the best print condition. Thus, many on-going research works are looking at applying ML to simplify process optimization.

A multi-objective optimization design method for drop-on-demand printing parameters through fully connected neural networks (FCNNs) was proposed; a hybrid multi-subgradient descent bundle with an adaptive learning rate algorithm was used for multi-objective optimization due to its rigorous convergence theorems; it can be used to optimize printing of droplets with smaller diameter, faster droplet speed with absence of satellite droplets using inputs such as applied voltage, viscosity, surface tension and nozzle diameter.[64] Another study used ensemble learning approach and its base learners (RF, least absolute shrinkage and selection operator (LASSO), extreme gradient boosting, and SVR) to predict the droplet velocity and volume using inputs such as polymer concentration, excitation voltage, dwell time, and rise time in inkjet-based bioprinting process; the experimental results showed extreme gradient boosting has highest predictive accuracy (R^2 = 0.977, RE = 0.044, and RMSE = 0.240) in accordance with the studied operating conditions.[65]

Another study utilized ML models to optimize the electrohydrodynamic jet printing of graphene-based biosensors.[66] Supervised ML models, trained on key printing parameters such as nozzle speed, ink flow rate, and voltage, could predict the conductivity of printed circuits in real time. The RF and K-NN (k = 10) models delivered the highest prediction accuracy of about 83%. The integration of ML aimed to streamline the manufacturing process, ensure resource efficiency, and produce devices with controlled electrical properties. Overall, the study emphasized the significant potential of ML in enhancing the manufacturing processes in the electronics industry.

ML models were used to predict ink-jetting behavior in the inkjet printing process based on 11 distinct ink and printer parameters.[67] Notably, small ensembles of DT such as boosted DTs and RF demonstrated superior predictive power for drop velocity and radius, with an RMSE of 0.39 ms^{-1} and 2.21 µm, respectively. Furthermore, a neural network model was constructed to categorize drop behavior into three categories: stable "single drop", "multiple drops", or "no ejection" and achieved an accuracy of 91.94%. The models were validated using an untried graphene oxide ink, which was not included in the training dataset. This innovative ML approach could accurately predict ink jetting behavior and eliminate the need for costly, time-consuming, and material-intensive jetting experiments. Overall, the research demonstrated that ML can significantly enhance the efficiency of inkjet printing, highlighting its potential for accelerating the development of new functional ink materials for printed electronics.

An innovative combination of a microfluidics-driven multiscale 3D printer with ML was implemented to enhance the precision of the freeform generation of active electronics.[68] A new printing and ML workflow was developed to modulate ink composition in real time and classify complex internal features. This was achieved by using an SVM-guided classification model for automated, in situ pattern classification. The ML model showed a balanced accuracy of 81.96% in classifying the internal textures of the evaporative-driven printed droplets. The developed ML-integrated printing system facilitated autonomous optimization of printing parameters and robust adaptation to unanticipated disturbances. This represented a significant step towards automated process parameter control for the 3D printing of electronics.

Another study applied RSM to investigate the interplay between aerosol jet printing parameters and the intense pulsed light (IPL) sintering process for silver nanoparticle film in printed electronics applications.[69] The correlation between print passes and sintering distance on surface morphology and sheet resistance was investigated to elucidate the

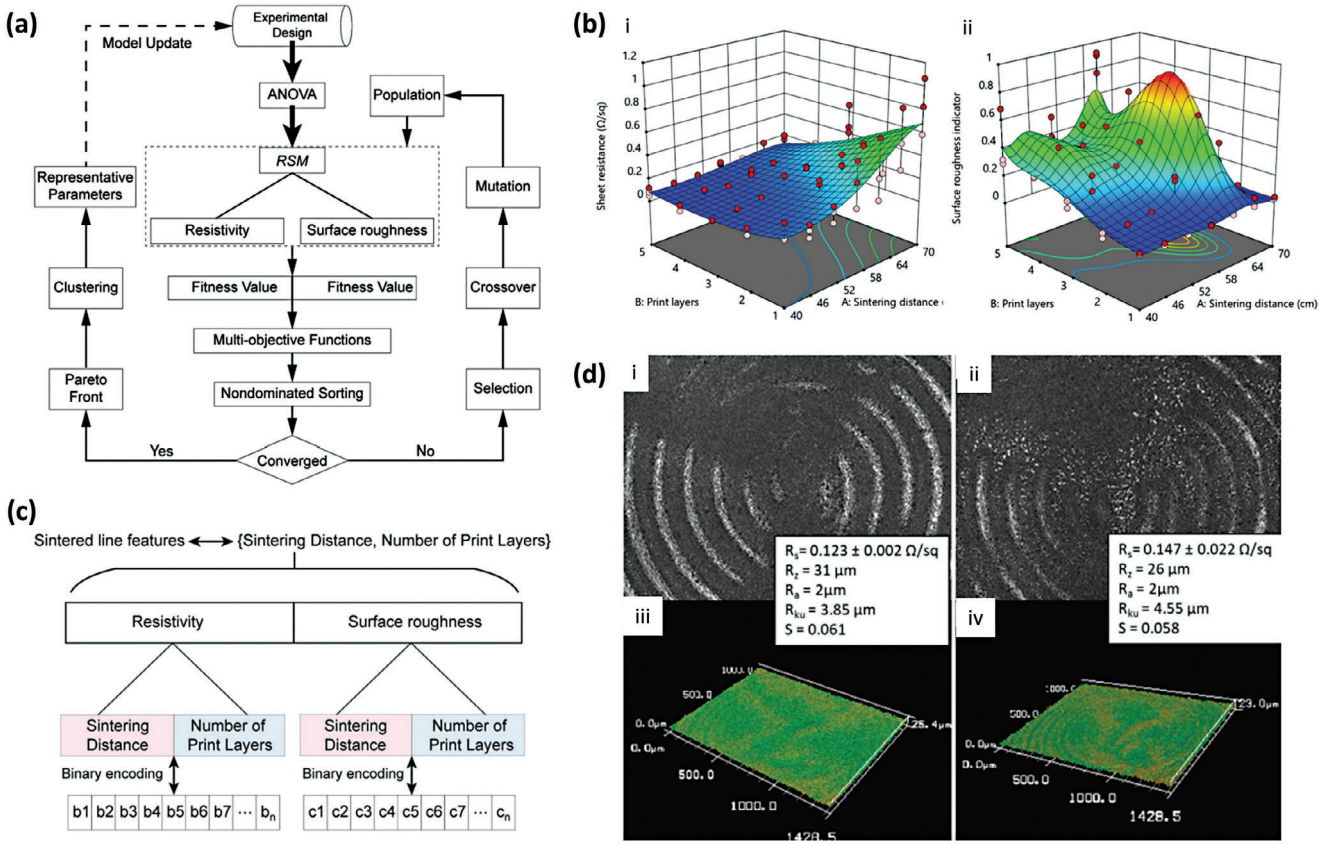

Figure 15. Schematic showing the workflow for a multi-objective optimization using RSM for optimizing the electrical conductivity and surface roughness in the IPL sintering process. Reproduced with permission.[69] 2022, AccScience Publishing.

complex relationships among the different parameters (**Figure 15**). A hybrid multi-objective optimization approach, including a modified central composite design (CCD) and non-dominated sorting genetic algorithm (GA), was applied to systematically manage these conflicting responses. The use of ML allowed for the identification of optimal windows for the IPL sintering process, resulting in films with low sheet resistance and low surface roughness. Compared to conventional trial-and-error methods, this optimization approach was found to be more efficient and systematic. This work lays a foundation for future optimization of IPL sintering parameters for various nanoparticle-based films and multi-layered electronics fabrication.

Various ML methods such as RSM, GA, and transfer learning were used to optimize the process parameters of the aerosol jet printing process and understand the complexity between their interactions.[70] The results showed that the Gaussian process regression performed better than the other ML models such as K-mean clustering and SVM in terms of prediction of the classification of printed features such as the line width, edge roughness, and film thickness. It is possible to use a very small dataset for the same prediction using transfer learning techniques such as feature representation, instance transfer, and model-based transfer. The feature representation technique outperformed the other methods as it resulted in smaller error in the prediction. Overall, the ML works for aerosol jet printing present a framework that can be effectively transferred and applied in other printing techniques.

3.2.4. Directed Energy Deposition (DED)

Besides toolpath optimization for LPBF processes, ML is often applied in other metal printing such as DED and gas-metal arc welding-AM to predict the spatial and temporal thermal fields to inform the designers of the producibility and the potential risk for cracks of the parts.[71] A study utilized a novel approach for discretizing the deposition process of gas-metal arc welding-AM process to enhance the adaptability and flexibility of numerical simulation in analyzing thermal aspects of the material deposition process (**Figure 16**).[71a] A unique data structure was used to obtain deposition state data from numerical simulation results. The data was then utilized to train a recurrent neural network and deep neural network (RNN-DNN), and one convolutional neural network (CNN) specifically designed for identifying correlations between deposition stages and their corresponding thermal fields. The validation results demonstrated that the developed method achieved a prediction accuracy exceeding 94% compared to numerical simulation results. Interestingly, the time required for a single prediction process was reduced to the millisecond level. Another study also RNN-DNN for thermal analysis in laser-aided AM (LAAM).[71b] A thermal field prediction numerical

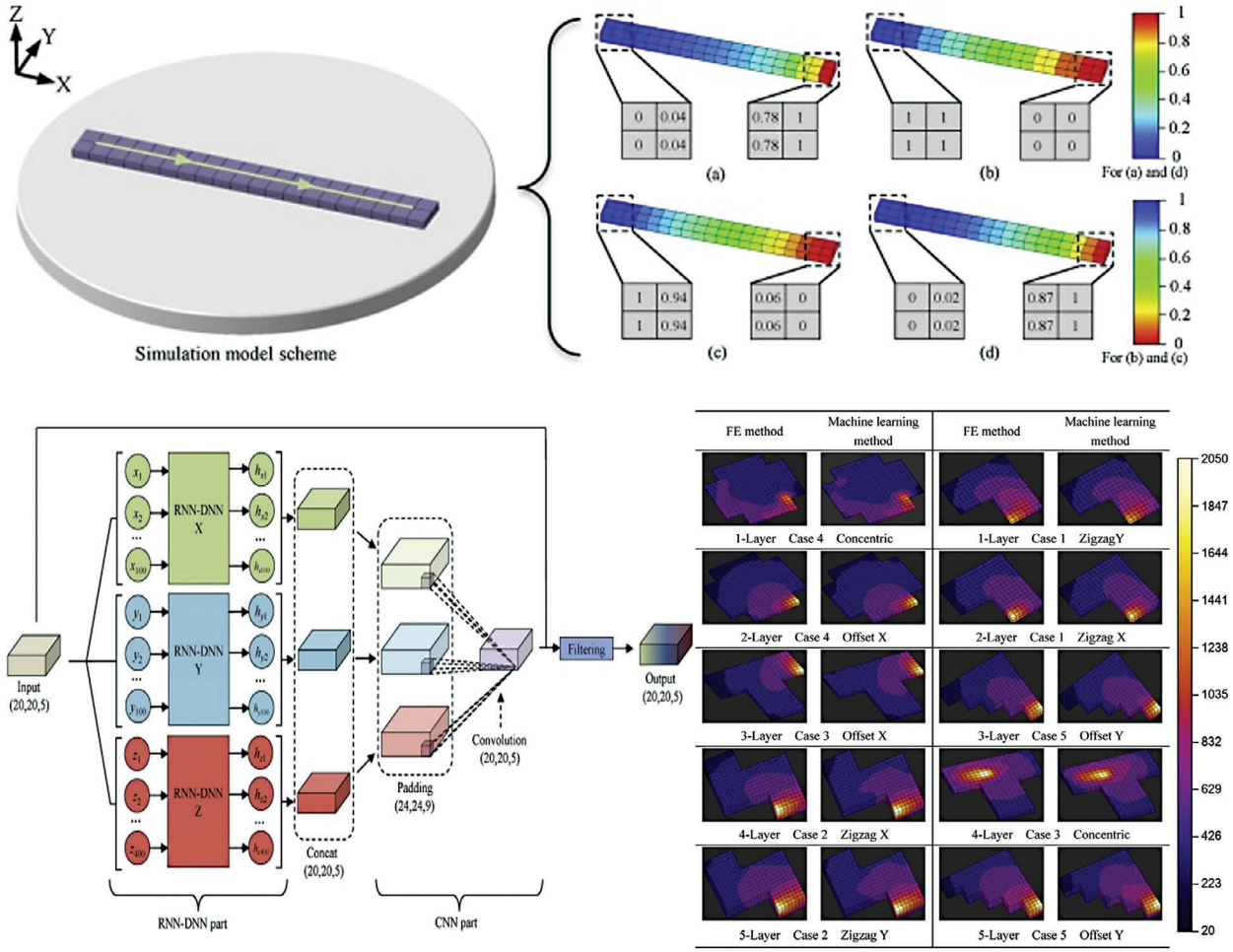

Figure 16. Illustration showing the use of RNN-DNN and CNN model to predict the temperature field of the 3D printing process. Reproduced with permission.[71a] 2021, Elsevier.

model was used to generate a comprehensive training dataset, the developed RNN-DNN model successfully correlated laser scanning patterns with their corresponding thermal history distributions. The high prediction accuracy of over 95% compared to finite element models highlighted the significance of ML in improving efficiency and decision-making in LAAM processes.

This advancement enables rapid evaluation of different scanning patterns within minutes, leading to potential cost savings and enhanced manufacturing outcomes. Furthermore, the integration of ML techniques paves the way for future research on multi-layered 3D deposition processes, expanding the understanding of complex geometries and optimizing deposition strategies for desired material properties. Overall, these studies underscore the importance of ML in revolutionizing thermal analysis in metal printing and accelerating its adoption in diverse industries.

3.2.5. Vat Photopolymerization

A recent work has demonstrated the use of NN to learn printing parameters for DLP process from a 3D-printed simulator to offset the cell-induced light scattering effect.[72] Single-layer trial prints were obtained from different sample masks and used to train the algorithm; a print simulator was used to generate a huge amount of new training data, which greatly reduced the required training samples by more than tenfold. The printed samples and the generated samples were then used to train the neural network which calculates the appropriate masks that compensate the cell scattering effect. The NN approach in the study is composed of two U-Net-like NNs—slave NN and master NN. The network architecture of the master NN is composed of 14 convolution or deconvolution layers with batch normalization, ReLU, and Tanh activation function, as well as U-net style skip connections. The slave NN learned the transformation of the physical 3D printer and provided gradient information to support the training of the master NN, while the master NN learned the inverse transformation of the 3D printer. This allowed the master NN to suggest a deformed mask for any given target structure and print it out under highly scattering condition. Furthermore, the algorithm enabled the use of a small sample size (as small as 32) for training data to generate grayscale masks that can print fine-detailed structures surpassing the traditional manual tuning method with identical masks.

Continuous liquid interface production (CLIP) is an advanced vat photopolymerization technique that uses an oxygen-permeable "dead zone" between the fabricated part and transparent window to continually cure the resin. There is an optimal range of printing speeds to achieve successful print for each defined geometry; a combination of physical modeling and ML approaches was used in a recent work to identify the optimum speed and appropriate speed range for continuous printing.[73] A synthetic dataset was first generated in the absence of an available experimental dataset to identify the significant factors using the design of experiments (DOE) for successful prints. The predicted results for the successful prints were then screened and collected as new experimental dataset that were subsequently used for training. Various ML algorithms such as conventional techniques (DT, naive Bayes, K-NN, and SVM), ensemble approaches (RF, gradient boost, and Ada boost), and DNN (Siamese networks) were evaluated and compared; Siamese Networks demonstrated superior performance (average training accuracy of 90.17% and testing accuracy of 88.42%) as critical information was extracted from the mathematical models-generated synthetic dataset (**Table 3**).

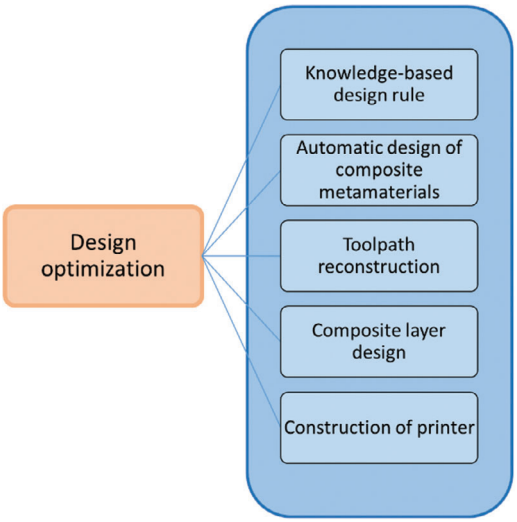

Figure 17. Graphical overview illustrating the utilization of ML for optimizing designs in the context of AM-related applications.

3.3. Design Optimization

The rapid evolution of 3D printing technologies has paved the way for innovative approaches in the design and fabrication of materials and structures. Amidst the plethora of techniques that have emerged to enhance the additive manufacturing process, the integration of ML stands out as a game-changer. Particularly in the realm of design and topology optimization, ML offers capabilities that have the potential to redefine the paradigms of 3D printing. Design and topology optimization traditionally involve intricate processes, where the objective is to derive the best material distribution within a given space, considering specific boundary conditions and loads. The challenge here is the vast solution space, which becomes computationally intensive and time-consuming to navigate. This is where ML comes into play. With its ability to analyze massive datasets, recognize patterns, and make predictions, ML can provide insights and solutions at a pace and precision that are often beyond traditional computational methods. Moreover, the iterative nature of design optimization aligns seamlessly with ML models. These models can be trained on a myriad of design variations, learning from each iteration, and subsequently suggesting optimal design strategies that not only meet but often surpass human-driven solutions. Furthermore, the incorporation of ML allows for real-time feedback during the design phase, which can be instrumental in making swift, informed decisions. In the context of AM, the choice of ML approach is dependent on the stage of design process. Supervised learning might be useful for the prediction of material properties at the early design stage, while reinforcement learning could be employed for fine-tuning and optimizing the design of 3D-printed parts. Most of the design optimization problems are multi-objective with conflicting design goals. Hence, a combination of approaches, like multi-objective optimization algorithms might be applied to determine the optimal solutions. **Figure 17** provides a summary of the application of ML for design optimization for various AM-related applications and more discussion on the use of different ML techniques for design optimization in AM will be provided in the subsequent sections.

A novel approach for constructing AM design rules was introduced using ML and knowledge graphs (**Figure 18**).[75] The framework extracted knowledge on predictive manufacturability from data, stored both existing and newfound AM knowledge in an ontology-based knowledge graph and applied reasoning to derive data-driven prescriptive AM design rules. The methodology enhanced the automated and autonomous construction and improvement of AM design rules, supporting AI-related decision-making in additive manufacturability analysis and (re-)design for AM. By providing shareable AM design rule knowledge with the AM community, this work promotes collaboration and facilitates advancements in the field.

An optimization framework that utilized variational autoencoder (VAEs) was proposed to design composite mechanical metamaterials (**Figure 19**).[76] The focus was on controlling macroscopic elastic moduli and designing optimal representative volume element. The approach employed a variational autoencoder to learn a reduced representation of representative volume element configurations, enabling Bayesian optimization for multi-material design problems. Bayesian optimization can be used to construct a probabilistic surrogate model for the objective function and query the next data point. This ML-based framework eliminated the need for subjective trial-and-error design decisions. Experimental validation using multi-material 3D-printed samples demonstrated good agreement between the optimized values by the ML model and the experimental counterparts.

A method utilizing StyleGAN was employed to design architected materials inspired by nature, specifically focusing on the generative formulation of original unit cell designs inspired by leaf microstructures.[77] By employing unsupervised learning, this approach facilitates the exploration of a latent space for pioneering material design, overcoming the limitations associated with labelled data. This methodology proves particularly pertinent to 3D printing workflows, where it can guide the development of materials and structures by translating natural language

Table 3. ML for process optimization in AM.

Research target	Fabrication process	ML technique	Sample size	Inputs	Outputs	Major findings	Refs.
Predict printability (% nano-TiB2 reinforced AlSi10Mg composite)	PBF (SLM)	**Supervised**: Backpropagation-based neural network model	2048	9 parameter combinations of laser power and scan speed	2 prediction classes (Good and bad printability)	A predictive approach for selective laser melting was developed, which makes use of a ML algorithm capable of recognizing faulty tracks and intelligently anticipating printable parameters	[53]
Toolpath optimization	PBF (SLS)	**Supervised**: Linear regression model and CNN	33 000	Laser toolpath	Good or bad classification based on median temperature gradient	It was noted that the linear model was not capable of accurately discerning the true optimal laser path pattern. Furthermore, when employing a Convolutional Neural Network (CNN), the Deep Learning simulation proved to be significantly faster compared to a brute force simulation.	[54]
Print information estimation	Material extrusion (FFF)	**Supervised**: MLP and CNN	24640	Extrusion width, layer height, print speed, infill percentage, volume area	Time, length, and weight	The proposed model does not need to consider the shape of the object but can perform the process automatically without external factors	[55]
Predict dimensional deviations	Material extrusion (FFF)	**Supervised**: random forest (RF), extreme gradient boosting (XGB), linear regression (LR), gradient boost (GB), light gradient boosting machine (LGBM), decision tree (DT), Ridge, Lasso, AdaBoost, and three deep learning algorithm models: 1DCNN, convolutional neural & long short-term memory network (CNN-LSTM)	N.A.	Temperature and vibration data from multiple sensors (thermocouples, infrared thermometers, and accelerometers)	Dimensional deviations	Deep learning algorithms often outperform traditional machine learning techniques, even with limited datasets. (R^2:0.9113) When tested on a dataset consisting only of process parameters and extruder vibrations, the Residual Attention model demonstrated strong resilience and was efficient in predicting the SDM of the printed components. The Residual Attention model shows improved generalization when exposed to varied data, and it can accurately forecast the three-layer SDM of components manufactured using the FDM process parameters and real-time sensing information. Unlike deep learning techniques such as 1DCNN, the attention feature in the Residual Attention model adjusts effectively to the dynamic interplays present in the AM procedure.	[56]

(*Continued*)

Table 3. (Continued)

Research target	Fabrication process	ML technique	Sample size	Inputs	Outputs	Major findings	Refs.
Printability optimization	Material extrusion	**Supervised**: Bayesian optimization framework	N.A.	Ink composition, reservoir temperature, extrusion pressure, print-head speed and platform temperature	Score system for filament morphology	It can be used to analyze the optimal printer parameters and accelerate the extrusion bioprinting experimentation process in comparison to the traditional trial and error approach	[57]
Optimization of printing outcome	Material extrusion	**Supervised**: Support Vector Machine (SVM)	12	Printing temperature, material composition, path height	Width index	Another work utilized Uniform Design (UD) technique to select 12 experiment data points based on three parameters four level data space $U_{12}(P_3^4)$[58] and Support Vector Machine algorithm to generate a process map that identified optimal printing parameters to fabricate high quality printed parts using Pluronic F127 bioink with high probability of > 75%	[59]
Printability optimization	Material extrusion (Hot melt extrusion)	**Supervised**: Artificial neural networks, support vector machines and random forests	1594 samples	Material type, glass transition temperature, melting temperature, molecular weight	Filament mechanical characteristics, extrusion temperature, printing temperature and printability	Random forest emerged as the best ML model for predicting all targeted variables (filament mechanical characteristics, extrusion temperature, printing temperature and printability) with the highest accuracy.	[60]
Optimization of print parameters	Material extrusion (FFF)	**Supervised**: ANN, DNN		Maximum tensile force, Type of part, Dimensions of part	Material, layer height, thicknesses (Top, Bottom Shell), fill density, print speed Temperatures (bed, 1st and 2nd nozzles)	Compared with the results from the traditional ANN approach, optimization based on DL decreased the calculating speed by up to 1.5 times with the same print quality, increased quality (both learning: 0.9577 and testing: 0.9721), decreased MSE (0.001), and a set of printing parameters not previously determined by trial and error was also identified.	[61]
In situ Process parameter closed-loop feedback control	Material extrusion (FFF)	Multi-Input-Multi-Output (MIMO) Fuzzy logic-based control algorithm	400 labeled data	Error and change in error of print states	Filament extrusion speed, Layer height, Line Distance, Print speed	Five supervised ML algorithms – deep neural network (DNN), support vector machine (SVM), decision tree (DT), random forest (RF), and logistic regression (LR) – are used for classification. The resulting models are used to decide the status of printed line connection given layer height, print speed, line distance and filament extrusion speed	[62]

(*Continued*)

Table 3. (Continued)

Research target	Fabrication process	ML technique	Sample size	Inputs	Outputs	Major findings	Refs.
Predicting cross section of extrudate (concrete)	Material extrusion	**Supervised**: ANN	101 extrudate cross-sectional samples were generated	Shape of the nozzle outlet and flow rate	Shape of the extrudate cross-section	The ML-based proposed approach improves the surface quality of three structures with varying curvatures by adjusting the nozzle geometry to match the desired extrudate shape for each structure.	[63]
Optimizing Droplet Formation	Material jetting (Inkjet printing)	**Supervised**: Fully connected NNs (FCNNs)	N.A.	Applied voltage, viscosity, surface tension and nozzle diameter	Droplet diameter, droplet speed, satellite droplets	It can be used to optimize droplet printing and propose an optimal range of bio-ink properties for best printing outcome based on nozzle diameter.	[64]
Droplet Prediction	Material jetting (Inkjet printing)	**Supervised**: Ensemble (random forest, LASSO, extreme gradient boosting, support vector regression)	243 data points	Polymer concentration, excitation voltage, dwell time, rise time	Droplet velocity, droplet volume	The experimental results showed extreme gradient boosting has highest predictive accuracy ($R^2 = 0.977$, RE = 0.044 and RMSE = 0.240) in accordance with the studied operating conditions	[65]
Prediction of electrical conductivity	Material jetting (Electrohydrodynamic-jet)	**Supervised**: Random forest, Logistic regression, K-NN	A set of 240 samples	Nozzle speed, voltage between the print head and the substrate, and the flow rate	Conductivity of electrodes	Random forest and K-NN (k = 10) models resulted in the highest accuracy (about 83%) in estimating the conductivity of graphene electrodes	[66]
Prediction of jetting window	Material jetting (Inkjet printing)	**Supervised**: 14 regressive models (linear regression, Bayes ridge, RANSAC, Decision tree, gradient boosting etc.) and deep neural network	3000 data points	11 features (frequency, rise time, fall time, dwell time, echo time, voltage, echo voltage, viscosity, surface tension, density, nozzle diameter)	Droplet jetting velocity, droplet radius, jettability prediction, jetting window prediction	Ensembles of DTs (GB and RF) were applied to predict the drop velocity and radius of 14 materials. The observed RMSE was 0.39 m s^{-1} and 2.12 µm respectively. The mean absolute percentage error is 3.87%. A neural network model was built to classify jetting category with 91.94% accuracy.	[67]
Tuning of colloidal ink composition and optimization of printing parameters	Material jetting (Microfluidic mixer-based printing)	**Supervised**: Support vector machine, random forest	N.A.	Feature maps	Deposition patterns	SVM model has achieved a balanced accuracy of 81.96% in classifying the internal textures of the evaporation-driven printed droplets.	[68]
Multi-objective optimization	Material jetting (Aerosol jet printing)	**Supervised**: Response surface method (RSM), genetic algorithm	105 samples	Sintering distance, print layers	Electrical resistivity, surface roughness	Response Surface Models (RSMs) were developed, and their associated statistical uncertainties were integrated with the NSGA-III algorithm to effectively optimize the printing quality in a two-dimensional (2D) space.	[69]

(*Continued*)

Table 3. (Continued)

Research target	Fabrication process	ML technique	Sample size	Inputs	Outputs	Major findings	Refs.
	Material jetting (Aerosol jet printing)	**Supervised**: Response surface method (RSM), genetic algorithm	100 data points	Sheath gas flow rate, carrier gas flow rate, print speed	Edge roughness, film thickness	The RSMs were employed to determine the optimal operating window in the 2D space, considering the trade-off between printed line features and print speed using the desirability function approach. The derived RSMs and corresponding statistical uncertainties were jointly utilized with the NSGA-III algorithm to systematically optimize the overall printing quality in a three-dimensional (3D) design space.	[70a]
	Material jetting (Aerosol jet printing)	**Supervised**: Noisy (input Gaussian process (NIGP))	25 samples	Sheath gas flow rate, carrier gas flow rate, print speed	Line width, edge roughness, thickness	Developed multi-objective optimization framework to optimize the overall printed line quality for customized line width printing using small data set and prediction uncertainty. Latin hyper sampling was combined with a noisy input Gaussian process (NIGP) approach for rapid modeling of the printing process	[70b]
Prediction of features using transfer learning	Material jetting (Aerosol jet printing)	**Supervised**: Transfer learning (instance transfer, feature representation), model-based transfer	90 data points	Sheath gas flow rate, carrier gas flow rate, print speed	Line width, edge roughness, thickness	It was found that Feature representation transfer generally produce much lower errors in the prediction of line width, line thickness and edge roughness. The errors are found to be 5% or smaller.	[70c]
Print quality optimization	Material jetting (Aerosol jet printing)	**Unsupervised and Supervised**: K-means clustering, SVM, GPR, genetic algorithm	N.A.	Sheath gas flow rate, carrier gas flow rate	Edge roughness, thickness, overspray	A ML method was introduced to optimize the quality of Additive Jet Printing (AJP) by investigating the connection between the morphology of deposited droplets and the characteristics of printed lines. The approach employed Gaussian process regression to establish a process model for the geometrical properties of droplets. The deposited droplet morphology was optimized while considering the dual conflicting objectives of customizing the droplet diameter and maximizing droplet thickness. By leveraging this ML-based approach, the AJP process could be fine-tuned to achieve desired droplet characteristics and enhance the overall printing quality.	[70d]

(*Continued*)

Table 3. (Continued)

Research target	Fabrication process	ML technique	Sample size	Inputs	Outputs	Major findings	Refs.
Temperature field prediction	DED (Gas metal arc welding)	**Supervised**: Recurrent neural network and deep neural network (RNN-DNN) parts, and one convolutional neural network (CNN), Feedforward Neural network	-	Spatial coordinates, material properties, and process parameters.	Thermal field, Temperature evolution	To detect the association between the deposition stage and its related thermal field, a physics-based ML approach based on an ensemble learning model was constructed. The time cost of a single prediction step was just milliseconds-minutes. Accuracy of 94%	[71a,b]
Print quality optimization	Vat photo-polymerization (Digital light processing)	**Supervised**: NN consisting of 2 U-Net-like NNs (master NN and slave NN)	24 samples	Grayscale mask image M of size 512 × 512	Binary image P of the same size	The U-net like NNs enabled the use of small sample size (as small as 32) for training data to generate grayscale masks that can print fine-detailed structures surpassing the traditional manual tuning method with identical masks.	[72]
Print speed optimization	Vat photo-polymerization (Continuous liquid interface production)	Siamese networks	N.A.	Manufacturing speed, resin viscosity, part radius, PDMS thickness, surface type, curing time per layer, total curing time	Printing success/failure	Siamese Networks worked the best among all the investigated models (average training accuracy of 90.17% and testing accuracy of 88.42%) as it can effectively extract useful information from the mathematical models-generated synthetic dataset	[73]
Control the print path of the aero-pendulum extruder (concrete)	Material Extrusion	**Deep Reinforcement Learning**: (twin-delayed deep deterministic policy gradient)	5000 simulations	Critic network: environment states and agent's actions Actor network: environment states	Trajectory of the toolpath Critic network: Expectation of the long-term reward Actor network: actions that maximize the long-term reward	A better performance in terms of process duration	[74]

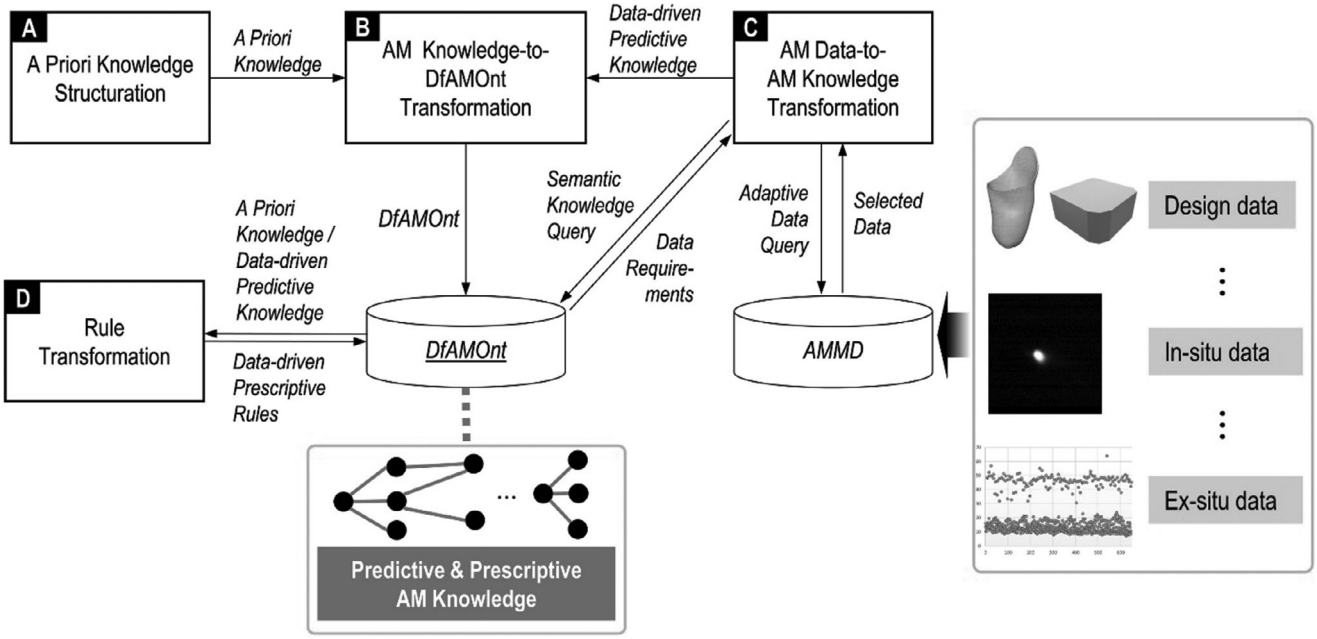

Figure 18. Schematic diagram of a framework that utilized ML and knowledge graphs to formalize unstructured AM guidelines into structured knowledge. The framework comprised four key components: a priori knowledge structuration, transformation of AM data into AM knowledge, transformation of AM knowledge into design for AM ontology, and rule transformation. By employing this approach, the framework facilitated automated and autonomous construction and enhancement of AM design rules by leveraging both existing knowledge and data-driven insights. Reproduced with permission.[75] 2021, Elsevier.

inputs or human design iterations into optimized 3D models. This process showcases the potential of integrating advanced ML techniques to augment material design and manufacturing processes, thereby enhancing the efficiency and responsiveness of intricate design workflows to human inputs.

A technique was developed to reverse engineer composite material parts using imaging methods and ML (**Figure 20**).[78] The approach captured the geometry of the parts and reconstructed the 3D printing tool path by examining the microstructure. The study utilized glass fiber reinforced acrylonitrile

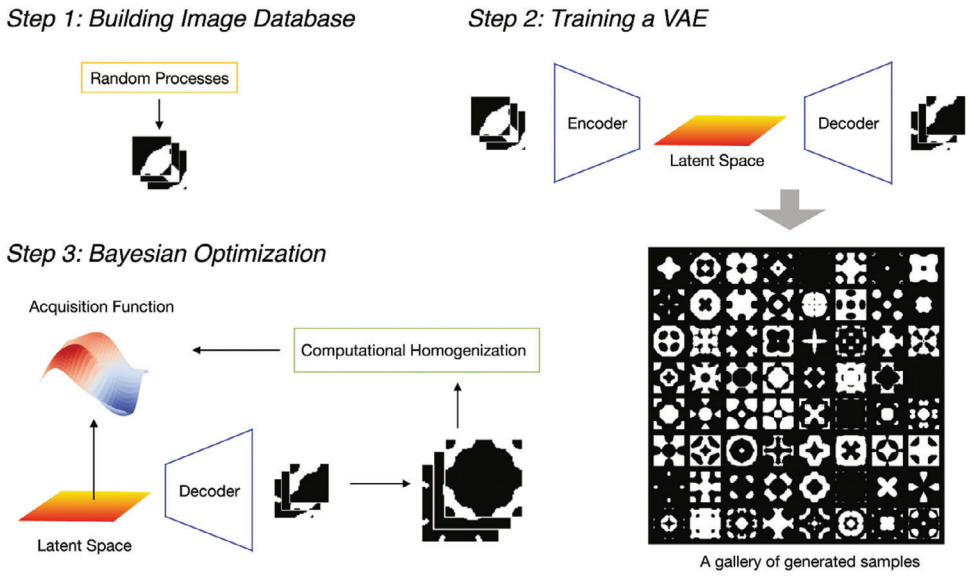

Figure 19. The metamaterial optimization framework involved three main steps. In Step 1, samples were drawn from a random process to create an artificial database of representative volume element images, each consisting of 28 × 28 pixels. Step 2 involved training a variational autoencoder to generate realistic output samples. By flipping the 28 × 28 images twice, larger 56 × 56 RVE images were obtained, which preserve symmetry. Finally, in Step 3, the framework employed Bayesian optimization to achieve the optimal design of a representative volume element that met the specified macroscopic elastic moduli requirements. Adapted with permission.[76] 2020, Elsevier.

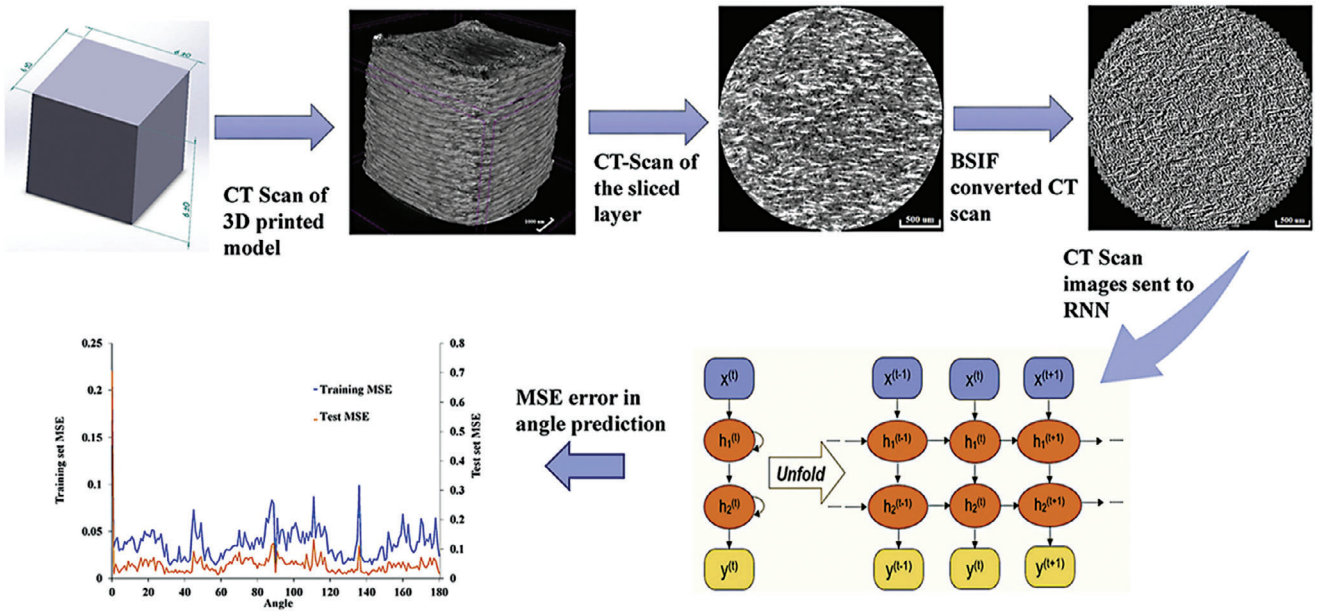

Figure 20. The implementation of a reverse engineering method using both μCT scan and SEM images of the model. The tool-path details are extracted by employing an RNN with LSTM architecture, which identifies the fiber orientation within each layer. This approach enabled the reconstruction of the model's toolpath based on the available imaging data. Reproduced with permission.[78] 2020, Elsevier.

butadiene styrene filaments for 3D printing specimens, which were then reverse-engineered using micro-computed tomography (μCT) scans and scanning electron microscopy (SEM) images. The tool-path information was extracted by identifying fiber orientation in each layer using an RNN with LSTM architecture. The results showed high accuracy in predicting printing orientation (error of 0.5°) and achieved high dimensional accuracy in the reverse-engineered models. The research demonstrated the potential to reverse engineer high-quality replicas of composite parts by leveraging the capabilities used for designing high-performance composites.

Researchers are advancing the field by integrating ML into AM processes for automating customization, optimizing parameters, improving part quality, and facilitating design rule development. These advancements enable efficient and cost-effective production, while also promoting collaboration and innovation within different research groups.

An optimization method for complex mechanical structures was demonstrated by combining the RSM and multi-objective genetic algorithm (MOGA).[79] After conducting experimental modal analysis and FEA on the inkjet printer, the method identified weak points and performance aspects of the structure. The central composite design (CCD) method was deployed to select sample points for numerical simulations and the initial second-order RSM, which focused on the printer's first-order natural frequency, weight, and maximum deformation of the inkjet head, was established. The approximation optimization of the RSM was then carried out using MOGA, resulting in a Pareto optimal solution set. The method demonstrated increased computational efficiency compared to conventional optimization methods and was good for multi-objective optimization of complex structures printed by the inkjet printer. The optimized solution increased the printer's first-order natural frequency by 36.3%, reduced the maximum deformation of the inkjet head by 33%, and lowered the printer's weight by 19.5%. There was a trade-off between computing costs and accuracy, hence it is necessary to discover the optimal balance for future research.

The synergy of ML with design and topology optimization for 3D printing holds the promise of pushing boundaries, that allows creating efficient and sustainable designs for specific applications. As we delve deeper into this intersection, we will explore the mechanisms through which ML augments the design process, addresses the challenges, and opens the horizons in the dynamic world of 3D printing (**Table 4**).

3.4. Microstructure Analysis

The microstructure of metal printed parts is critical for determining their mechanical, thermal, and functional properties. However, there are several challenges in characterizing the microstructure in AM parts. The AM process introduces unique complexities such as rapid solidification and cooling rates, which results in distinct microstructural features compared to conventional manufacturing methods. Moreover, spatial variations within a single part and the need for non-destructive evaluation further complicate microstructural analysis. To address these challenges, advanced imaging techniques such as electron backscatter diffraction (EBSD), X-ray CT, and high-resolution microscopy have emerged as powerful tools for microstructural characterization in metal printing. These techniques enable the visualization and quantification of grain morphology, crystallographic orientations, and defects. However, analyzing the vast amounts of data obtained from these techniques requires sophisticated data analysis methods. This is where ML and DL algorithms come into play, offering automated approaches to

Table 4. ML for design optimization in AM.

Research type	Research target	Fabrication process	ML technique	Sample size	Inputs	Outputs	Major findings	Refs.
Design optimization	ML and KG based design rule construction for AM	-	Supervised: Classification and regression tree CART	N.A.	Prior knowledge and surface roughness measurement data from a LPBF build	Design rule for overhang features	Data-Knowledge-Design Rule (DKDR) framework, which comprises of a prior knowledge structuration, AM knowledge to-DfAMOnt transformation, AM data-to-AM knowledge transformation, and Rule transformation, is a unique framework based on ML and KG.	[75]
Design optimization	Automatic design of composite mechanical metamaterials	-	Unsupervised: Variational autoencoder (VAEs)	200	28 × 28 image pattern (representative volume element)	Elastic moduli	Bayesian optimization was used to get the necessary elastic moduli.	[76]
Design optimization	Toolpath reconstruction using imaging	Material extrusion (FFF)	Supervised: Recurrent neural network with LSTM	78373 images (70:30)	CT-scan images	Direction of fiber	The original models were reverse engineered with just a 0.33% discrepancy in dimensional correctness.	[78]
Design optimization	Design optimization	Material jetting (Inkjet printing)	Supervised: RSM Multi-objective genetic algorithm	N.A.	8 parameters as design variables for optimization	Natural frequency, maximum deformation weight	The optimal solution proposed in this study demonstrates a significant improvement in the first-order natural frequency of the inkjet printer, resulting in a remarkable 36.3% increase. This enhancement effectively mitigates the resonance region caused by the excitation of the servo motor. Additionally, the maximum deformation of the inkjet head is reduced by 33%, leading to enhanced stability and performance. Furthermore, the weight of the inkjet printer can be reduced by 19.5%, resulting in a more lightweight and compact design.	[79]
Design optimization	Crack prediction	PBF	Supervised: High-fidelity surrogate model based on an Attention-based U-Net architecture	540	3D geometries	Maximum shear strain index	Maximum Shear Strain Index (MSSI) as a dependable index for crack formation, it demonstrated how a deep convolutional neural network equipped with an attention-based 3D U-Net architecture could be trained as a trustworthy surrogate of the time-consuming construction process simulation, capable of reliably forecasting MSSI based on the object's shape. Using the surrogate, they applied automated differentiation to directly compute the gradients of maximum MSSI relative to the input design variables. This was then combined with a typical topology optimization engine's performance-based sensitivity field to enable successful design optimization. This method considers the trade-off between weight, manufacturability, and multi-physics performance, demonstrating a complete approach to dealing with these numerous factors.	[80]

(*Continued*)

Table 4. (Continued)

Research type	Research target	Fabrication process	ML technique	Sample size	Inputs	Outputs	Major findings	Refs.
Design optimization	Composite layer design for tissue-mimicking anatomical models	Material jetting (Inkjet Printing)	Supervised: ANN and GE	216 specimens (with 72 combinations of design parameters)	Infill type, coating shore hardness, base shore hardness, height, coating & base thickness	Shore hardness and compressive modulus	By 3.5%, the ML technology surpasses the surface response method. Material characteristics ranging from 20A to 65A may be simulated using the multi-layer model.	[81]

extract meaningful microstructural descriptors and establish quantitative relationships between processing parameters and microstructure variations.

The choice of ML approach for microstructure analysis in AM is dependent on the specific objectives and the nature of the microstructure data. Microstructure analysis in AM involves examining the internal structure of 3D-printed parts to understand their properties and quality. Supervised learning is suitable when there is labeled microstructure data with corresponding information about the specific microstructure characteristics or properties, while unsupervised learning is suitable for discovering patterns, clusters, or anomalies in microstructure data without having pre-defined labels. A combination of supervised and unsupervised techniques may be beneficial for microstructure analysis in AM; the initial use of unsupervised learning to discover patterns in the data, followed using supervised learning to predict specific microstructure based on those patterns. More discussion on the use of different ML techniques for microstructure analysis in AM will be provided in the subsequent sections.

Optimization of AM processes can be performed by leveraging ML models to correlate processing parameters with specific microstructural characteristics. A DL framework for the quantitative analysis of microstructural variations in metals fabricated through additive friction stir deposition technique was developed to predict the grain size, grain orientation, and grain boundary morphology.[82] Microstructural descriptors were extracted by utilizing EBSD patterns and were used to represent the differences in microstructures under different processing conditions. A regeneration neural network was employed to predict new microstructures within the reduced representation domain. The framework was validated using samples produced through additive friction stir deposition, known for equiaxed microstructures. The study addressed challenges in high-dimensional data processing and the identification of principal microstructure descriptors that aligned with specific problem goals. The results demonstrated the effectiveness of the framework in capturing salient changes within microstructures and accurately regenerating them. The physical insights in microstructure descriptors obtained through mapping the regenerated microstructures provided valuable understanding. The study establishes a foundation for quantifying processing-microstructure linkages in metal AM and holds promise for applications in materials science, including heterogeneous material design and optimization. **Figure 21** provides a summary of the applications of ML in AM for the prediction of various microstructure-related properties.

3.4.1. Powder Bed Fusion

Determining the mechanical properties of 3D-printed metal parts is crucial for ensuring their reliability, functionality, and safety. However, there are unique challenges in determining the mechanical properties of 3D-printed metal parts. The microstructure and defects in the printed material can significantly affect its properties, making it essential to consider factors like porosity, grain structure, and residual stresses. Furthermore, the complex geometry and layer-by-layer fabrication process of 3D printing make it difficult to perform standardized testing. ML techniques offer a promising solution to address the associated chal-

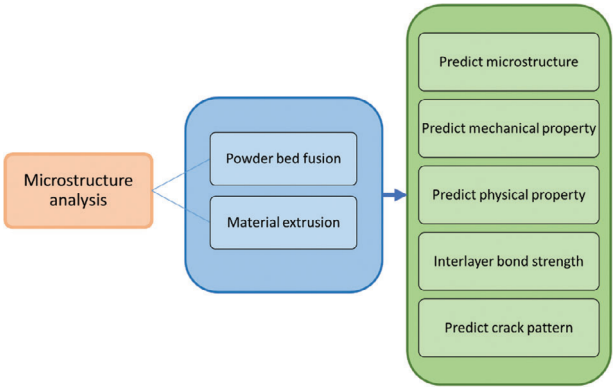

Figure 21. Graphical overview depicting the applications of ML in the field of AM for predicting various properties related to microstructure.

lenges. By analyzing diverse datasets, ML algorithms can predict mechanical properties based on geometrical and microstructural features, reducing the need for extensive experimental testing. These algorithms can also identify correlations between printing parameters and mechanical properties, optimizing the printing process. ML aids in defect detection and classification, enhancing quality control and it enables more efficient and effective characterization of 3D-printed metal parts by leveraging the power of AI.

Various ML techniques such as NN,[83] gradient boosting regression,[84] SVM,[85] and GA[86] have been utilized for predicting the mechanical property of 3D-printed metal parts with a good coefficient of determination (R^2: 0.84–0.98). The mechanical properties that were explored include the ultimate tensile strength, the maximum elongation, the fatigue life, and the microhardness of the 3D-printed metal parts. The inputs were dependent on the type of mechanical properties (static or dynamic). Inputs for static mechanical properties include process parameters, parts and build orientations, surface roughness, relative density, and crystal orientation, while the inputs for dynamic mechanical properties include stress, build orientation, defect size and depth, and loading conditions.

For most cases, the mechanical properties of 3D-printed materials are assessed at the specimen level, employing a range of standardized testing methodologies to ensure consistency, reliability, and comparability of results. The American Society for Testing and Materials (ASTM) provides several standards that are widely adopted in evaluating the mechanical properties of materials produced by additive manufacturing processes. These standards help in defining the procedures for preparing specimens, conducting tests, and interpreting the results for materials such as metals, polymers, and composites. ASTM F2971-13,[87] ASTM E8/E8M,[88] and ASTM E9[89] are some notable ASTM standards used in the testing of 3D-printed materials. Utilizing these ASTM standards in testing 3D-printed materials ensures that the mechanical properties are measured accurately and consistently, facilitating the comparison of data across different studies and applications. It also helps in validating the performance of 3D-printed parts against traditional manufacturing methods, aiding in the broader acceptance and adoption of additive manufacturing technologies. These standards guide the testing of uniformly prepared specimens that are assumed to represent the material's overall characteristics. The results, such as tensile strength, elongation, compressive strength, and flexural modulus, are considered to reflect the average or bulk properties of the material across the entire specimen. This assumption is valid under the premise that the specimen is homogeneous, and the material properties are uniform throughout the specimen. In 3D printing, however, the layer-by-layer manufacturing process and the potential variability in microstructure across different regions of a part may challenge this assumption.

The repeatability of LPBF-printed metal parts was investigated using ML models (**Figure 22**a).[90] The mechanical properties of the printed metal parts (standard deviation of yield strength, tensile strength, and maximum elongation) were used to quantify the repeatability. The study showed that the DT method was the most efficient method to classify and predict the quality of the part, achieving an F1 score of 95%. While most ML models are trained with homogenized properties, derived from standardized testing of uniform specimens, their application extends beyond simple predictions to encompass the complex and varied nature of arbitrary 3D-printed parts. This potential is rooted in the ability of these models to analyze and predict based on diverse inputs, offering a nuanced understanding of material behavior. For instance, the ML models can be trained on a dataset that captures a wide range of mechanical properties, geometries, materials, and print parameters, allowing the model to recognize patterns and correlations that apply across different printing scenarios. By extracting detailed features of an arbitrary part, including its geometry, material composition, and print settings, ML models could potentially predict its localised mechanical properties so that designers can rapidly iterate on designs by incorporating predictive insights into mechanical properties, effectively tailoring parts to specific performance criteria.

The adaptation of new printers requires a lot of effort due to the high variability of 3D printers in determining the optimal process window to fabricate AM parts with good mechanical strength. The main challenge involves the collection of a large dataset which can be time consuming and costly. Notably, this can be solved using ML models to predict the performance of the printed parts that are fabricated by a new printer using a small dataset via a transfer learning technique. The published data of LPBF Ti-6Al-4 V parts was used for the model training to predict process parameters for different hardness-porosity property combinations (Figure 22b).[86] The challenges of predicting process-property relationship include 1) adopting a new printer model from the same manufacturer, 2. adopting a printer from different manufacturers but with similar technology, and 3) adopting a printer from a new manufacturer with different technology. Bayesian optimization models were found to be effective in modeling process-property relations and outperformed other models. The framework demonstrated the feasibility of cross-machine knowledge transfer and multi-property optimization experiments. The work highlights that data mining-assisted ML efforts can accelerate the development and optimization of metal 3D printing processes, emphasizing the need for standardized reporting of data and the creation of a comprehensive metals AM database.

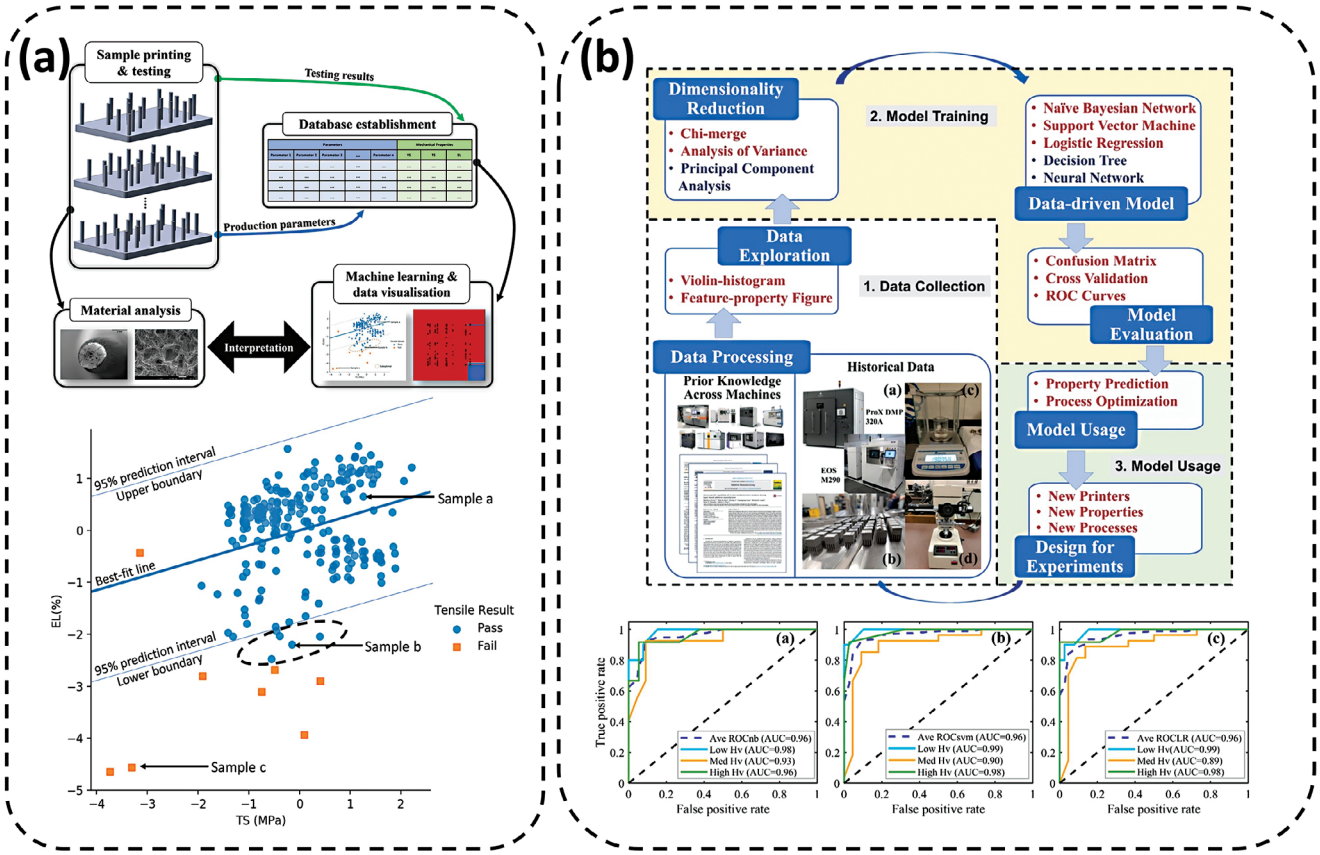

Figure 22. a) Schematic showing the workflow of ML technique for predicting the mechanical property of 3D-printed metal parts. Reproduced with permission.[90] 2021, Elsevier. b) Schematic showing the workflow for training an ML model for predicting the performance of the 3D-printed parts from a new printer. Reproduced with permission.[86] 2021, Elsevier.

3.4.2. Material Extrusion

A study demonstrated prediction of mechanical properties in 3D FDM-printed parts. This was addressed by developing a data-driven predictive model using LSTM networks for FDM processes.[91] The model took into account the layer-by-layer printing process and related cyclic layer thermal history to improve accuracy and reliability. Layer-wise activities were captured using sensors (IR sensor, thermocouple, and accelerometer) and their data were incorporated into the LSTM network. The LSTM-based predictive model outperformed traditional ML techniques such as support vector regression (SVR) and RF by 9.8% and 24.3% respectively. Key findings of the study included significant improvements in prediction performance by incorporating in-process sensing data, high relevance of infrared sensor and accelerometer data for tensile strength prediction, and substantial contributions of process parameters to tensile strength prediction. The LSTM model demonstrated the effectiveness of sequential layer-by-layer modeling of the FDM process, paving the way for improved microstructure analysis in AM applications.

To address the issue of poor part strength in extrusion-based additive manufacturing processes, another study developed an ANN model to predict the tensile strength of 3D-printed parts.[92] The ANN model considered various input variables such as layer thickness, orientation, raster angle, nozzle temperature, bed temperature, room temperature, air gap, and barrel temperature and showed higher accuracy and lower errors compared to existing response surface methodology (RSM) models with root-mean-square-error (RMSE) values for ANN and RSM models at 0.49 and 0.90, respectively. This approach offers significant improvement in predicting part strength, enabling better optimization of manufacturing process conditions and cost-effective additive manufacturing. Another study utilized RF and ANN (known for their ability to capture nonlinearity) to predict the dynamic strength of 3D-printed continuous ramie fiber reinforced biocomposites (CRFRC) under various conditions (varying layer thicknesses, hatch spacings, and strain rates).[93] The ANN model outperformed RF in prediction accuracy (5% error compared to 9% error) and provided insights into the importance of different factors. ML proved advantageous in accurately predicting CRFRC's dynamic strength, optimizing printing parameters, and understanding the influence of microstructural characteristics on composite performance.

A comparative analysis of selected ML algorithms (ANN, SVM, and RF) was performed for construction printing to evaluate the interlayer bonding in layered cementitious composites using non-destructive testing and measurements.[94] The objective was to simplify the mathematical models by reducing the number of input parameters, making it more practical for implementation in real-world scenarios. The study concluded that ANN yielded

the most accurate results in predicting interlayer bond strength, yielding a linear correlation coefficient R^2 of 0.883 and RMSE of 0.341 MPa. The ANN model was trained using data from various mixtures and it effectively predicted the interlayer bond strength and determined the optimal printing parameters for obtaining strong interlayer bonding.

ML models were used to classify 3D-printed boron-based geopolymer samples based on their compressive strength.[95] Supervised ML algorithms such as recursive-partitioning functions rpart and ctree, were used to build separate classification models. The models were compared in terms of simplicity and cumulative accuracy. The rpart function demonstrated slightly better performance, with a cumulative accuracy of 70% as compared to the ctree function's 63% accuracy. Furthermore, the rpart function required fewer parameters for prediction. The study highlighted the importance of the slag content and the ratio of boron ions in determining the compressive strength of samples. The application of machine learning significantly reduces the error in predicting compressive strength, demonstrating its potential for developing a guide or standard for classifying 3D-printed boron-based geopolymer samples based on compressive strength.

Another study proposed a hybrid approach combining the multi-objective grasshopper optimization algorithm (MOGOA) and ANN to predict the compressive strength of 3D-printed concrete.[96] The MOGOA was used to optimize the architecture of the ANN model, considering the number of hidden layers and neurons in each layer. The results showed that the hybrid MOGOA-ANN model achieved accurate predictions (mean absolute percentage error (MAPE) of 92%) of the compressive strength, even with simplified neural network architectures. This approach can reduce computational complexity and enable faster predictions in the material design process (**Table 5**).

3.5. Material Formulation

Material formulation is a pivotal process in achieving desired properties for various applications. Two key considerations in this endeavor are processability and the targeted end-use properties. Achieving this balance can be intricate due to the multifaceted nature of material behavior and the interplay between different parameters. Processability entails ensuring that the material can be effectively and reliably processed into the desired form. On the other hand, tailoring materials to exhibit specific properties such as mechanical strength, thermal conductivity, or electrical resistivity is crucial for meeting the demands of diverse applications. However, this pursuit is often a delicate balancing act. Enhancing one aspect may inadvertently impact another. For instance, increasing mechanical strength might result in reduced flexibility. Moreover, this trade-off is complicated by the multitude of factors at play, including chemical composition, processing conditions, and material microstructure. This is where ML steps in as a powerful tool. By ingesting and analyzing vast datasets encompassing various material compositions and their corresponding properties, ML algorithms can identify complex relationships and patterns that might elude traditional analysis. This enables the formulation of predictive models that guide the selection of optimal material compositions to achieve desired properties, while also considering processability constraints.

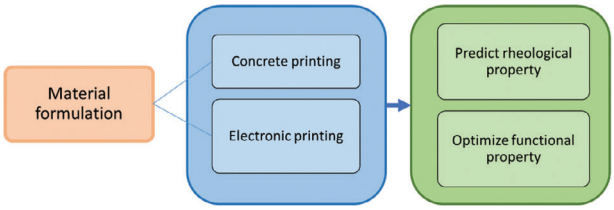

Figure 23. A graphical overview summarizing the applications of ML in material formulation for AM.

The choice of ML approach for material formulation in AM is dependent on the specific goals and challenges associated with the material development process in AM. Material formulation in AM involves designing and optimizing the materials with desired properties for 3D printing. Supervised learning is suitable when there is labeled data that associates material compositions with specific material properties or performance metrics, while unsupervised learning is suitable for discovering patterns, clusters, or similarities among materials or their properties without pre-defined labels. A combination of supervised and unsupervised techniques may be beneficial for material formulation in AM; the initial use of unsupervised learning to discover complex relationship in the data followed by using supervised learning to build predictive models for specific material properties. More discussion on the use of different ML techniques for material formulation in AM will be provided in the subsequent sections (**Figure 23**).

3.5.1. Powder Bed Fusion

Alloy selection profoundly influences the entire AM process, spanning from the initial energy-source-material interactions to the final component characteristics. The degree to which lasers are reflected or absorbed by a powder bed is contingent upon the powder's makeup.[100] Both the internal and external granular densities of the feedstock contribute significantly to the density of the end products.[101] Moreover, the thermal properties of the selected alloy partially dictate the conduction pathways in the molten state.[102] Variations in solidification rates among alloys can result in significantly diverse post-manufacture microstructures.[103] Certain AM-related challenges, such as the evaporation of elemental constituents due to intense thermal changes, can be attributed to material composition. This can affect the stoichiometry of the melt pools and ultimately the quality of the finished product.[104] Furthermore, some research has probed the influence of feedstock attributes, like particle size distribution and shape, on process outcomes.[100b,105] Yet, the exact effects remain to be fully elucidated.

Databases offering a myriad of alloy attributes serve as indispensable tools in the realm of materials science. Notably, the International Crystal Structure Database (ICSD) hosts crystallographic structures of countless materials, while the Linus Pauling files extend from atomic specifics, such as radii and electron valence, to more advanced crystallographic information.[106] Contemporary platforms like Aflow[107] and the Materials Project[108] empower users with sophisticated search functionalities across diverse alloy datasets. The efficacy of data mining in advancing AM alloy development has been underscored by several

Table 5. ML for microstructure analysis in AM.

Research target	Fabrication process	ML technique	Sample size	Inputs	Outputs	Performance	Refs.
Predict microstructure	Additive friction stir deposition	**Supervised**: convolutional neural network (VGG16)	Nil	EBSD scans	Grain size, grain orientation, and grain boundary morphology	Near 100% accuracy	[82]
Predict mechanical property	PBF	**Supervised**: a custom 3D convolutional neural network (CNN) based on VGGNet	7680	Crystal orientation as input (with or without auxiliary input features)	Mechanical properties	R^2 value of 0.84 and a root mean square error (RMSE) value of 16.57 MPa.	[83a]
Prediction of fatigue life	PBF	**Supervised**: Backpropagation neural network	32800 data points	Stress, build orientation, defect size, defect depth, defect distance to surface	Fatigue life	R^2 value of greater than 0.98	[83b]
Mechanical property prediction	PBF	**Supervised**: Gradient boosting regression	3000	Surface roughness and void position, number density and size	Mechanical property	R^2 value of greater than 0.98	[84]
Fatigue life	PBF	**Supervised**: ANN, random forest, Support vector machine	-	Process parameters, fatigue loading conditions	Fatigue life	R^2 value of greater than 0.95 for random forest and SVM	[85]
Transfer learning for property prediction	PBF	**Supervised**: Multi-Objective Genetic Algorithm (MOGA)	Data from 120 manuscripts	Laser power, scan speed, energy density, hatch spacing, layer thickness, powder size	Relative density, microhardness,	Overall prediction accuracy of 88%	[86]
Repeatability of printed parts	PBF	**Supervised**: Tree-based models	167	Production parameters such as build mass, height and time, part volume, sample locations and temperature parameters.	Static mechanical properties such as yield strength, tensile strength, and maximum elongation.	F1 score > 0.95	[90]
Tensile strength prediction	Material extrusion (FFF)	**Supervised**: LSTM		Material property, extruder temp, printing speed, layer height	Tensile strength	With an RMSE of roughly 2%, the developed LSTM model outperforms previous ML models in predicting the tensile strength of 3D-printed parts.	[91]

(*Continued*)

Table 5. (Continued)

Research target	Fabrication process	ML technique	Sample size	Inputs	Outputs	Performance	Refs.
Part strength prediction	Material extrusion (FFF)	**Supervised**: ANN, RSM	120 (70:15:15)	Layer thickness, orientation, raster angle, raster width, air gap	Tensile strength	Pellet based printing: The RMSE for the ANN results are lower in most of the cases, which shows the adequacy of this model, but ANN is not suitable for less data, while RMSE for the RSM sometimes performs better in cases with less data using thermal imaging to predict the strength.	[92]
Dynamic tensile strength prediction	Material extrusion (FFF)	**Supervised**: Random forest, ANN	108 (81:27)	Hatching spacing, layer thickness, strain rate	Tensile strength	The workflow combines dual-resolution Robotic Scanning, Neural Network prediction and printing of PETG plastic. This integrated approach offers the advantage of responding directly to unknown geometries through automated performance design customization.	[93]
Interlayer bond strength prediction (concrete)	Material extrusion	**Supervised**: ANN, SVM, RF	338	Parameters of concrete surface repair cover thickness: 10-point height, core height, reduced peak height, average mobility, overlay thickness, frequency of the sound wave reflection from the bottom of a sample	Pull-off adhesion	ANN provided the most accurate assessment of the interlayer bonding pull-off adhesion of layered concrete, with an average relative error of 10.13 percent.	[94]
Compressive Strength prediction (concrete)	Material extrusion	**Supervised**: The conditional inference trees (ctree) and recursive partitioning (rpart) methods	114 targets	Weight percentages of the fly ash and Ground granulated blast-furnace slag (GGBFS) (%S), as well as the ratios of boron ions silicon ions and the ratio of sodium ions in the alkaline solution	Compressive strength	Ctree function has a 100% positive predictive value, while rpart has a positive predictive value of up to 81%.	[95]

(*Continued*)

Table 5. (Continued)

Research target	Fabrication process	ML technique	Sample size	Inputs	Outputs	Performance	Refs.
Compressive strength prediction (concrete)	Material extrusion	**Supervised**: Multi-objective Grasshopper Optimization algorithm's hybridization with ANN (ANNMOGOA)	N.A.	Water-cement ratio (W/C), amount of coarse aggregate (CA), amount of fine aggregate (FA), amount of super-plasticizer (S)	Compressive strength	Accuracy of ANNMOGOA-1 is about 92%	[96]
Surrogate model to predict peak and maximum displacement of beam of cellular design (concrete)	Material extrusion	**Supervised**: ANN	1800	Number of TPMS layers and volume fraction	Peak load Maximum displacement	The maximum deviations of 2.5% and 3.5% for peak loads and maximum midpoint displacements	[97]
Predicting the auxetic behavior of cementitious cellular composite (concrete)	Material extrusion	**Supervised**: perceptron-based neural network (NN) Shapley additive explanations (SHAP)	850 combinations FEA simulation results	Design parameters: aspect ratio, length of the major axis, number of voids along the X- and Y-directions	Poisson's ratio	$R^2 > 0.99$ and MSE < 0.0004	[98]
Crack prediction of air-void structure (concrete)	Material extrusion	**Supervised**: U-net CNN	193989 (95:5)	2D microstructure image containing pores (32 by 32 pixels)	Crack patterns	CNN model predictions show excellent agreement with lattice numerical analyses, with an Intersection over Union (IoU) of 0.85 for crack pattern prediction and an R^2 value of 0.75 for stress-crack width curve prediction.	[99]

studies. A study employed this method to optimize the chemistry of aluminum alloys for enhanced processing during LPBF.[102] The printed Al alloys historically faced challenges such as limited grain nucleation, resulting in the coalescence of expansive grains and concomitant intergranular stresses, predisposing the material to hot-cracking. To mitigate this, a study sought potential grain inoculant compounds, generated via chemical reactions during LPBF, which could refine grain properties. A notable solution emerged when silicon and carbon reactions birthed SiC particles, promoting more uniform grain nucleation. However, the lattice disparities between certain compounds and the aluminum alloy could induce substantial stresses at their interface, perpetuating cracking issues. Consequently, the focus shifted to identifying inoculants with lattice parameters aligning with the primary aluminum alloy. Through the deployment of a search algorithm probing around 4500 potential nucleants, hydrogen-stabilized Zr emerged as the optimal candidate.

The challenges of data mining from existing literature include missing values from isolated studies of individual parameters or properties. A database linking process parameters and material properties in SLM-fabricated Ti6Al4V alloys was developed.[109] Various data imputation methods such as K-NN, multivariate imputation by chained equations, and graph imputation neural network (GINN) were explored to fill missing data. The K-NN model excelled in process parameters, whereas GINN model excelled in material properties. The imputation quality was enhanced by using the median of the values from the three models, and a self-organizing map provided visualization of the relationships between process parameters and material properties.

3.5.2. Material Extrusion

One key area of focus in material formulation for material extrusion technique is the rheological properties of the extrudate to ensure good flowability and extrudability. A study was conducted to investigate the effects of various admixtures on the rheological properties of cement paste for 3D printing applications.[110] An empirical formula was proposed to analyze the relationship between dynamic yield stress and mini-slump. ANN model was used to predict dynamic yield stress and mini slump based on admixture proportions. The model was validated by simulating new mixes, and the results demonstrated a high level of effectiveness in predicting the correlation between mini-slump and dynamic yield stress. This work opens avenues for future research to consider the time factor in ANN models for predicting printability over time.

A novel ML algorithm called gene expression programming (GEP) was used to develop mathematical models that predict the rheological properties of concrete such as yield stress and plastic viscosity.[111] A comprehensive database was built using previous experimental results and the significant input parameters that influence concrete rheology (cement, sand, water, small and medium-sized coarse gravels, and superplasticizer) were identified. The GEP models, which use simple arithmetic expressions to describe the relationships between the input parameters and the rheological properties, exhibited a strong correlation with experimental data (R^2 of 0.998 for yield stress and R^2 of 0.978 for plastic viscosity). The models demonstrated high efficiency and predictability, with performance index factors indicating their accuracy. Various statistical parameters and external validation checks further confirmed the precision and generalization capacity of the GEP models in predicting the rheological properties of fresh concrete.

Another study focused on predicting the static yield stress (τS_n) of blended cement pastes containing supplementary cementitious materials (SCMs) using ML models.[112] A dataset from previous experimental work was collected and eight input parameters, including SCM properties, cement reactivity, mixture design parameters, and resting time were identified. A comparison of different ML models (MLP, RF, and SVR) was conducted and the MLP model demonstrated the highest accuracy with low RMSE and high coefficient of determination (R^2). The study revealed that τS_n was primarily influenced by the amount of pseudo-contact points, while the amount of cement replacement by SCM had the least effect by analyzing the importance of different input parameters using Shapley-value and permutation feature importance analysis. These ML models show promise in improving mix design for innovative concrete technologies that require better workability control such as concrete printing or self-consolidating concrete.

Apart from the rheological properties, ML has also been used to predict the optimal composition of additives for the feedstock material. A study investigated the 3D-printing of polylactic acid (PLA) composites reinforced with chopped long carbon fiber using an FDM printer.[113] The study employed gaussian process modeling, an ML technique suitable for small dataset, to predict the optimal carbon fiber content for the composites The model predicted the best mechanical performance at 6.7 wt.% carbon fiber, closely aligning with the experimental result of 5 wt.% carbon fiber. The use of ML demonstrated its advantages in accurately predicting material properties and optimizing composite performance, potentially saving time and resources in the manufacturing process.

3.5.3. Material Jetting

Material design plays a crucial role in 3D printing of electronics, as it directly influences printability and the final properties of the printed traces (conducting, semi-conducting, or insulating). Additives such as surfactants or binders are typically added to the functional materials to ensure good printability of the functional inks. The proportion of different solvents is important in determining the printability and the final deposition pattern for certain inks. Important factors such as particle loading, and particle size can influence the printability and final electrical property of the printed structures. It can be a daunting task in identifying the optimal parameters and ratios for the materials. Therefore, researchers are increasingly turning to ML techniques to predict the performance of the final printed electrical circuits and components, streamlining the process, and improving overall outcomes.

A study introduced a strategy that leveraged ML models to guide the 3D printing process of Cu anode scaffolds directly onto solid-state NASICON-type $Li_{1+x}Al_x^{3+}M_{2-x}^{4+}(PO_4)_3$ (LATP)

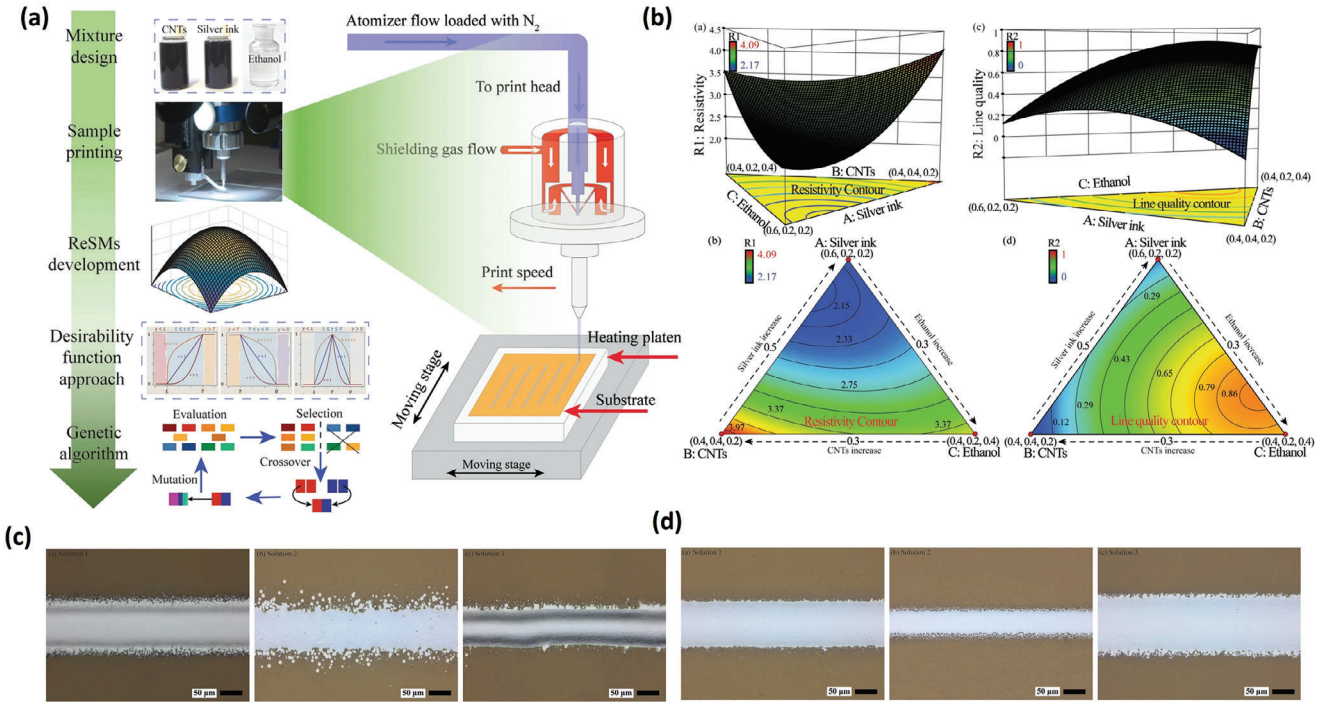

Figure 24. Illustration showing the ink formulation optimization using RSM to improve the electrical resistivity and line quality. Reproduced with permission.[115] 2023, Nature Portfolio.

electrolytes, thereby addressing obstacles associated with lithium batteries.[114] A sequential learning method based on mixture design was employed to refine the formulation of the printing ink, the rheological parameters, and the operational conditions of the 3D printing process. The method streamlined experimental work by systematically enhancing the design variables through a sequence of experiments, resulting in a sturdy methodology for ink characterization. The printed hierarchical scaffold and copper oxide (CuO) interlayer substantially decreased overpotential in comparison to unadorned lithium anodes, which was achieved by improving interfacial contact to mitigate the formation of lithium dendrites and inhibit side reactions. In summary, the research introduced a novel methodology for swiftly exploring anode geometries and 3D printable inks for lithium batteries, exploiting both experimental design and machine learning techniques.

A hybrid multi-objective optimization technique was used to identify the best functional ink composition for aerosol jet printing technology and obtain low electrical resistivity and good printed line quality (**Figure 24**).[115] The suggested method systematically examined the causal relationship between several ink components (ethanol, nanoparticle silver ink, and carbon nanotube (CNT) ink) and printing outcomes. Two RSM were created based on the analysis of variance; a non-dominated sorting genetic algorithm III (NSGA-III) was then merged with these models to provide a more reliable optimization in the 3D mixture design space. This data-driven methodology extended the process of creating materials with multi-component and multi-property in aerosol jet printing technology, resulting in higher electrical performance and broader applications in the field of printed electronics (**Table 6**).

4. Outlook

4.1. Advanced ML Models

Large Language Models (LLMs) are revolutionizing the ML landscape, showcasing broad applicability across domains due to their profound understanding of language and context. These advanced AI systems are designed to comprehend, generate, and interact with human language at scale, excelling in tasks like writing, translating, summarizing, and question-answering. Fuelled by DL techniques and the transformer architecture, exemplified by OpenAI's GPT series, LLMs process and generate coherent, contextually relevant text. "MechGPT", developed by Buehler's group, exemplifies their prowess in modeling mechanics and materials, showcasing the model's proficiency in knowledge retrieval, hypothesis generation, and bridging disparate areas for understanding and predicting material behavior and failure mechanisms.[116]

Recent efforts have also focused on enhancing the efficiency of in-context learning for LLMs through active learning strategies, specifically targeting the optimization of demonstration selection for few-shot learning tasks.[117] By employing methods such as uncertainty sampling, diversity sampling, and similarity-based selection, the study identifies the most informative examples that significantly improve LLM performance. The principles from this research can be adapted to 3D printing in several ways – 1. optimizing printing parameters through active learning to enhance the quality of 3D-printed objects while minimizing resource use, 2. accelerating the design iteration process through active learning to facilitate rapid prototyping of models based on feedback and predicted outcomes, 3. developing new printable materials

Table 6. ML for material formulation in AM.

Research target	Fabrication process	ML technique	Sample size	Inputs	Outputs	Major findings	Refs.
Rheological properties prediction (concrete)	Material extrusion	**Supervised**: ANN	16	Dosage of high efficiency water reducing agent, hydrated calcium silicate, nano-clay, viscosity-modified agents, accelerating agent	Dynamic yield stress, mini slump	The suggested model can precisely forecast the dynamic yield stress and mini-slump of 3D-printed cementitious materials using a variety of admixtures of different kinds and quality.	[110]
Rheological parameters prediction (concrete)	Material extrusion	**Supervised**: Gene expression programming (GEP)	137 data sets of yield stress and 142 for plastic viscosity	Percentages of Cement, water, sand, small coarse gravel, medium coarse gravel, and super plasticizer	Yield stress and plastic viscosity	For yield stress and plastic viscosity, the mathematical models based on GEP demonstrated greater efficiency with significant correlation factors R2 of 0.978 and 0.998, respectively, with the experimental data (R2 ∼1).	[111]
Yield stress evolution prediction (concrete)	Material extrusion	**Supervised**: ANN, Random Forest, SVR	280 data points (75:25)	SCM properties (i.e., particle number density (NPSD), specific surface area (SSAPSD), surface potential (ζ), and hydraulicity (SCMR)), cement reactivity (CR), main mixture parameters, and resting time (t)	Static yield stress	The best model to predict τS0 was MLP, which had an average RMSE of 20.97 Pa and an R2 of 98.4%.	[112]
Mechanical properties prediction	Material extrusion	**Supervised**: Gaussian Process Modeling	-	Composition of CF/PLA	Tensile strength, tensile modulus, elongation at break, flexural strength, flexural modulus, hardness	It can accurately gauge uncertainty metrics and offer a distribution for the predicted value.	[113]
Optimization of ink formulation	Material extrusion (Direct ink writing – pneumatic)	**Supervised**: Mixture design RSM, sequential learning	N.A.	Solid loading, binder humectant	Herschel-Bulkley shear thinning index, dynamic yield stress, static yield stress, ink stiffness G' LVR, line continuity, % spreading	Successfully identified the optimal range of ink formulation, referred to as the printable window, within which the desired printing results were achieved. The optimal rheological parameters for the selected ink deviated from the initial projections and previous findings reported in the literature	[114]
Optimization of ink composition	Material jetting (Aerosol jet printing)	**Supervised**: Mixture design RSM, non-dominated sorting GA	13 data points	Ink composition of silver, CNT, and ethanol	Resistivity, line quality	Investigated the causal relationship between various ink components, namely nanoparticle silver ink, CNTs ink, and ethanol, and their corresponding effects on the printing outcomes. To optimize the composition of functional ink to achieve desirable characteristics, specifically low electrical resistivity, and high quality of printed lines.	[115]

through active learning to prioritize the exploration of material compositions to yield novel properties and expedite innovation in material science within the 3D printing domain.

Moreover, LLMs, with their vast knowledge base, prove valuable in troubleshooting 3D printing issues by offering language-based solutions. They can understand descriptions of issues encountered during the 3D printing process and provide relevant solutions or suggestions for parameter adjustments. Their capacity to learn from diverse data sources enables them to offer guidance on a wide range of problems, from hardware malfunctions to software glitches and material issues, making them valuable tools for both novice and experienced users seeking to optimize their 3D printing workflows. For instance, ChatGPT was explored to optimize the G-code generation process in AM, particularly focusing on fused filament fabrication (FFF) with thermoplastic polyurethane (TPU) as the feedstock.[118] It assesses ChatGPT's capabilities in addressing common 3D printing challenges such as warping, bed detachment, and stringing by optimizing printing parameters. The study demonstrates ChatGPT's effectiveness in generating optimized G-code, leading to improved print quality and material savings. It highlights the potential of integrating AI tools like ChatGPT in additive manufacturing to enhance efficiency, reduce trial and error, and accelerate innovation in material science.

Incorporating generative AI into design workflows holds promise for transforming 3D modeling and printing. This vision entails a collaborative experience where designers articulate ideas in natural language, and AI translates them into tangible 3D models. The iterative cycle of feedback and refinement between human designers and AI could significantly accelerate the design process, allowing for rapid prototyping and optimization, thereby blurring the lines between imagination and materialization in the realm of 3D printing. A method was proposed for generating 3D architected materials from natural language inputs using a combination of a vector quantized generative adversarial network (VQGAN) and contrastive language-image pre-training (CLIP) neural networks.[119] This approach translates natural language descriptions into 2D images, which are then converted into 3D models for printing, applying both to materials with varying rigidity and to molecular dynamics modeling of nano-architectures. This innovative method allows for the direct materialization of concepts derived from language, offering new pathways for complex design workflows in 3D printing by leveraging human-readable inputs to drive the creation and optimization of 3D models and materials. Despite their capabilities, these models face challenges such as bias, interpretability, and adaptability in novel situations.

4.2. Advanced Sensors

Various sensors, ranging from image-based to sensor signal-based types, are utilized to monitor and detect defects in AM, providing comprehensive insights into the processes.[120] Image-based sensors, capturing visual and sequential images through cameras, offer a detailed representation of the printing process.[121]Sensor signal-based techniques, including acoustic emission with fibre Bragg grating (FBG) sensors,[122] optical emission with multispectral sensors[123] and X-ray computed tomography,[124] and infrared signal-based sensors like pyrometers[125] and high-speed infrared cameras, focus on different aspects of monitoring. Notably, multi-sensor signal integration, combining accelerometers, acoustic emission sensors, and optical emission spectrometers with CCD cameras, enhances simultaneous monitoring.[126] Employing ML models alongside the various existing sensors aids in detecting macroscale or mesoscale defects. However, a trade-off exists between the speed of processing 1D data and higher information density for 2D or 3D data, posing a challenge in balancing processing speed and information richness in AM defect detection strategies.

In the dynamic realm of AM, the integration of advanced sensor technology with ML models presents a transformative opportunity to push the boundaries of innovation. Looking ahead, the adoption of three-dimensional data acquisition, particularly using stereoscopic cameras, emerges as a significant advancement over traditional two-dimensional imaging methods.[127] These cameras capture the manufacturing process in three dimensions, unlocking a previously inaccessible depth of data. This enhancement allows ML algorithms to predict the quality and performance of the final product more precisely, shifting from a flat perspective to a comprehensive, volumetric analysis that could revolutionize quality assessment practices. Expanding the data spectrum for ML models, the incorporation of advanced measuring techniques such as scanning electron microscopy (SEM),[128] surface roughness measurement,[129] and in situ computed tomography (CT) scans provide abundant information on both micro- and macro-scales.[130] SEM offers insights into microstructural integrity crucial for predicting mechanical properties, surface roughness serves as a direct quality metric, and CT scanning non-destructively verifies internal structure and dimensional accuracy. The convergence of these diverse data streams holds the potential to create a comprehensive dataset for ML models, capable of transforming process optimization, and real-time quality control in AM.

The concept of data fusion is particularly promising in this context, holding the potential to establish robust, predictive ML models providing comprehensive insights into the AM process. By amalgamating data from various sources, such as stereoscopic images, SEM analyses, surface topology, and CT scans, a more nuanced view of the printing process emerges. ML models can be trained on datasets reflecting the complexity of AM, enabling more accurate predictions and the ability to proactively identify and address potential failures. Furthermore, the use of augmented and virtual reality (AR/VR) technologies can potentially enhance this advanced sensory ecosystem, offering an immersive interface for design and decision-making.[131] When integrated with ML, AR/VR creates a virtual testing ground for refining designs and simulating manufacturing outcomes, pre-empting potential issues and optimizing parameters for optimal results.[132] Informed by both virtual simulations and real-time sensory data, ML models guide users through the design-to-production journey, suggesting modifications that enhance the end product's functionality and design fidelity.

The integration of these technologies into AM not only elevates the precision and reliability of the manufacturing process but also represents a stride toward a fully integrated, intelligent manufacturing system. These advancements signal the potential for a new era of "smart" AM, where machines evolve beyond tools

of creation to become design partners capable of learning, adapting, and optimizing in real-time, ensuring the delivery of products meeting the highest standards of quality and performance.

4.3. ML Applications in Emerging AM-Related Fields

In the vibrant landscape of AM, 3D printing has taken center stage, metamorphosing various industries by offering unprecedented customization, precision, and efficiency. As this transformative technology continues to evolve, the integration of machine learning emerges as a compelling frontier, promising to amplify the capabilities of 3D printing across diverse AM-related research areas. In this section, the unique applications of ML in various fields such as metal printing, polymer printing, bioprinting, construction printing, drug printing, and electronic printing will be discussed.

4.3.1. Bioprinting

Over the years, the widespread adoption of 3D bioprinting technologies (including extrusion-based,[133] jetting-based,[134] vat photopolymerization-based)[135] in tissue engineering, regenerative medicine, and biomedical applications can be attributed to its remarkable ability to accurately deposit multiple types of living cells and bio-inks at pre-defined positions. This capability facilitates the fabrication of biomimetic 3D tissue-engineered constructs.[136] The pivotal functional units in 3D bioprinted tissue constructs are the living cells, and ML proves to be a potent tool for unraveling the complexities of cellular behavior. It achieves this by handling large datasets, identifying patterns, and making predictions at various stages of the bioprinting process (**Figure 25**).

Cell expansion is a crucial step in the bioprinting process to attain sufficient and well-characterized cell populations for the development of functional and viable tissue constructs. A study implemented an innovative ML approach, employing just-in-time learning to calibrate Raman spectroscopic models. This enabled real-time predictions of critical cell culture performance parameters for optimal cell growth.[137] ML has also been applied to differentiate healthy from apoptotic cells based on cell size and granularity information.[138] Flow cytometry-based analysis of cell size and granularity, combined with ML, offers an automated, reliable, and stain-free classification of healthy and apoptotic cells. ML plays a pivotal role in optimizing cell proliferation and selecting healthy cells for the fabrication of 3D biomimetic tissue constructs.

Numerous publications discuss the use of ML for optimizing printability in bioprinting[36,139] and a comprehensive understanding of the influence of printing parameters is essential to enhance the viability of the printed cells. Various factors such as shear stress, nozzle size in extrusion-based bioprinting,[140] shear stress, droplet impact velocity, droplet volume and polymer concentration in jetting-based bioprinting[141] and the wavelength and intensity of light, exposure time, type and concentration of photo-initiators and presence of unreacted free radicals in vat photopolymerization-based bioprinting[142] significantly affect the cell viability post-printing. Recent studies have demonstrated the use of ML approaches to predict cell viability during the bioprinting processes with high accuracies.[143] Various parameters were evaluated in the extrusion-based bioprinting system[143a] and vat photo-polymerization bioprinting,[143b] and the live-dead assays provided the dataset for ML training to predict cell viability post-printing. Additionally, a recent study demonstrated the ability to predict the number of printed cells in inkjet-based bioprinting based on the droplet velocity profile captured using a high-speed camera.[144] The ability to precisely predict the number of printed cells is important for fabrication of 3D tissue constructs in a scalable and reproducible manner.

Finally, the tissue maturation process plays a vital role in cell proliferation and differentiation over time, ultimately resulting in 3D tissues/organs with some degree of functionality. This intricate process involves critical biochemical cues that regulate cellular behavior within 3D-bioprinted tissue constructs. Biomechanical conditioning, including mechanical conditioning,[145] electromechanical stimulation,[146] macromolecules,[147] air-liquid interface cultivation,[148] or short-term hypoxic conditions,[149] has been explored to expedite the maturation of 3D-bioprinted constructs into vascularized, functional tissues. ML approaches have been applied to assess the differentiation potential of cells using morphological-based prediction by measuring gene-expression profiles and various biomarkers of undifferentiated cells.[150] Furthermore, a recent study utilized mineral apposition rate and mineralizing surface area as input loading parameters in a DL model to predict and accelerate loading-induced osteogenesis during the bone remodeling process.[151] The interplay between advanced ML models with detailed biological parameters promises to revolutionize the ability to predict and influence tissue maturation, marking a significant stride toward the realization of functional, bioprinted tissues.

4.3.2. Bioelectronics

The convergence of bioprinting and electronics printing in bioelectronics printing marks a revolutionary development, ushering in a new era of advancements in healthcare and related domains.[152] This technology fundamentally revolves around creating a platform that combines biomaterials with electronic components, paving the way for a spectrum of devices, from portable benchtop platforms to wearable or implantable platforms. These devices seamlessly interact with biological systems, holding transformative potential in areas such as regenerative medicine, neural interfaces, biosensors, and in-vitro diagnostic tools for medical assessments and drug testing. The advent of 3D multi-material printing technology has enabled the fusion of diverse materials, spanning biomaterials to functional electronic inks. This synergy provides unparalleled integration, design flexibility, and functionalities that traditional platforms struggle to achieve. Nevertheless, bioelectronics printing encounters challenges, including the development of biocompatible conductive inks (demanding meticulous selection and optimization of conductive biomaterials) and maintaining high cell viability during printing (requiring careful selection of techniques and precise calibration of parameters). Effectively addressing these challenges involves navigating a complex optimization problem, balancing factors such as electronic material conductivity,

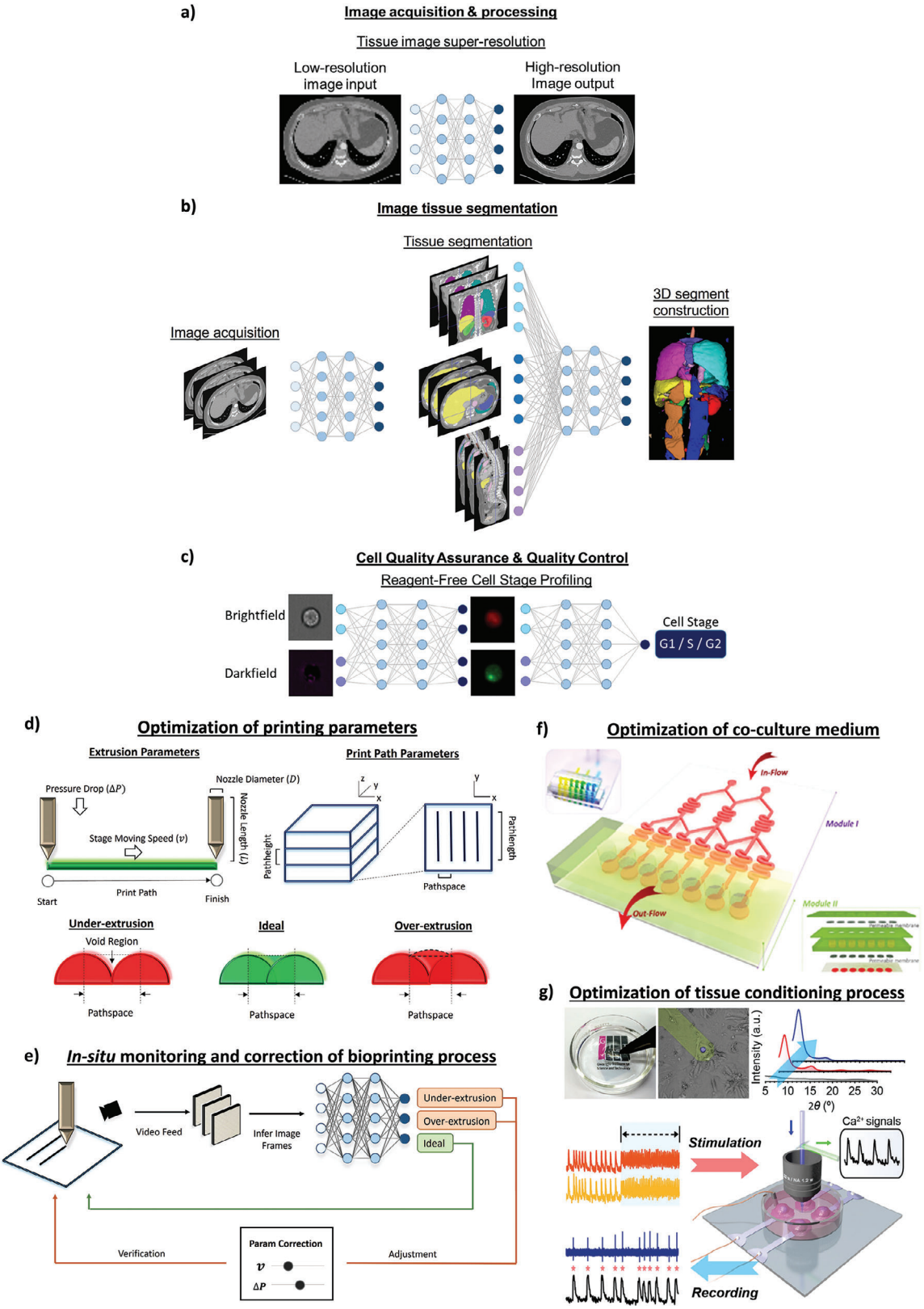

Figure 25. An overview of ML application in typical bioprinting processes. ML can be used to a) generate high-resolution images, b) perform image segmentation, c) control cell quality, d) optimize printing parameters, e) monitor and correct bioprinting process, f) optimize co-culture medium, and g) optimize external stimuli for tissue conditioning process. Reproduced with permission.[136a] 2020, Taylor & Francis.

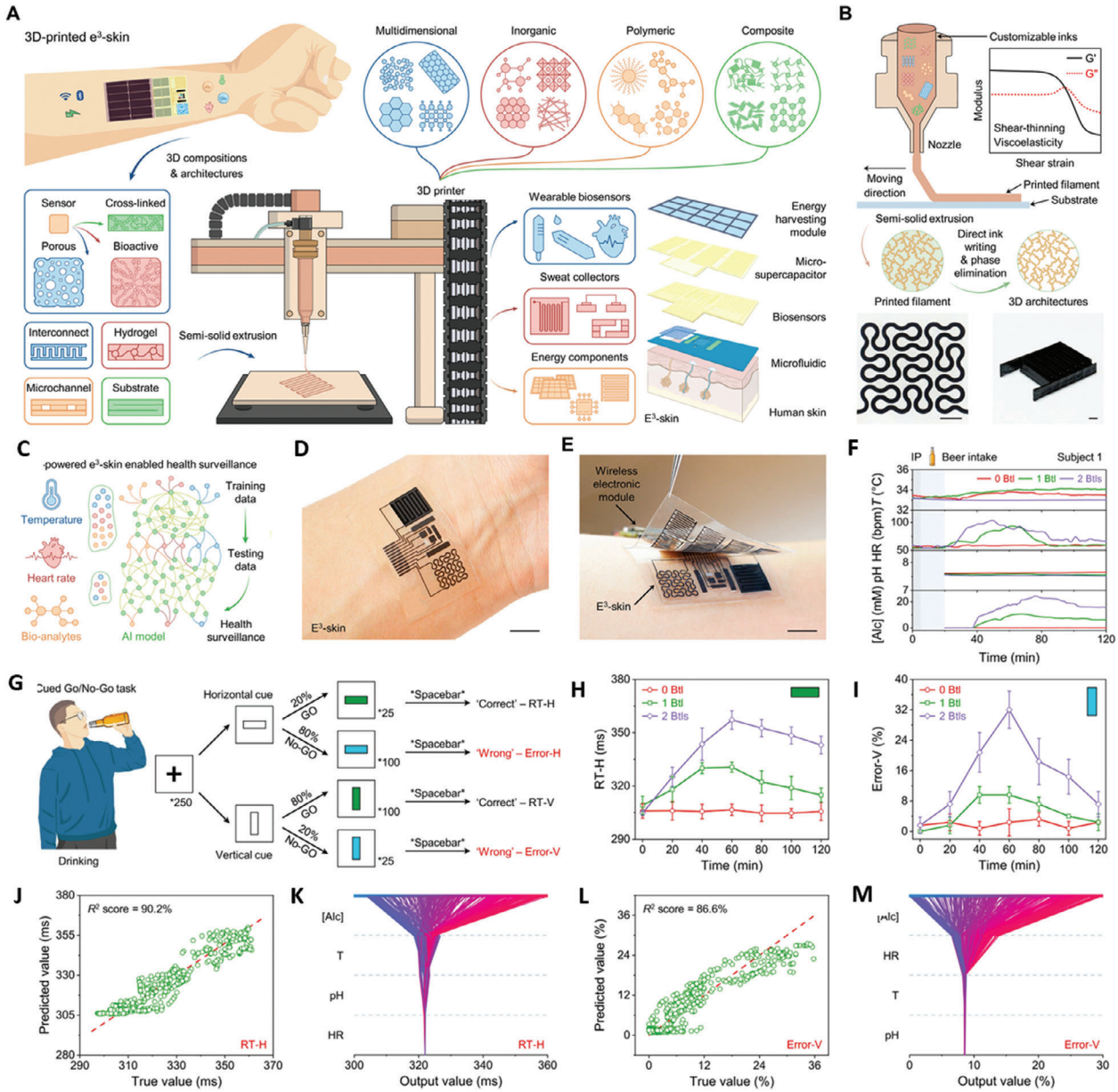

Figure 26. A) Schematic illustration of the material extrusion-based 3D printing that features highly customizable inks based on versatile materials to construct all main building blocks of the wearable electronic (e^3)-skin with multimodal sensing and power management capabilities. B) Schematic illustration of material extrusion printing procedures to prepare 2D and 3D architectures. Top right inset, typical rheological properties of printable inks; bottom, optical images of as printed 2D and 3D MXene architectures. G_0, storage modulus; G_{00}, loss modulus. Scale bars, 2 mm. C) A machine learning framework for multimodal e^3-skin. (D and E) Figure showing the 3D-printed electronic skin. F–M) On-body evaluation using e3-skin for real-time health surveillance and ML-powered health condition prediction. F) Multiplexed multimodal physiological monitoring of a subject after consuming an alcoholic beverage with different doses. G) Workflow of the cued Go/No-Go task for quantitative measurements of the deviation in reaction time (RT) and commission errors (%) for the degree of impairment (DI) for inhibitory control due to the influence of alcohol. H–M) The actual performance versus ML-predicted RT-H (J) and Error-V (L), and the corresponding SHAP decision plot explaining how each regression model arrives at final task performance outcome of RT-H (K) and Error-V (M). Reproduced with permission.[153] 2023, American Association for the Advancement of Science.

platform printability, biocompatibility, and cell survival rates. A recent demonstration showcased the potential application of ML in bioelectronics printing (**Figure 26**).[153] ML emerges as a powerful tool, assisting researchers in identifying patterns among various parameters and guiding decision-making to optimize performance in bioelectronics platforms.[154]

4.3.3. Construction

ML finds application in diverse facets of construction printing, including architectural design, structural analysis, structural health monitoring, and durability.[155] In the realm of architectural design, ML plays a pivotal role in generating both 2D and 3D

innovative layouts. ML models excel in classifying architectural styles and recognizing building components from drawings. A recent study showcased the utilization of the House-GAN model, demonstrating its capacity to explore new designs by learning from existing data, generating diverse house layouts based on input sketches.[156] Additionally, techniques such as semantic segmentation and CNNs are employed to analyze architectural drawings, identify space usage, and simulate interior layouts.[157]

In the domain of structural analysis, ML algorithms are instrumental in predicting structural behavior (such as seismic response, buckling, and fatigue analysis). Neural networks are employed to predict material properties and assess structural components, contributing to the safety and stability evaluation of existing structures.[158] Furthermore, ML, coupled with vibration-based data, facilitates the detection, localization, and quantification of damage in steel beams.[159] Notably, ML can also be applied to structural health monitoring for 3D-printed buildings, evaluating the condition of structures over time, detecting defects, deterioration, and potential failures.[160] ML algorithms analyzed sensor data from strain gauges and accelerometers to predict structural health, identify anomalies, and provide recommendations for maintenance or repairs.[161] Durability assessment, considering factors like material properties, environmental exposure, and load-bearing capacity, benefits from ML by predicting the lifespan of structures and optimizing their design for longevity.

Despite notable progress, challenges such as data quality, model interpretability, and real-world implementation necessitate careful consideration. The ongoing evolution of ML is poised to have a profound impact on the construction industry, reshaping the entire lifecycle of structures from conceptual design to operational maintenance. ML-driven innovations are ushering in a revolution in construction, facilitating the creation of safer, more efficient, and sustainable built environments.

4.3.4. Drug

To date, 3D printing technology has garnered increasing attention within the pharmaceutical sector, revolutionizing drug manufacturing. One of the key advantages of drug printing lies in its ability to facilitate production in small batches, offering unprecedented flexibility in customized dosages, geometries, dimensions, and controllable drug release profiles. This breakthrough in manufacturing capability leads to the on-demand fabrication of personalized medicines. Remarkably, drug printing finds applications across the entire spectrum of the drug development process, ranging from preclinical drug development and human clinical trials to the actual intake of medicines.[162]

Numerous studies have reported the use of ML to optimize the printing parameters in the drug printing process.[163] Notably, an intriguing application of ML involves predicting the drug dissolution behavior of 3D-printed medicine based on the drug's composition. Several studies have demonstrated the capability to predict drug dissolution profiles by considering various input parameters, including material composition, glass transition temperature, melting temperature, molecular weight, infill pattern, density, and surface area-to-volume ratio.[164] This predictive modeling proves invaluable in understanding how different factors influence the release of drugs over time, contributing to more informed and efficient drug development processes.

Furthermore, another captivating application is the optimization of loading efficiency for 3D-printed drugs through the utilization of ML models and advanced Design of Experiments (DOE) techniques.[165] By leveraging ML algorithms and systematic experimentation, researchers can fine-tune the parameters influencing loading efficiency, ensuring that the maximum amount of drug is effectively incorporated into the 3D-printed structure. The marriage of 3D drug printing and ML models holds immense promise for the future of pharmaceutical research and development, paving the way for more personalized and efficient drug therapies.

4.3.5. Electronics

3D-printed electronics have emerged as a ground-breaking frontier in AM, introducing novel opportunities for integrating circuits, sensors, and devices directly within printed structures.[166] ML plays a dual role in this domain: 1) optimizing the printing processes and detecting anomalies during fabrication, 2) processing data collected from the 3D-printed sensors. These printed sensors, enhanced by ML algorithms, can exhibit adaptive behaviors, dynamically responding to their environment and ensuring optimal performance in end-use applications. The synergy between 3D printing and ML thus presents a unique avenue for creating intelligent electronics that are both fabricated and functionally enhanced by advanced computational techniques.

The advances in additive nanomanufacturing of flexible wearable electronics have been presented, showcasing the potential of printed bioelectronic systems for portable healthcare, human-machine interfaces, and advanced wearable technologies.[167] Aerosol jet printing was used to fabricate soft electromyography (EMG) electrodes for recording signals from the skin and CNN was applied for pose-prediction. The results achieved over 97% accuracy in classifying six muscle activities, enabling real-time, wireless control of external machines. In another work, a graphene-based electrode was fabricated, and a similar ML technique was applied for pose prediction (Figure 22). It demonstrated about 99% accuracy in detecting seven classes of finger motions, facilitating wireless control of a robotic hand. Both studies emphasize the reliability, mechanical flexibility, and high-fidelity recording capabilities of the printed bioelectronic systems. The integration of ML algorithms enhances classification accuracy and ensures precise control and continuous monitoring in wearable devices. These quantitative findings validate the feasibility and effectiveness of these technologies in revolutionizing healthcare and human performance.

A novel wearable biosensing system that used surface EMG and hyperdimensional computing for real-time hand gesture recognition was demonstrated.[168] The device comprised of a screen-printed, conformal electrode array and custom-designed application-specific integrated circuit and it incorporated adaptive learning and inference capabilities within the sensor. It classified 13 hand gestures with 97.12% accuracy and maintained high accuracy (92.87%) even when expanded to 21 gestures. The device facilitated real-time updates of its ML models to adapt to changes such as different arm positions or sensor

replacement, recovering accuracy by 9.5% without needing additional external computation. The system offers potential advancements in human-machine interface applications, allowing fast initial training and on-the-fly adaptation, and future work could consider additional situational contexts and gesture transitions, potentially improving classification performance. The low-cost, low-complexity design could also be adapted for other physiological signal processing applications, like electrocardiography or electroencephalography (**Figure 27**).

4.3.6. Food

In recent years, the global food industry has been at the forefront of a transformative paradigm shift, responding to pressing challenges such as environmental sustainability, animal welfare, and the escalating demand for protein-rich diets. This shift has given rise to the innovative concept of 3D cultivated meat, often referred to as lab-grown or cell-based meat. This cutting-edge approach to meat production is currently in its infancy, with researchers working intensively to surmount technical, cost, and regulatory hurdles. The ultimate goal is to provide a sustainable and ethical alternative to conventional meat production, addressing the growing concerns associated with traditional practices.[169]

Notably, the incorporation of ML offers a myriad of advantages to produce 3D-printed cultivated meat. These advantages span from the meticulous fabrication of 3D meat-like structures to the precise regulation of food texture and the customization of nutritional profiles, ushering in a new era of precision and customization.[170] Recent studies have already demonstrated the use of ML in various aspects of 3D-printed cultivated meat, showing its potential for optimization and enhancement. These applications range from the optimization of culture medium formulation,[171] to the prediction and regulation of food flavor,[172] and even quality control measures.[173] A pivotal stage in cultivated meat production lies in cell production within bioreactors, and ML is proving to be a valuable tool for real-time adjustments. Parameters such as temperature, pH, oxygen levels, and nutrient circulation can be dynamically optimized through ML, facilitating optimal cell growth. A recent study showcased the application of ML to sustainably optimize serum-free media development, identifying the optimal combination of media ingredients that strike a balance between yield, environmental impact, and cost for cultivated meat production.[171a]

Furthermore, ML also plays a pivotal role in various facets of 3D-cultivated meat production. ML contributes to the development, optimization, and scale-up of the entire process. By analyzing data on different cell types, ML can identify the most suitable type of cells for cultured meat production based on factors such as growth rate, nutrient requirements, and flavor profile to achieve the best-quality cultured meat products.[174] In essence, ML proves to be an invaluable tool in the development of 3D-printed cultivated meat, aiding researchers in overcoming challenges related to cell selection, bioreactor control, product quality, and nutritional requirements. The role of ML has become increasingly pivotal in shaping the future of sustainable and ethical meat production.

5. Concluding Remarks

The integration of ML in AM processes has attracted increasing attention due to its superior performance for various AM-related applications; the ML models can recognize complex patterns from large, curated datasets and elucidate the complex relationships among different parameters to improve decision-making during the AM process. Some common ML applications in AM research include quality control, process optimization, design optimization, microstructure analysis, and material formulation. The implementation of ML in AM helps to enhance the efficiency and reliability of AM processes. Quality control involves the collection of signals from in situ sensors to train ML models for monitoring process stability and detecting defects within printed layers. Process optimization relies on large datasets from previous printing runs for the prediction of optimal process parameters under a given set of conditions. The incorporation of ML in design optimization enables training on a myriad of design variations, learning from previous iterations, and providing real-time feedback during the design phase. Advanced imaging techniques were used to collect vast amounts of data which can be processed and extracted easily using ML algorithms to decipher the relationships between the processing parameters and microstructure variations. ML algorithms can be used to guide the selection of optimal material compositions to achieve desired properties within the processability constraints. Furthermore, ML applications in emerging AM-related fields such as bioprinting, bioelectronics, construction printing, drug printing, electronics printing, and food printing were highlighted.

In AM, even seemingly straightforward calibration can be subject to a multitude of variable factors, including environmental conditions, equipment wear and tear, and batch-to-batch material inconsistencies. ML, particularly adaptive algorithms, can continuously learn from new data to adjust for these variations, thereby maintaining and even improving the calibration over time without manual re-calibration. The AM landscape is rapidly evolving, with the development of new materials and complex geometries that present high-dimensional challenges suitable for advanced ML techniques. In these scenarios, ML can be integral not just for calibration, but for optimizing printing strategies for novel materials, predicting mechanical properties of printed objects, and enabling real-time quality control for intricate structures that are beyond the capabilities of traditional manufacturing processes.

While current DL research indeed focuses on complex domains such as image and language processing, the principles and models developed in these domains can be adapted to the high-dimensional aspects of AM. For example, CNNs, primarily used for image data, can be repurposed to analyze topological features of printed layers, and recurrent neural networks can model time-series data from the printing process to predict and compensate for potential defects. The intersection of AM with high-dimensional data becomes evident in the pursuit of customizable manufacturing, such as for medical implants or aerospace components, where bespoke designs are the norms. Here, ML can navigate the vast design space to optimize for specific performance criteria, considering individualized constraints and objectives. The application of ML in AM is not limited to simple calibration problems but extends to tackling the intrinsic complexity and evolving challenges of the field. The potential for ML to

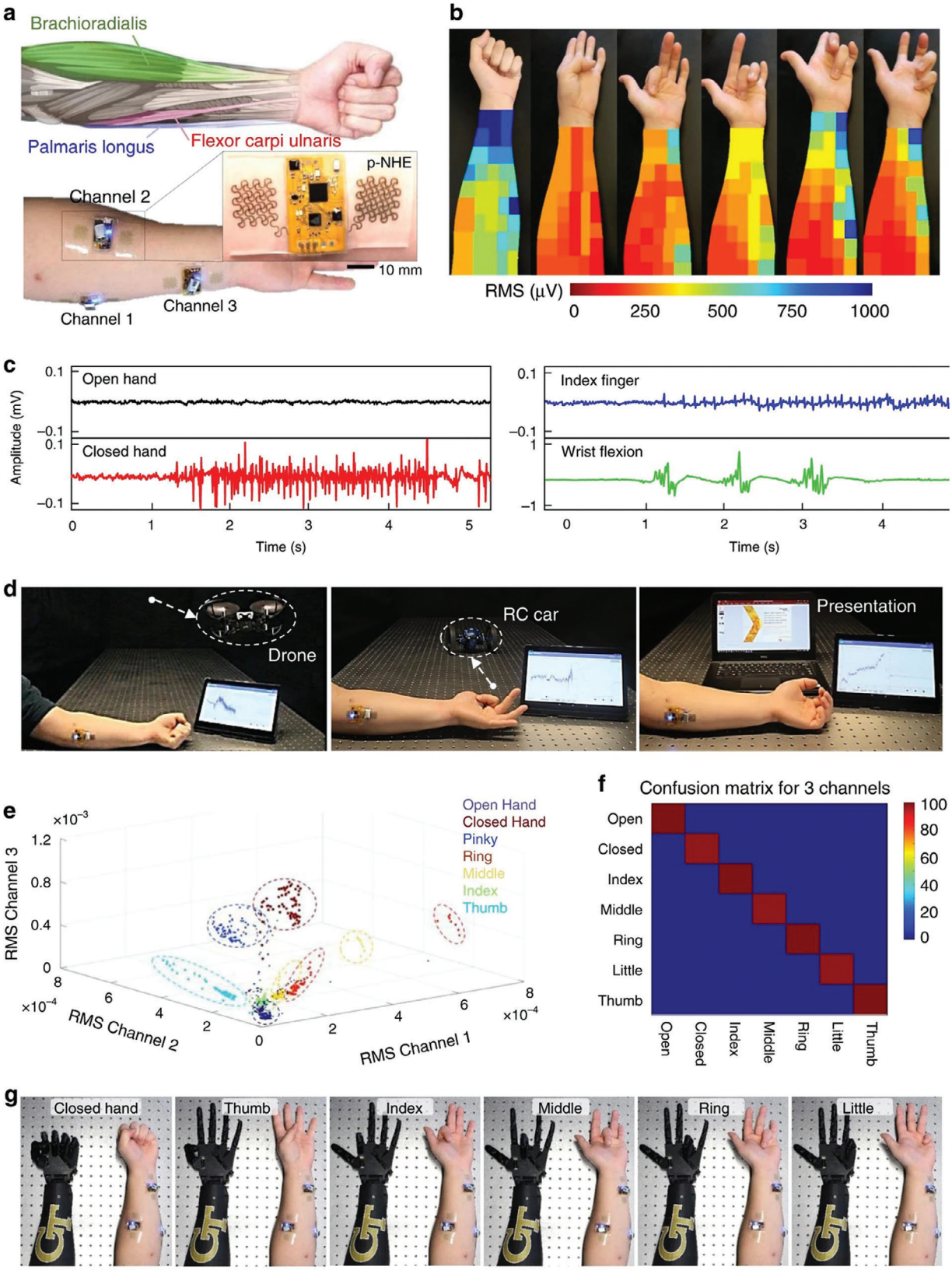

Figure 27. Schematics showing the application of ML to process the output signals from the printed electrodes and sensors. Reproduced with permission.[167b] 2020, Nature Portfolio.

contribute to AM is vast and varied, and we anticipate further integration of advanced ML techniques as the technology and materials of AM continue to advance.

Lastly, establishing a unified data community could serve as a catalyst for overcoming current bottlenecks in ML-driven 3D printing research. By ensuring that data and insights are freely shared, researchers can build on each other's work, accelerating the path from experimental prototypes to practical applications. Additive Manufacturing Materials Database (AMMD) is an initiative that fosters data sharing and collaboration within the AM community.[175] The AMMD enables users to browse and search for specific datasets, facilitating easy access to a wealth of information regarding AM materials and processes. For users who have data but lack a framework to structure it, AMMD provides a data schema and a tool called "Curate Data" to assist in organizing their information according to standardized practices. The database is built upon the National Institute of Standards and Technology's Material Data Curation System (MDCS), utilizing a structure defined by NIST's AM schema. This suggests a robust, standards-driven approach to data curation in the field of additive manufacturing. Nonetheless, currently available databases consist primarily of data extracted from powder bed fusion process and more effort from the AM community to contribute to the development of the database. We strongly believe that ML is an indispensable tool in realizing the full potential of AM, paving the way for unprecedented innovation and efficiency in AM processes. The integration of ML in AM processes would significantly enhance its efficiency and reliability and amplify the 3D printing capabilities across various AM-related research areas.

Acknowledgements

W.L.Ng would like to acknowledge support from the NTU Presidential Postdoctoral Fellowship. W.Y.Yeong would like to acknowledge the support of the National Research Foundation for NRF Investigatorship Award No.: NRF-NRFI07-2021-0007. Part of this research was supported by A*STAR under its RIE2015 JCO Career Development Award (Grant No 202D800024).

Conflict of Interest

The authors declare no conflict of interest.

Keywords

additive manufacturing, bioelectronics, bioprinting, construction, cultivated meat, drug, machine learning

Received: September 26, 2023
Revised: March 1, 2024
Published online:

[1] a) M. D. Xames, F. K. Torsha, F. Sarwar, *J Intell Manuf* **2022**, 1; b) G. D. Goh, S. L. Sing, W. Y. Yeong, *Artif. Intell. Rev.* **2021**, *54*, 63.
[2] R. Caruana, A. Niculescu-Mizil, *ICML '06* **2006**, 161.
[3] a) Z. Ghahramani, in *Advanced Lectures on Machine Learning: ML Summer Schools 2003*, (Eds: O. Bousquet, U. von Luxburg, G. Rätsch), Springer, Berlin, Heidelberg **2004**; b) T. Hastie, R. Tibshirani, J. Friedman, in *The Elements of Statistical Learning: Data Mining, Inference, and Prediction*, (Eds: T. Hastie, R. Tibshirani, J. Friedman), Springer, New York **2009**.
[4] J. E. Van Engelen, H. H. Hoos, *Machine Learning* **2020**, *109*, 373.
[5] a) K. Arulkumaran, M. P. Deisenroth, M. Brundage, A. A. Bharath, *IEEE Signal Process Mag* **2017**, *34*, 26; b) M. A. Wiering, M. Van Otterlo, *Adapt., Learn., Optimiz.* **2012**, *12*, 729; c) L. P. Kaelbling, M. L. Littman, A. W. Moore, *J. Artif. Intell. Res.* **1996**, *4*, 237.
[6] G. L. Goh, G. D. Goh, J. W. Pan, P. S. P. Teng, P. W. Kong, *Sensors* **2023**, *23*, 9759.
[7] G. L. Goh, X. Huang, W. Toh, Z. Li, S. Lee, W. Y. Yeong, B. S. Han, T. Y. Ng, *Int. J. AI Mater. Design* **2024**, *1*, 2328.
[8] J. Zhang, C. Yin, Y. Xu, S. L. Sing, *Int. J. AI Mater. Design* **2024**, *1*, 2301.
[9] L. Scime, J. Beuth, *Addit. Manuf.* **2018**, *19*, 114.
[10] C. Gobert, E. W. Reutzel, J. Petrich, A. R. Nassar, S. Phoha, *Addit. Manuf.* **2018**, *21*, 517.
[11] C. Liu, R. R. Wang, I. Ho, Z. J. Kong, C. Williams, S. Babu, C. Joslin, *J. Intell. Manuf.* **2023**, *34*, 2673.
[12] a) P. Yadav, V. K. Singh, T. Joffre, O. Rigo, C. Arvieu, E. Le Guen, E. Lacoste, *Adv. Eng. Mater.* **2020**, *22*, 2000660; b) S. Feng, Z. Chen, B. Bircher, Z. Ji, L. Nyborg, S. Bigot, *Mater. Des.* **2022**, *222*, 111115.
[13] H. Baumgartl, J. Tomas, R. Buettner, M. Merkel, *Progress Additive Manuf.* **2020**, *5*, 277.
[14] S. Oster, P. P. Breese, A. Ulbricht, G. Mohr, S. J. Altenburg, *J. Intell. Manuf.* **2023**.
[15] S. Oster, T. Fritsch, A. Ulbricht, G. Mohr, G. Bruno, C. Maierhofer, S. J. Altenburg, *Metals* **2022**, *12*, 947.
[16] L. Scime, J. Beuth, *Addit. Manuf.* **2019**, *25*, 151.
[17] A. Gaikwad, R. J. Williams, H. de Winton, B. D. Bevans, Z. Smoqi, P. Rao, P. A. Hooper, *Mater. Des.* **2022**, *221*, 110919.
[18] Z. Ren, L. Gao, S. J. Clark, K. Fezzaa, P. Shevchenko, A. Choi, W. Everhart, A. D. Rollett, L. Chen, T. Sun, *Science* **2023**, *379*, 89.
[19] J. R. Tempelman, A. J. Wachtor, E. B. Flynn, P. J. Depond, J.-B. Forien, G. M. Guss, N. P. Calta, M. J. Matthews, *Addit. Manuf.* **2022**, *55*, 102735.
[20] M. Ghayoomi Mohammadi, D. Mahmoud, M. Elbestawi, *Opt. Laser Technol.* **2021**, *143*, 107338.
[21] S. Luo, X. Ma, J. Xu, M. Li, L. Cao, *Sensors* **2021**, *21*, 7179.
[22] R. Drissi-Daoudi, V. Pandiyan, R. Logé, S. Shevchik, G. Masinelli, H. Ghasemi-Tabasi, A. Parrilli, K. Wasmer, *Virtual Phys. Prototyping* **2022**, *17*, 181.
[23] K. Wasmer, T. Le-Quang, B. Meylan, S. A. Shevchik, *J. Mater. Eng. Perform.* **2019**, *28*, 666.
[24] V. Pandiyan, G. Masinelli, N. Claire, T. Le-Quang, M. Hamidi-Nasab, C. de Formanoir, R. Esmaeilzadeh, S. Goel, F. Marone, R. Logé, S. Van Petegem, K. Wasmer, *Addit. Manuf.* **2022**, *58*, 103007.
[25] Z. Snow, E. W. Reutzel, J. Petrich, *J. Mater. Process. Technol.* **2022**, *302*, 117476.
[26] E. Westphal, H. Seitz, *Addit. Manuf.* **2022**, *50*, 102535.
[27] G. A. R. Sampedro, D. J. S. Agron, G. C. Amaizu, D.-S. Kim, J.-M. Lee, *Appl. Sci.* **2022**, *12*, 8753.
[28] Z. Jin, Z. Zhang, G. X. Gu, *Manuf. Lett.* **2019**, *22*, 11.
[29] G. D. Goh, N. M. B. Hamzah, W. Y. Yeong, *3D Print. Addit. Manuf.* **2022**, *10*, 428.
[30] L. Tan, T. Huang, J. Liu, Q. Li, X. Wu, *Computers Industrial Eng.* **2023**, *176*, 108887.
[31] D. A. J. Brion, S. W. Pattinson, *Nat. Commun.* **2022**, *13*, 4654.
[32] O. Davtalab, A. Kazemian, X. Yuan, B. Khoshnevis, *J Intell Manuf* **2022**, *33*, 771.
[33] S. Garfo, M. Muktadir, S. Yi, *J. Mechatron. Robot* **2020**, *4*, 74.

[34] J. Villacrés, R. Guamán, O. Menéndez, F. A. Cheein, presented at IECON 2021 – 47th Annual Conference of the IEEE Industrial Electronics Society, Toronto, ON, October **2021**.
[35] D. Ahlers, presented at *2021 International Solid Freeform Fabrication Symposium*, Austin, TX, August **2021**.
[36] A. F. Bonatti, G. Vozzi, C. K. Chua, C. De Maria, *Int. J. Bioprint.* **2022**, *8*, 620.
[37] A. Gaikwad, T. Chang, B. Giera, N. Watkins, S. Mukherjee, A. Pascall, D. Stobbe, P. Rao, *J. Intell. Manuf.* **2022**, *33*, 2093.
[38] M. Ogunsanya, J. Isichei, S. K. Parupelli, S. Desai, Y. Cai, *Proc. Manuf.* **2021**, *53*, 427.
[39] S. Stoyanov, C. Bailey, presented at *2017 40th Int. Spring Seminar on Electronics Technology (ISSE)*, Sofia, Bulgaria, May **2017**.
[40] S. Stoyanov, C. Bailey, G. Tourloukis, presented at *2016 6th Electronic System-Integration Technology Conference (ESTC)*, Grenoble, France, September, **2016**.
[41] X. Li, S. Siahpour, J. Lee, Y. Wang, J. Shi, *Proc. Manuf.* **2020**, *48*, 643.
[42] Z. Zhang, Z. Liu, D. Wu, *Addit. Manuf.* **2021**, *37*, 101692.
[43] H. Lee, W. Heogh, J. Yang, J. Yoon, J. Park, S. Ji, H. Lee, *J Manuf Syst* **2022**, *62*, 575.
[44] J. Ertveldt, P. Guillaume, J. Helsen, *Proc. CIRP* **2020**, *94*, 456.
[45] F. Kaji, H. Nguyen-Huu, A. Budhwani, J. A. Narayanan, M. Zimny, E. Toyserkani, *J. Manuf. Processes* **2022**, *81*, 624.
[46] L. Chen, X. Yao, P. Xu, S. K. Moon, G. Bi, *Virtual Phys, Prototyping* **2021**, *16*, 50.
[47] M. Montazeri, A. R. Nassar, C. B. Stutzman, P. Rao, *Addit. Manuf.* **2019**, *30*, 100916.
[48] a) L. Chen, X. Yao, S. K. Moon, *Mater Today Proc* **2022**, *70*, 136; b) L. Chen, X. Yao, C. Tan, W. He, J. Su, F. Weng, Y. Chew, N. P. H. Ng, S. K. Moon, *Addit. Manuf.* **2023**, *69*, 103547.
[49] V. Akhil, G. Raghav, N. Arunachalam, D. Srinivas, *J Comput Inf Sci Eng* **2020**, *20*, 021010.
[50] X. Zhang, J. Saniie, W. Cleary, A. Heifetz, *JOM* **2020**, *72*, 4682.
[51] D. Cannizzaro, A. G. Varrella, S. Paradiso, R. Sampieri, E. Macii, E. Patti, S. Di Cataldo, presented at *2021 Design, Automation & Test in Europe Conference & Exhibition (DATE)*, February **2021**.
[52] V. Mahato, M. A. Obeidi, D. Brabazon, P. Cunningham, *J Intell Manuf* **2022**, *33*, 845.
[53] Y. Chen, H. Wang, Y. Wu, H. Wang, *Materials* **2020**, *13*, 5063.
[54] D. Kim, T. Zohdi, *Computational Mechanics* **2022**, *69*, 383.
[55] P. D. Nguyen, T. Q. Nguyen, Q. B. Tao, F. Vogel, H. Nguyen-Xuan, *Virtual Phys. Prototyping* **2022**, *17*, 768.
[56] X. Li, M. Zhang, M. Zhou, J. Wang, W. Zhu, C. Wu, X. Zhang, *J. Manuf. Processes* **2023**, *90*, 274.
[57] K. Ruberu, M. Senadeera, S. Rana, S. Gupta, J. Chung, Z. Yue, S. Venkatesh, G. Wallace, *Appl. Mater. Today* **2021**, *22*, 100914.
[58] K.-T. Fang, D. K. Lin, P. Winker, Y. Zhang, *Technometrics* **2000**, *42*, 237.
[59] Z. Fu, V. Angeline, W. Sun, *Int J Bioprint* **2021**, *7*, 434.
[60] J. J. Ong, B. M. Castro, S. Gaisford, P. Cabalar, A. W. Basit, G. Pérez, A. Goyanes, *Int. J. Pharm: X* **2022**, *4*, 100120.
[61] I. Rojek, D. Mikołajewski, P. Kotlarz, K. Tyburek, J. Kopowski, E. Dostatni, *Materials* **2021**, *14*, 7625.
[62] T. S. Tamir, G. Xiong, Q. Fang, Y. Yang, Z. Shen, M. Zhou, J. Jiang, *Int. J. Computer Integr. Manuf.* **2022**, 1.
[63] W. Lao, M. Li, T. N. Wong, M. J. Tan, T. Tjahjowidodo, *Virtual Model. Rapid Manuf.: Adv. Res. Virtual Rapid Prototyping, Proc. Int. Conf. Adv. Res. Rapid Prototyping, 2nd* **2020**, *15*, 178.
[64] J. Shi, J. Song, B. Song, W. F. Lu, *Engineering* **2019**, *5*, 586.
[65] D. Wu, C. Xu, *J. Manuf. Sci. Eng.* **2018**, *140*, 101007.
[66] M. Abbasi Shirsavar, M. Taghavimehr, L. J. Ouedraogo, M. Javaheripi, N. N. Hashemi, F. Koushanfar, R. Montazami, *Biosens. Bioelectron.* **2022**, *212*, 114418.
[67] F. P. Brishty, R. Urner, G. Grau, *Flexible Printed Electron.* **2022**, *7*, 015009.
[68] S. Ghosh, M. V. Johnson, R. Neupane, J. Hardin, J. D. Berrigan, S. R. Kalidindi, Y. L. Kong, *Flexible Printed Electron.* **2022**, *7*, 014011.
[69] G. L. Goh, H. Zhang, G. D. Goh, W. Y. Yeong, T. H. Chong, *Mater. Sci. Addit. Manuf.* **2022**, 1.
[70] a) H. Zhang, J. P. Choi, S. K. Moon, T. H. Ngo, *Addit. Manuf.* **2020**, *33*, 101096; b) H. Zhang, J. P. Choi, S. K. Moon, T. H. Ngo, *J. Mater. Process. Technol.* **2020**, *285*, 116779; c) H. Zhang, J. P. Choi, S. K. Moon, T. H. Ngo, *Advanced Engineering Informatics* **2021**, *48*, 101264; d) H. Zhang, E. Hong, X. Chen, Z. Liu, *ACS Appl. Mater. Interfaces* **2023**, *15*, 14532.
[71] a) Z. Zhou, H. Shen, B. Liu, W. Du, J. Jin, *J. Manuf. Processes* **2021**, *64*, 960; b) K. Ren, Y. Chew, Y. Zhang, J. Fuh, G. Bi, *Comput Methods Appl Mech Eng* **2020**, *362*, 112734.
[72] J. Guan, S. You, Y. Xiang, J. Schimelman, J. Alido, X. Ma, M. Tang, S. Chen, *Biofabrication* **2021**, *14*, 015011.
[73] H. He, Y. Yang, Y. Pan, *J Manuf Syst* **2019**, *50*, 236.
[74] F. Parisi, V. Sangiorgio, N. Parisi, A. M. Mangini, M. P. Fanti, J. M. Adam, *VINYLTEC 2005, PVC Build. Constr* **2023**, ahead-of-print.
[75] H. Ko, P. Witherell, Y. Lu, S. Kim, D. W. Rosen, *Addit. Manuf.* **2021**, *37*, 101620.
[76] T. Xue, T. J. Wallin, Y. Menguc, S. Adriaenssens, M. Chiaramonte, *Extreme Mech Lett* **2020**, *41*, 100992.
[77] S. C.-y. Shen, M. J. Buehler, *Communications Engineering* **2022**, *1*, 37.
[78] K. Yanamandra, G. L. Chen, X. Xu, G. Mac, N. Gupta, *Compos. Sci. Technol.* **2020**, *198*, 108318.
[79] L. Zhou, X. Wu, C. Gu, *Journal of Vibroengineering* **2015**, *17*, 3160.
[80] N. S. Iyer, A. M. Mirzendehdel, S. Raghavan, Y. Jiao, E. Ulu, M. Behandish, S. Nelaturi, D. M. Robinson, *arXiv preprint arXiv:2112.04552* **2021**.
[81] G. D. Goh, S. L. Sing, Y. F. Lim, J. L. J. Thong, Z. K. Peh, S. R. Mogali, W. Y. Yeong, *Mater. Des.* **2021**, *211*, 110125.
[82] Y. Han, R. J. Griffiths, Z. Y. Hang, Y. Zhu, *J. Mater. Res.* **2020**, *35*, 1936.
[83] a) C. Herriott, A. D. Spear, *Comput. Mater. Sci.* **2020**, *175*, 109599; b) J. Li, Z. Yang, G. Qian, F. Berto, *Int J Fatigue* **2022**, *158*, 106764.
[84] E. Hu, I. P. Seetoh, C. Q. Lai, *Int J Mech Sci* **2022**, *221*, 107190.
[85] Z. Zhan, H. Li, *Int J Fatigue* **2021**, *142*, 105941.
[86] S. Liu, A. P. Stebner, B. B. Kappes, X. Zhang, *Addit. Manuf.* **2021**, *39*, 101877.
[87] A. International, ASTM F2971-13 Standard Practice for Reporting Data for Test Specimens Prepared by Additive Manufacturing, **2021**.
[88] A. International, ASTM E8/E8M-22 Standard Test Methods for Tension Testing of Metallic Materials, **2022**.
[89] A. International, ASTM E9-19 Standard Test Methods of Compression Testing of Metallic Materials at Room Temperature, **2019**.
[90] D. J. Huang, H. Li, *Mater. Des.* **2021**, *203*, 109606.
[91] J. Zhang, P. Wang, R. X. Gao, *Comput Ind* **2019**, *107*, 11.
[92] A. K. Gupta, M. Taufik, *Austr. J. Mech. Eng.* **2022**, 1.
[93] R. Cai, H. Lin, P. Cheng, Z. Zhang, K. Wang, Y. Peng, Y. Wu, S. Ahzi, *Polym. Compos.* **2022**, *43*, 5235.
[94] S. Czarnecki, Ł. Sadowski, J. Hoła, *Autom Constr* **2021**, *132*, 103977.
[95] A. Bagheri, C. Cremona, *Mater. Adv.* **2020**, *1*, 720.
[96] H. Izadgoshasb, A. Kandiri, P. Shakor, V. Laghi, G. Gasparini, *Appl. Sci.* https://doi.org/10.3390/app112210826.
[97] K. Tran-Quoc, L. B. Nguyen, V. H. Luong, H. Nguyen-Xuan, *Vietnam J. Mech.* **2022**, *44*, 538.
[98] G. A. Lyngdoh, N.-K. Kelter, S. Doner, N. M. A. Krishnan, S. Das, *Mater. Des.* **2022**, *213*, 110341.
[99] Z. Chang, Z. Wan, Y. Xu, E. Schlangen, B. Šavija, *Eng. Fract. Mech.* **2022**, *271*, 108624.

[100] a) C. D. Boley, S. C. Mitchell, A. M. Rubenchik, S. S. Q. Wu, *Appl. Opt.* **2016**, *55*, 6496; b) J. Trapp, A. M. Rubenchik, G. Guss, M. J. Matthews, *Appl. Mater. Today* **2017**, *9*, 341.
[101] G. Bi, C. N. Sun, A. Gasser, *J. Mater. Process. Technol.* **2013**, *213*, 463.
[102] J. H. Martin, B. D. Yahata, J. M. Hundley, J. A. Mayer, T. A. Schaedler, T. M. Pollock, *Nature* **2017**, *549*, 365.
[103] P. C. Collins, D. A. Brice, P. Samimi, I. Ghamarian, H. L. Fraser, *Annu. Rev. Mater. Res.* **2016**, *46*, 63.
[104] C. A. Brice, W. A. Tayon, J. A. Newman, M. V. Kral, C. Bishop, A. Sokolova, *Mater. Charact.* **2018**, *143*, 50.
[105] a) J. A. Slotwinski, E. J. Garboczi, P. E. Stutzman, C. F. Ferraris, S. S. Watson, M. A. Peltz, *J Res Natl Inst Stand Technol* **2014**, *119*, 460; b) A. Strondl, O. Lyckfeldt, H. Brodin, U. Ackelid, *JOM* **2015**, *67*, 549.
[106] P. Villars, N. Onodera, S. Iwata, *J. Alloys Compd.* **1998**, *279*, 1.
[107] S. Curtarolo, W. Setyawan, S. Wang, J. Xue, K. Yang, R. H. Taylor, L. J. Nelson, G. L. W. Hart, S. Sanvito, M. Buongiorno-Nardelli, N. Mingo, O. Levy, *Comput. Mater. Sci.* **2012**, *58*, 227.
[108] A. Jain, S. Ong, G. Hautier, W. Chen, W. Richards, S. Dacek, S. Cholia, D. Gunter, D. Skinner, G. Ceder, **2013**, *1*, 011002.
[109] G. D. Goh, X. Huang, S. Huang, J. L. J. Thong, J. J. Seah, W. Y. Yeong, *Mater. Sci. Addit. Manuf.* **2023**, *2*.
[110] M. Charrier, C. M. Ouellet-Plamondon, *Cem. Concr. Res.* **2022**, *156*, 106761.
[111] S. Nazar, J. Yang, M. Faisal Javed, K. Khan, L. Li, Q.-f. Liu, *Structures* **2023**, *48*, 1670.
[112] I. Navarrete, I. L. Fé-Perdomo, J. A. Ramos-Grez, M. Lopez, *Constr. Build. Mater.* **2023**, *371*, 130632.
[113] C. Hu, W. N. G. J. Hau, W. Chen, Q.-H. Qin, *J. Compos. Mater.* **2020**, *55*, 1459.
[114] D. Cipollone, H. Yang, F. Yang, J. Bright, B. Liu, N. Winch, N. Wu, K. A. Sierros, *J. Mater. Process. Technol.* **2021**, *295*, 117159.
[115] H. Zhang, Z. Liu, S. Yin, H. Xu, *Sci. Rep.* **2023**, *13*, 2513.
[116] M. J. Buehler, *Appl. Mech. Rev.* **2024**, 76.
[117] K. Margatina, T. Schick, N. Aletras, J. Dwivedi-Yu, *presented at Findings of the Association for Computational Linguistics: EMNLP 2023, Singapore*, **2023**.
[118] S. Badini, S. Regondi, E. Frontoni, R. Pugliese, *Adv. Ind. Eng. Polym. Res.* **2023**, *6*, 278.
[119] Y.-C. Hsu, Z. Yang, M. J. Buehler, *APL Mater.* **2022**, 10.
[120] Y. Zhang, G. S. Hong, D. Ye, K. Zhu, J. Y. Fuh, *Mater. Des.* **2018**, *156*, 458.
[121] Y. Zhang, H. G. Soon, D. Ye, J. Y. H. Fuh, K. Zhu, *IEEE Trans Industr Inform* **2019**, *16*, 5769.
[122] S. A. Shevchik, C. Kenel, C. Leinenbach, K. Wasmer, *Addit. Manuf.* **2018**, *21*, 598.
[123] M. Montazeri, A. R. Nassar, A. J. Dunbar, P. Rao, *IISE Trans* **2020**, *52*, 500.
[124] W. Ren, G. Wen, Z. Zhang, J. Mazumder, *Mater. Manuf. Processes* **2022**, *37*, 1339.
[125] M. Khanzadeh, S. Chowdhury, M. Marufuzzaman, M. A. Tschopp, L. Bian, *J Manuf Syst* **2018**, *47*, 69.
[126] J. S. Kim, C. S. Lee, S.-M. Kim, S. W. Lee, *Int. J. Precision Eng. Manuf. Green Technol.* **2018**, *5*, 479.
[127] Z. Ye, C. Liu, C. Kan, *Manuf. Lett.* **2023**, *35*, 1155.
[128] a) T. DebRoy, T. Mukherjee, H. Wei, J. Elmer, J. Milewski, *Nat. Rev. Mater.* **2021**, *6*, 48; b) S. Nasiri, M. R. Khosravani, *J Mater Res Technol* **2021**, *14*, 1137.
[129] F. García-Martínez, D. Carou, F. de Arriba-Pérez, S. García-Méndez, *Rapid Prototyping J.* **2023**.
[130] O. Ero, K. Taherkhani, E. Toyserkani, *Addit. Manuf.* **2023**, *78*, 103894.
[131] a) N. Rane, S. Choudhary, J. Rane, *Virtual Reality (VR), Augmented Reality (AR) D* **2023**, 4; b) L. O. S. Bozzi, K. D. Samson, S. Tadeja, T. Bohné, S. Pattinson, *presented at 2023 IEEE Conference on Virtual Reality and 3D User Interfaces Abstracts and Workshops (VRW)*, **2023**.
[132] J. Urlings, G. de Jong, T. Maal, D. Henssen, *J Digit Imaging* **2023**, 1.
[133] a) P. Zhuang, W. L. Ng, J. An, C. K. Chua, L. P. Tan, *PLoS One* **2019**, *14*, 0216776; b) I. T. Ozbolat, M. Hospodiuk, *Biomaterials* **2016**, *76*, 321; c) W. L. Ng, W. Y. Yeong, M. W. Naing, *Proc. of the 1st Int. Conf. on Progress in Additive Manufacturing* **2014**, 441; d) W. L. Ng, W. Y. Yeong, M. W. Naing, *Int J Bioprint* **2016**, *2*, 53; e) W. L. Ng, W. Y. Yeong, M. W. Naing, *Proc. CIRP* **2016**, *49*, 105.
[134] a) R. Suntornnond, W. L. Ng, X. Huang, E. C. H. Yeow, W. Y. Yeong, *J. Mater. Chem. B* **2022**, *10*, 5989; b) W. L. Ng, W. Y. Yeong, M. W. Naing, *Proc. of the Int. Conf. on Progress in Additive Manufacturing* **2016**, 397; c) W. L. Ng, J. M. Lee, W. Y. Yeong, M. W Naing, *Biomater. Sci.* **2017**, *5*, 632.
[135] W. Li, L. S. Mille, J. A. Robledo, T. Uribe, V. Huerta, Y. S. Zhang, *Adv. Healthcare Mater.* **2020**, *9*, 2000156.
[136] a) W. L. Ng, A. Chan, Y. S. Ong, C. K. Chua, *Virtual Phys. Prototyping* **2020**, *15*, 340; b) W. L. Ng, C. K. Chua, Y.-F. Shen, *Prog. Polym. Sci.* **2019**, *97*, 101145; c) R. Levato, T. Jungst, R. G. Scheuring, T. Blunk, J. Groll, J. Malda, *Adv. Mater.* **2020**, *32*, 1906423; d) J. He, M. Mao, X. Li, C. K. Chua, *Int J Bioprint* **2021**, *7*, 395; e) W. L. Ng, S. Wang, W. Y. Yeong, M. W. Naing, *Trends Biotechnol.* **2016**, *34*, 689; f) J. M. Lee, W. L. Ng, W. Y. Yeong, *Appl Phys Rev* **2019**, *6*, 011307; g) W. L. Ng, J. M. Lee, M. Zhou, W. Y. Yeong, in *Rapid Prototyping of Biomaterials*, (Ed.: R. Narayan), Elsevier, Chapel Hill, NC **2020**.
[137] A. Tulsyan, G. Schorner, H. Khodabandehlou, T. Wang, M. Coufal, C. Undey, *Biotechnol. Bioeng.* **2019**, *116*, 2575.
[138] Y. Li, C. M. Nowak, U. Pham, K. Nguyen, L. Bleris, *npj Syst. Biol. Appl.* **2021**, *7*, 23.
[139] a) Y. Lu, R. Rai, N. Nitin, *Food Res Int* **2023**, *173*, 113384; b) H. Chen, Y. Liu, S. Balabani, R. Hirayama, J. Huang, *Research* **2023**, *6*, 0197; c) D. Oh, M. Shirzad, M. C. Kim, E.-J. Chung, S. Y. Nam, *Int J Bioprint* **2023**, *9*, 1280.
[140] a) S. Han, C. M. Kim, S. Jin, T. Y. Kim, *Biofabrication* **2021**, *13*, 035048; b) L. Fischer, M. Nosratlo, K. Hast, E. Karakaya, N. Ströhlein, T. U. Esser, R. Gerum, S. Richter, F. Engel, R. Detsch, *Biofabrication* **2022**, *14*, 045005.
[141] a) W. L. Ng, V. Shkolnikov, *Int J Bioprint* **2024**, 2135; b) A. Blaeser, D. F. Duarte Campos, U. Puster, W. Richtering, M. M. Stevens, H. Fischer, *Adv. Healthcare Mater.* **2016**, *5*, 326; c) W. L. Ng, X. Huang, V. Shkolnikov, G. L. Goh, R. Suntornnond, W. Y. Yeong, *Int J Bioprint* **2022**, *8*, 424; d) W. L. Ng, X. Huang, V. Shkolnikov, R. Suntornnond, W. Y. Yeong, *Bio-Des. Manuf* **2023**, *6*, 676; e) W. L. Ng, W. Y. Yeong, M. W. Naing, *Materials* **2017**, *10*, 190.
[142] W. L. Ng, J. M. Lee, M. Zhou, Y.-W. Chen, K.-X. A. Lee, W. Y. Yeong, Y.-F. Shen, *Biofabrication* **2020**, *12*, 022001.
[143] a) D. Mohammadrezaei, L. Podina, J. De Silva, M. Kohandel, *Biofabrication* **2023**; b) H. Xu, Q. Liu, J. Casillas, M. McAnally, N. Mubtasim, L. S. Gollahon, D. Wu, C. Xu, *J Intell Manuf* **2022**, *33*, 995.
[144] X. Huang, W. L. Ng, W. Y. Yeong, *J Intell Manuf* **2023**.
[145] a) B.-S. Kim, J. Nikolovski, J. Bonadio, D. J. Mooney, *Nat. Biotechnol.* **1999**, *17*, 979; b) D. Seliktar, R. A. Black, R. P. Vito, R. M. Nerem, *Ann. Biomed. Eng.* **2000**, *28*, 351.
[146] a) A. Llucià-Valldeperas, C. Soler-Botija, C. Gálvez-Montón, S. Roura, C. Prat-Vidal, I. Perea-Gil, B. Sanchez, R. Bragos, G. Vunjak-Novakovic, A. Bayes-Genis, *Stem Cells Transl. Med.* **2017**, *6*, 970; b) K. Ronaldson-Bouchard, S. P. Ma, K. Yeager, T. Chen, L. Song, D. Sirabella, K. Morikawa, D. Teles, M. Yazawa, G. Vunjak-Novakovic, *Nature* **2018**, *556*, 239.
[147] a) A. Satyam, P. Kumar, X. Fan, A. Gorelov, Y. Rochev, L. Joshi, H. Peinado, D. Lyden, B. Thomas, B. Rodriguez, *Adv. Mater.* **2014**, *26*, 3024; b) W. L. Ng, M. H. Goh, W. Y. Yeong, M. W. Naing, *Biomater. Sci.* **2018**, *6*, 562; c) P. Benny, C. Badowski, E. B. Lane, M. Raghunath, *Tissue Eng Part A* **2014**, *21*, 183.

[148] a) M. Pruniéras, M. Régnier, D. Woodley, *J. Invest. Dermatol.* **1983**, *81*, S28; b) W. L. Ng, Z. Q. Tan, W. Y. Yeong, M. W. Naing, *Biofabrication* **2018**, *10*, 025005; c) J.-E. Chang, S. K. Basu, V. H. Lee, *Pharm. Res.* **2000**, *17*, 670; d) S. Wang, C. E. Ghezzi, R. Gomes, R. E. Pollard, J. L. Funderburgh, D. L. Kaplan, *Biomaterials* **2017**, *112*, 1; e) G. Lacroix, W. Koch, D. Ritter, A. C. Gutleb, S. T. Larsen, T. Loret, F. Zanetti, S. Constant, S. Chortarea, B. Rothen-Rutishauser, *Appl. In Vitro Toxicol.* **2018**, *4*, 91; f) W. L. Ng, T. C. Ayi, Y.-C. Liu, S. L. Sing, W. Y. Yeong, B.-H. Tan, *Int J Bioprint* **2021**, *7*, 332.

[149] a) S. Rey, G. L. Semenza, *Cardiovasc. Res.* **2010**, *86*, 236; b) M. A. Kuss, R. Harms, S. Wu, Y. Wang, J. B. Untrauer, M. A. Carlson, B. Duan, *RSC Adv.* **2017**, *7*, 29312.

[150] a) H. Sasaki, I. Takeuchi, M. Okada, R. Sawada, K. Kanie, Y. Kiyota, H. Honda, R. Kato, *PLoS One* **2014**, *9*, e93952; b) F. Matsuoka, I. Takeuchi, H. Agata, H. Kagami, H. Shiono, Y. Kiyota, H. Honda, R. Kato, *PLoS One* **2013**, *8*, e55082.

[151] M. Dattatrey, A. K. Tiwari, B. Ghoshal, J. Singh, *IEEE Access* **2019**, *7*, 122561.

[152] S. Agarwala, J. M. Lee, W. L. Ng, M. Layani, W. Y. Yeong, S. Magdassi, *Biosens. Bioelectron.* **2018**, *102*, 365.

[153] Y. Song, R. Y. Tay, J. Li, C. Xu, J. Min, E. Shirzaei Sani, G. Kim, W. Heng, I. Kim, W. Gao, *Sci. Adv.* **2023**, *9*, eadi6492.

[154] G. D. Goh, J. M. Lee, G. L. Goh, X. Huang, S. Lee, W. Y. Yeong, *Tissue Eng Part A* **2023**, *29*, 20.

[155] S. K. Baduge, S. Thilakarathna, J. S. Perera, M. Arashpour, P. Sharafi, B. Teodosio, A. Shringi, P. Mendis, *Autom Constr* **2022**, *141*, 104440.

[156] N. Nauata, K.-H. Chang, C.-Y. Cheng, G. Mori, Y. Furukawa, *presented at Computer Vision–ECCV 2020: 16th European Conference, Glasgow, UK, August 23–28, 2020, Proceedings, Part I 16*, **2020**.

[157] J. Seo, H. Park, S. Choo, *Appl. Sci.* **2020**, *10*, 7347.

[158] a) M. Jimenez-Martinez, M. Alfaro-Ponce, *Int J Fatigue* **2019**, *124*, 42; b) P. Mandal, *Eng. Struct.* **2017**, *152*, 843; c) U. K. Mallela, A. Upadhyay, *Thin-Walled Structures* **2016**, *102*, 158; d) S. Tohidi, Y. Sharifi, *Thin-Walled Structures* **2015**, *94*, 359.

[159] a) K. H. Padil, N. Bakhary, H. Hao, *Mech Syst Signal Process* **2017**, *83*, 194; b) O. Avci, O. Abdeljaber, S. Kiranyaz, M. Hussein, M. Gabbouj, D. J. Inman, *Mech Syst Signal Process* **2021**, *147*, 107077.

[160] a) O. Abdeljaber, O. Avci, M. S. Kiranyaz, B. Boashash, H. Sodano, D. J. Inman, *Neurocomputing* **2018**, *275*, 1308; b) S. Dorafshan, R. J. Thomas, M. Maguire, *Constr. Build. Mater.* **2018**, *186*, 1031; c) W. R. L. d. Silva, D. S. d. Lucena, *presented at Proceedings*, **2018**; d) Y. Bao, Z. Tang, H. Li, Y. Zhang, *Struct Health Monit* **2019**, *18*, 401; e) Y. J. Cha, W. Choi, O. Büyüköztürk, *Computer-Aided Civil and Infrastructure Engineering* **2017**, *32*, 361.

[161] a) C.-c. Liu, J. Liu, L.-j. Liu, *presented at 2009 International Conference on Information Engineering and Computer Science*, **2009**; b) M. H. Rafiei, H. Adeli, *Eng. Struct.* **2018**, *156*, 598.

[162] J. Vamathevan, D. Clark, P. Czodrowski, I. Dunham, E. Ferran, G. Lee, B. Li, A. Madabhushi, P. Shah, M. Spitzer, *Nat. Rev. Drug Discovery* **2019**, *18*, 463.

[163] a) M. Elbadawi, B. M. Castro, F. K. Gavins, J. J. Ong, S. Gaisford, G. Pérez, A. W. Basit, P. Cabalar, A. Goyanes, *Int. J. Pharm.* **2020**, *590*, 119837; b) M. Elbadawi, T. Gustaffson, S. Gaisford, A. W. Basit, *Int. J. Pharm.* **2020**, *590*, 119868; c) Y. Abdalla, M. Elbadawi, M. Ji, M. Alkahtani, A. Awad, M. Orlu, S. Gaisford, A. W. Basit, *Int. J. Pharm.* **2023**, *633*, 122628; d) C. S. O'Reilly, M. Elbadawi, N. Desai, S. Gaisford, A. W. Basit, M. Orlu, *Pharmaceutics* **2021**, *13*, 2187; e) P. Carou-Senra, J. J. Ong, B. M. Castro, I. Seoane-Viano, L. Rodríguez-Pombo, P. Cabalar, C. Alvarez-Lorenzo, A. W. Basit, G. Pérez, A. Goyanes, *Int. J. Pharm. X* **2023**, *5*, 100181.

[164] a) T. Tagami, C. Morimura, T. Ozeki, *Int. J. Pharm.* **2021**, *604*, 120721; b) S. Obeid, M. Madžarević, M. Krkobabić, S. Ibrić, *Int. J. Pharm.* **2021**, *601*, 120507; c) B. M. Castro, M. Elbadawi, J. J. Ong, T. Pollard, Z. Song, S. Gaisford, G. Pérez, A. W. Basit, P. Cabalar, A. Goyanes, *J. Controlled Release* **2021**, *337*, 530; d) A. Lu, J. Zhang, J. Jiang, Y. Zhang, B. R. Giri, V. R. Kulkarni, N. H. Aghda, J. Wang, M. Maniruzzaman, *Pharm. Res.* **2022**, *39*, 2905.

[165] J. Wang, N. H. Aghda, J. Jiang, A. M. Habib, D. Ouyang, M. Maniruzzaman, *Int. J. Pharm.* **2022**, *628*, 122302.

[166] a) A. K. Sinha, G. L. Goh, W. Y. Yeong, Y. Cai, *Adv. Mater. Interfaces* **2022**, *9*, 2200621; b) G. L. Goh, V. Dikshit, R. Koneru, Z. K. Peh, W. Lu, G. D. Goh, W. Y. Yeong, *Int J Adv Manuf Technol* **2022**, *120*, 2573; c) S. Agarwala, G. L. Goh, W. Y. Yeong, **2018**; d) G. L. Goh, H. Zhang, T. H. Chong, W. Y. Yeong, *Adv. Electron. Mater. n/a*, 2100445.

[167] a) Y.-T. Kwon, H. Kim, M. Mahmood, Y.-S. Kim, C. Demolder, W.-H. Yeo, *ACS Appl. Mater. Interfaces* **2020**, *12*, 49398; b) Y.-T. Kwon, Y.-S. Kim, S. Kwon, M. Mahmood, H.-R. Lim, S.-W. Park, S.-O. Kang, J. J. Choi, R. Herbert, Y. C. Jang, Y.-H. Choa, W.-H. Yeo, *Nat. Commun.* **2020**, *11*, 3450.

[168] A. Moin, A. Zhou, A. Rahimi, A. Menon, S. Benatti, G. Alexandrov, S. Tamakloe, J. Ting, N. Yamamoto, Y. Khan, *Nat. Electron.* **2021**, *4*, 54.

[169] M. J. Post, S. Levenberg, D. L. Kaplan, N. Genovese, J. Fu, C. J. Bryant, N. Negowetti, K. Verzijden, P. Moutsatsou, *Nat Food* **2020**, *1*, 403.

[170] W. L. Ng, J. S. Tan, *Int. J. AI Mater. Design* **2024**, *1*, 2279.

[171] a) A. Nikkhah, A. Rohani, M. Zarei, A. Kulkarni, F. A. Batarseh, N. T. Blackstone, R. Ovissipour, *Sci. Total Environ.* **2023**, 164988; b) Z. Cosenza, D. E. Block, K. Baar, *Biotechnol J* **2021**, *16*, 2100228.

[172] H. Ji, D. Pu, W. Yan, Q. Zhang, M. Zuo, Z. Yuyu, *Trends Food Sci. Technol.* **2023**, *138*, 738.

[173] A. Soni, Y. Dixit, M. M. Reis, G. Brightwell, *Compr Rev Food Sci Food Saf* **2022**, *21*, 3717.

[174] J. Wang, S. Ding, C. Da, C. Chen, Z. Wu, C. Li, G. Zhou, C. Tang, *J. Agric. Food Chem.* **2023**, *71*, 18613.

[175] NIST, National Institute of Standards and Technology, Vol. *2024*, 2024.

[176] S. L. Sing, Y. Y. Wai, E. W. Florencia, *J. of Alloys and Comp.* **2016**, *660*, 461.

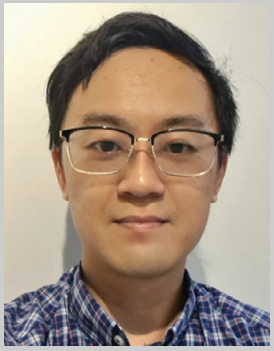

Wei Long Ng is a NTU Presidential Postdoctoral Fellow at the Singapore Centre for 3D Printing (SC3DP), Nanyang Technological University (NTU), Singapore. He received his Ph.D. degree from School of Aerospace & Mechanical Engineering, Nanyang Technological University under the A*STAR Graduate Scholarship. Dr. Ng served as a Research Assistant Professor at the HP-NTU Digital Manufacturing Corporate Lab, Singapore from 2020 to 2022. His expertise lies in the intersection of additive manufacturing and machine learning, where he fabricates 3D biomimetic constructs using novel bioprinting strategies for applications ranging from tissue engineering to the emerging field of cultivated meat production.

Guo Liang Goh is a Research Fellow at the School of Mechanical and Aerospace Engineering, Nanyang Technological University, Singapore. He obtained his Ph.D. degree in Mechanical Engineering from the Nanyang Technological University. He specializes in the innovative fields of 3D printing, additive manufacturing, 3D-printed electronics and machine learning. His expertise spans wearables, soft robotics, bioelectronics and more. He has led numerous research projects, secured substantial funding, and contributed to pioneering advancements in sensor technology, UAVs, and sports technology.

Guo Dong Goh is a scientist at Singapore Institute of Manufacturing Technology (SIMTech). He obtained his Ph.D. degree in Mechanical Engineering from the Nanyang Technological University. His research interests include using additive manufacturing process to create multifunctional polymer parts and applying machine learning techniques to advance the field of 3D printing in terms of design and quality. He has led numerous research projects, secured substantial funding, and contributed to pioneering advancements in fracture mechanics in 3D printing composites, UAVs, and sports technology.

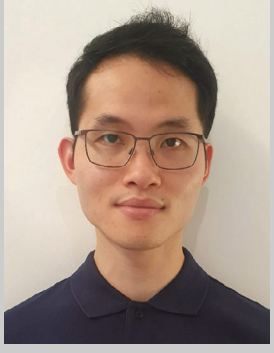

Jyi Sheuan Jason Ten is currently the Deputy Group Manager of the Additive Technology Innovation Group within the Additive Manufacturing Division at the Singapore Institute of Manufacturing Technology. He received a Ph.D. degree in lasers for manufacturing from the University of Cambridge in 2018. Dr. Ten's research interests are in additive manufacturing: including in-process monitoring for defect detection and quality assurance, sustainability of powder within re-use cycles with correlation to part properties, fine feature part production, multi-material laser powder bed fusion, materials for additive manufacturing, and machine learning in AM.

Wai Yee Yeong is a Professor and Chair of School of Mechanical & Aerospace Engineering, Nanyang Technological University (NTU). She joined NTU since 2013 and was promoted to Full Professor in 2022. She is currently serving as a Program Director at HP-NTU Digital Manufacturing Corporate Lab, Editor-in-Chief of International Journal of AI for Materials and Design (IJAMD) and Associate Editor for Virtual and Physical Prototyping and International Journal of Bioprinting. Her current research interest focuses on the convergence of 3D printing and machine learning, particularly in the realms of printing multi-functional structures, printed electronics, and bio-electronic platforms.